

Aus der Klinik für Innere Medizin III
im Universitätsklinikum Schleswig-Holstein, Campus Kiel
an der Christian-Albrechts-Universität zu Kiel
Direktor: Prof. Dr. Norbert Frey

**Functional characterization of TRIM24 and TRIM32 proteins in the
heart through their interaction with Dysbindin**

Dissertation
zur Erlangung des Doktorgrades
der Mathematisch-Naturwissenschaftlichen Fakultät
der Christian-Albrechts-Universität zu Kiel
Vorgelegt von

Ankush Borlepawar

Kiel, 2019

First Examiner: Prof. Dr. Dennis Schade

Second Examiner: Prof. Dr. Norbert Frey

Date of the oral examination: 05.11.2019

Declaration:

I hereby declare that, apart from the supervisor's guidance the content and design of the current thesis is all of my own work. This doctoral thesis has never been submitted either partially or wholly as part of a doctoral degree to another examining body and has never been published nor has been submitted for publication. This thesis has been prepared in accordance to the Rules of Good Scientific Practice of the German Research Foundation. No academic degree has ever been withdrawn from me.

Kiel, _____

(Date)

Doctoral candidate's signature

Preface

The work presented in this doctoral thesis has been performed under supervision of Prof. Dr. Norbert Frey in the Institute of Molecular Cardiology. The experimental work and its dissertation were conducted from August 2015 to November 2019. Various results arising from this doctoral thesis work have been published in renowned scientific journals, which also have been enlisted below.

1	Index	
2	Summary.....	12
3	Zusammenfassung.....	13
4	Introduction.....	15
4.1	Prelude.....	15
4.2	Cardiomyopathies.....	16
4.3	Cardiac hypertrophy.....	17
4.3.1	Dysbindin is a potent inducer cardiac of hypertrophy.....	18
4.3.2	TRIM24 and TRIM32 are potential cardiac interaction partners of Dysbindin.....	19
4.4	Proteostasis is essential for normal heart functioning.....	20
4.5	Components of the cellular proteostasis machinery.....	22
4.5.1	Component 1: Heat shock proteins.....	22
4.5.2	HSPs in cardioprotection.....	23
4.5.3	Component 2: Autophagy.....	25
4.5.4	Autophagy in the heart.....	26
4.5.5	Component 3: Ubiquitin-Proteasome system (UPS).....	28
4.5.6	E3 ligases provide substrate recognition specificity.....	30
4.5.7	E3 ubiquitin ligases in the heart.....	30
4.6	TRIM E3 ubiquitin ligases.....	31
4.6.1	N-terminal invariable domains in TRIM24 and TRIM32.....	32
4.6.2	C-terminal variable domains occurring in TRIM24/32.....	34
4.6.3	Roles of TRIM family in cardiac proteostasis.....	35
5	Aims of the study.....	39
6	Materials.....	40
6.1	Hardware and consumables.....	40
6.2	Chemicals.....	42
6.3	Enzymes.....	44
6.4	Antibodies.....	45
6.5	Vectors.....	46

6.6	Kits.....	47
6.7	Buffers and solutions	48
6.8	Media	50
6.9	Bacteria	50
7	Methods.....	51
7.1	Microbiological methods	51
7.1.1	Generation of electro-competent bacteria.....	51
7.1.2	Electroporation.....	51
7.1.3	Agar plate preparation	51
7.1.4	Spreading of bacterial cultures	52
7.1.5	The growth of the bacteria in liquid-culture.....	52
7.1.6	Storage of positive clones as glycerol stocks	52
7.1.7	Plasmid DNA extraction: Mini preparation	52
7.1.8	Plasmid DNA extraction: Midi preparation	53
7.1.9	Agarose gel electrophoresis	53
7.1.10	DNA extraction from agarose gels	54
7.1.11	DNA and RNA concentration measurement	54
7.2	Cell culture methods.....	54
7.2.1	Culturing of immortalized HEK293A cell line	54
7.2.2	Cell Transfection in HEK293A cells	55
7.2.3	Cryo-conservation of the HEK293A cell line.....	55
7.2.4	Isolation of neonatal rat ventricular cardiomyocytes.....	56
7.3	Generation of mammalian vectors	58
7.3.1	Open reading frame (ORF) PCRs using target specific and attB site-specific primers	58
7.3.2	Recombination using BP and LR clonase from Gateway® technology.....	60
7.3.3	Generation of artificial micro-RNA constructs using the Gateway®-compatible Block-iT system	60
7.3.4	Generation of adenoviruses for recombinant protein or miRNA expression.....	61
7.3.5	Virus particle titration	62

7.4	Interaction studies	63
7.4.1	Co-immunoprecipitation in HEK293A cells	63
7.4.2	Co-immunoprecipitation in NRVCMs	64
7.4.3	Co-localization in NRVCMs: Confocal immunofluorescence microscopy	65
7.4.4	Co-localization in NRVCMs: Analysis	65
7.5	Animal experiments	66
7.5.1	Transverse Aortic Constriction (TAC)	66
7.5.2	Phenylephrine osmotic pump implantation	66
7.6	Cellular assays	67
7.6.1	SRF reporter gene assay	67
7.6.2	MTT assay for cell viability in NRVCMs	67
7.7	Immunofluorescence studies.....	68
7.7.1	Immunofluorescence microscopy	68
7.7.2	Cell surface area measurement using BZ-9000 microscope	68
7.7.3	TUNEL assay.....	69
7.7.4	Cleaved Caspase3 staining	70
7.7.5	Propidium Iodide (PI) staining.....	70
7.8	Molecular biology methods	70
7.8.1	RNA isolation and qRT-PCR	70
7.8.2	Protein isolation and Western blotting.....	74
7.9	Human DCH and HCM heart samples	78
7.10	Statistical analyses	78
8	Results.....	79
8.1	TRIM24 and TRIM32 are putative cardiac interaction partners of Dysbindin.....	79
8.2	TRIM24 and TRIM32 exhibit endogenous cardiac expression.....	81
8.3	TRIM24 and TRIM32 are differentially expressed after biochemical and biomechanical stress.....	82
8.4	TRIM24 and TRIM32 are differentially expressed in human cardiomyopathies.....	83
8.5	TRIM24 and TRIM32 interact with Dysbindin in HEK293A cells	84
8.6	Dysbindin interacts with TRIM24 via its coiled-coil domain.....	86

8.7	Validation of vector expression efficiency in cardiomyocytes	88
8.8	Dysbindin interacts with TRIM24 and TRIM32 in cardiomyocytes.....	89
8.9	Dysbindin localizes with TRIM24 and TRIM32 in cardiomyocytes	90
8.10	Expression of TRIM24 and TRIM32 discordantly affects cellular levels of Dysbindin	92
8.11	TRIM24 and TRIM32 affect cellular levels of Dysbindin via ubiquitination.....	93
8.12	TRIM24 and TRIM32 have a differential effect on SRF signaling.....	95
8.13	TRIM24 and TRIM32 inversely affect cell surface area in cardiomyocytes	96
8.14	TRIM24 protects Dysbindin from TRIM32-mediated degradation and further promotes cardiomyocyte hypertrophy	97
8.15	TRIM32 expression adversely affects cell viability	99
8.16	TRIM32 expression induces apoptosis in NRVCMs.....	101
8.17	TRIM32 induces apoptosis via regulation of Caspases	103
9	Discussion	105
9.1	TRIM24 and TRIM32 are differentially regulated in cardiac hypertrophy and cardiomyopathy.....	106
9.2	TRIM24 and TRIM32 interact with cardiac Dysbindin	107
9.3	TRIM32 but not TRIM24 targets Dysbindin for UPS-mediated degradation.....	108
9.4	TRIM24 is additive, whereas TRIM32 is inhibitory for SRF signaling.....	109
9.5	TRIM24 protects Dysbindin from TRIM32-mediated degradation.....	110
9.6	TRIM32 affects cellular viability and induces apoptosis in cardiomyocytes	110
9.7	Molecular mechanism of cardiac hypertrophy and apoptosis regulated by TRIM24/32	112
9.8	Expression data suggest the involvement of additional TRIMs in heart function.....	114
9.9	Concluding remarks and wider prospectives.....	115
10	Abbreviations.....	117
11	References	123
12	Curriculum vitae.....	141
13	Acknowledgment.....	143

List of figures

Figure 1: Worldwide causes of mortality in the year 2015.....	15
Figure 2: Major protein Homeostasis processes.....	20
Figure 3: Heat shock proteins and their functions in the heart.....	24
Figure 4: Autophagy in the heart.	27
Figure 5: The process of Ubiquitination.....	28
Figure 6: Fate of ubiquitination.....	28
Figure 7: Classification of Tripartite motif family proteins	31
Figure 8: TRIM24 and TRIM32 are endogenously present in mouse heart..	80
Figure 9: TRIM24 and TRIM32 are differentially regulated in biochemical and biomechanical stress in mouse heart..	82
Figure 10: TRIM24 and TRIM32 are differentially regulated in human dilated and hypertrophic cardiomyopathies.....	83
Figure 11: TRIM24 and TRIM32 are interaction partners of Dysbindin.....	86
Figure 12: Dysbindin interacts with TRIM24 through the coiled-coil domain..	87
Figure 13: Validation for the efficiency of adenoviral overexpression vectors.	87
Figure 14: Validation for knockdown of native Dysbindin, TRIM24, and TRIM32 in NRVCMs	88
Figure 15: TRIM24 and TRIM32 are cardiac interaction partners of Dysbindin..	89
Figure 16: Dysbindin co-localizes with TRIM24 and TRIM32 in NRVCMs..	90
Figure 17: TRIM24 and TRIM32 have an antagonistic effect on Dysbindin protein levels in NRVCMs.....	93
Figure 18: Dysbindin protein levels are regulated by TRIM24 and TRIM32 via ubiquitination.	93
Figure 19: TRIM24 and TRIM32 antagonistically regulate SRF activity in NRVCMs.....	95
Figure 20: TRIM32 adversely affects cell surface area in cardiomyocytes.	96
Figure 21: TRIM24 protects Dysbindin from TRIM32-mediated degradation.	97
Figure 22: TRIM32 negatively affects cellular viability.....	99
Figure 23: TRIM32 induces apoptosis and cell death in NRVCMs.	102
Figure 24: TRIM32 induces apoptosis in cardiomyocytes via cleavage and activation of caspases.	104

Figure 25: Pictorial representation of the effects of TRIM24/32 on Dysbindin levels and its downstream signaling in cardiomyocytes.....113

Figure 26: Expression of TRIM proteins in various heart compartments.....114

Figure 27: Expression of TRIM proteins in various cardiovascular diseases.....115

List of tables

Table 1: List of primary antibodies.....	45
Table 2: List of secondary antibodies.....	46
Table 3: List of overexpression plasmids.....	46
Table 4: Adenoviral constructs.....	47
Table 5: Cell seeding density for NRVCMs.	57
Table 6: ORF cloning primers.	59
Table 7: Synthetic oligonucleotide sequences for microRNA generation.	61
Table 8: Resuspension mix for RNA isolation with DNase I enzyme.....	71
Table 9: Contents for cDNA synthesis master mix.....	72
Table 10: cDNA synthesis conditions.	73
Table 11: Quantitative real-time PCR protocol.....	73
Table 12: Quantitative real-time PCR primers.	74
Table 13: List of putative Dysbindin-binding partners.....	80

2 Summary

Ubiquitination is one of the important post-translational modifications and a vital cellular process involved in various tasks of targeted protein degradation via the Ubiquitin-Proteasome system (UPS), intracellular signaling, cell death, transcriptional control, etc. Importantly, it prevents the aggregation of non-functional, misfolded, and potentially harmful proteins to maintain protein homeostasis. Ubiquitination is accomplished by the concerted action of three enzymatic steps involving E1 activating enzymes, E2 conjugating enzymes, and E3 ligases. Tripartite motif-containing (TRIM) proteins are one of the integral members of E3 ubiquitin ligases in metazoans, modulating essential cellular pathways. For long, MuRFs (Muscle ring finger proteins) were the most extensively studied TRIMs for their cardiac function. Recent advances in the field, however, have demonstrated broader and ever-increasing reports of various TRIM E3 ligases in the (patho-) physiology of the heart. A schizophrenia susceptibility protein, Dysbindin was reported by our group to also play a role in the heart and to be the robust inducer of cardiomyocyte hypertrophy via activation of Rho-dependent serum-response factor (SRF) signaling pathway. A Yeast two-hybrid screen was performed using Dysbindin as bait against a human cardiac cDNA library to identify the cardiac Dysbindin interactome. Among several putative binding proteins, TRIM24 was identified and confirmed to be interacting with Dysbindin by experimental methods of co-immunoprecipitation and co-immunostaining. Another TRIM family protein, TRIM32, has earlier been reported as an E3 ubiquitin ligase for Dysbindin in skeletal muscle. Consistently, TRIM32 degraded Dysbindin in neonatal rat ventricular cardiomyocytes (NRVCMs) as well. Surprisingly, however, TRIM24 did not promote Dysbindin decay but rather protected Dysbindin against possible degradation by TRIM32. Correspondingly, TRIM32 attenuated the activation of SRF signaling and hypertrophy through Dysbindin decay, whereas TRIM24 promoted Dysbindin-induced hypertrophic effects in NRVCMs. Further experiments in this study also signify that TRIM32 is a key regulator of cell viability and apoptosis in cardiomyocytes via simultaneous activation of p53 and caspase-3/-7 and inhibition of X-linked inhibitor of apoptosis. In conclusion, we here provide a novel mechanism of post-translational regulation of Dysbindin and hypertrophy via TRIM24 and TRIM32 and show the importance of TRIM32 in cardiomyocyte apoptosis *in vitro*.

3 Zusammenfassung

Die Hauptkomponente von post-translationalen Modifikationen, die Ubiquitinierung durch das Ubiquitin-Proteasome-System (UPS), ist ein entscheidender zellulärer Prozess. Sie ist an verschiedenen Aufgaben beteiligt, beispielsweise dem gezielten Proteinabbau, der intrazellulären Signalkaskaden bei Apoptose sowie an der transkriptionellen Kontrolle. Wichtig dabei ist, dass es die Aggregation von nicht-funktionalen, falsch gefalteten und potentiell schädlichen Proteinen verhindert und somit die Proteinhomöostase unterstützt. Die Ubiquitinierung wird durch die gemeinsame Aktivität von drei enzymatischen Prozessen erreicht. Diese bestehen aus E1 (aktivierende Enzyme), E2 (konjungierende Enzyme), sowie E3 (Ligasen). Dabei gehören TRIM (tripartite motif) Proteine in Metazoen zu den wichtigsten Gruppen von E3-Ubiquitin-Ligasen, die essenzielle Signalwege modulieren. Aufgrund ihrer kardialen Funktion waren MuRFs (Ringfinger-Muskel-Proteine) lange Zeit die am meisten untersuchten TRIMs. Jüngste Forschungsergebnisse in diesem Bereich zeigen jedoch eine breitere und stets wachsende Palette an Funktionen von verschiedenen TRIM-E3-Ligasen in der (Patho-)Physiologie des Herzens. Für das mit Schizophrenie assoziierte Protein Dysbindin konnte unsere Gruppe zeigen, dass es die Hypertrophie in Kardiomyozyten durch das Aktivieren von Signalwegen via des Rho-abhängigen Serum-Response-Faktors (SRF) stark beeinflusst. Mit Hilfe des Hefe-Zwei-Hybrid-Systems wurde, unter der Verwendung einer cDNA-Datenbank aus dem humanen Herzen und Dysbindin als Köderprotein, unter mehreren Bindungsproteinen TRIM24 identifiziert. Zusätzlich wurde die Interaktion mit Dysbindin durch experimentelle Methoden wie Co-Immunpräzipitation und Co-Immunfärbung bestätigt. Ein weiteres Protein aus der TRIM-Familie, TRIM32, ist als E3 Ubiquitin Ligase für Dysbindin in der Skelettmuskulatur bekannt. Es wurde herausgefunden, dass TRIM32 in neonatalen ventrikulären Kardiomyozyten aus Ratten (NRVCMs) Dysbindin-Level ebenfalls abschwächt. Überraschenderweise unterstützte TRIM24 jedoch nicht den Abbau von Dysbindin, sondern schützte es vor einer Degradierung durch TRIM32. Entsprechend mildert TRIM32 die Aktivierung von SRF-Signalen und hypertrophe Effekte durch den Abbau von Dysbindin, wohingegen TRIM24 Dysbindin-induzierte hypertrophe Effekte in NRVCMs fördert. Weitere Experimente in dieser Studie zeigen auch, dass TRIM32 ein Schlüsselregulator für die Überlebensfähigkeit von Zellen ist und Apoptose in Kardiomyozyten über die simultane Aktivierung von p53 sowie Caspase-3/-7 und die Inhibierung von

X-verknüpften Inhibitoren der Apoptose (XIAP) induziert. Zusammenfassend wird hier ein neuer Mechanismus der post-translationalen Regulation von Dysbindin und kardialer Hypertrophie über TRIM24 und TRIM32 vorgestellt. Außerdem wird die Bedeutung von TRIM32 in Apoptose-Signalwegen in Kardiomyozyten *in vitro* dargelegt.

4 Introduction

4.1 Prelude

A collective highlight in research areas related to biomedical studies in the last decades directs to the increased toll of pathophysiology, instigating metabolic imbalance and piloting various organ related disorders and diseases, particularly like the heart diseases. Regardless of several years of cardiac research and circulatory understanding over the decades, cardiovascular diseases (CVDs) remain at the top of epidemic deaths in the modern world. With vastly changing lifestyles ensuing diminutive physical activity, addiction to drugs, tobacco & alcohol and detrimental dietary orientations, these numbers are on the constant rise. The death toll by CVDs is increasing particularly in developing countries with low and middle income, according to the World Health Organization, where CVDs are the primary causes of deaths, irrespective of gender. In 2015 alone, CVDs accounted for 17.7 million deaths globally, representing 31% of all deaths, with coronary heart disease and stroke contributing the biggest share with 14.1 million deaths (WHO-CVDs data) (Figure 1). Dietary malpractices leading to various metabolic disorders like obesity, diabetes, and high blood pressure sequentially result in numerous CVDs like cardiomyopathies, cardiac arrest, hypertension, cardiac valve calcification, and arrhythmias among others.

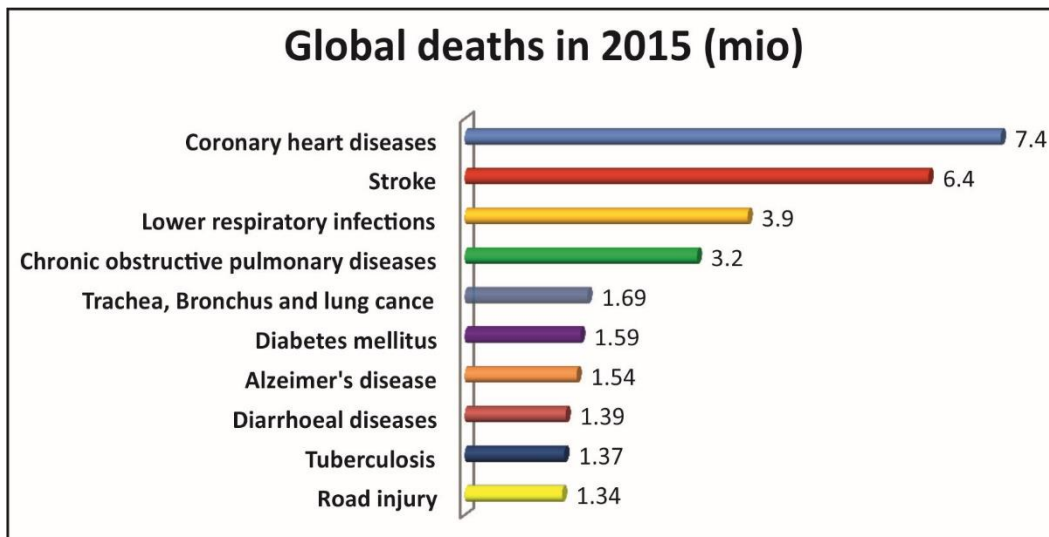


Figure 1: Worldwide causes of mortality in the year 2015. As per the World Health Organization mortality data, cardiovascular diseases are still the biggest reason for deaths globally with a share of 31% deaths.

Thus, these amplifying numbers of global deaths collectively craft a call for effective tools that can alleviate the burden of various CVDs, shaping the current stream of cardiovascular research into exemplified inter-systemic approaches aimed at generating therapeutic strategies.

4.2 Cardiomyopathies

Cardiomyopathy is a general terminology for dysfunctional heart muscle predominately culminating in cardiac-related disease conditions. Historically, definitions and classifications of cardiomyopathies or CMPs have been attempted by several physicians consistently with the occurrence of newer cases. Most prominently, CMPs were classified into three major groups by British physicians (Goodwin et al., 1961) depending on the clinical presentation of the disease, like congestive heart failure (often with atrioventricular valvular incompetence), constrictive cardiomyopathy and obstructive cardiomyopathy. Better research understanding, genetic studies, and diverse disease occurrence have led to establishing several newly adapted definitions of cardiovascular diseases.

The most noted one, accepted by the American Heart Association defines cardiac muscle diseases as, *“Cardiomyopathies are a heterogeneous group of diseases of the myocardium associated with mechanical and/or electrical dysfunction that usually (but not invariably) exhibit inappropriate ventricular hypertrophy or dilatation and are due to a variety of causes that frequently are genetic. Cardiomyopathies either are confined to the heart or are part of generalized systemic disorders, often leading to cardiovascular death or progressive heart failure-related disability”* (Maron et al., 2006).

However, the classification of CMPs has developed in a similar direction as suggested by Goodwin, with congestive (now being referred as dilated) cardiomyopathy (DCM), hypertrophic cardiomyopathy (HCM), and constrictive (now referred to as restrictive) cardiomyopathy (RCM). A fourth category, arrhythmogenic cardiomyopathy has been added recently. In further efforts to accommodate all varieties of CMPs, each of these categories has been subdivided by their pathogenesis, like a systemic disorder, an infection, inflammation, or an inherited disorder. In the absence of pathogenesis identification, CMPs are termed idiopathic cardiomyopathies in their respective category (Braunwald, 2017).

The most common indicators of several CMPs are increased heart weight to body weight ratio, reduction of ejection fraction, and an increased cardiomyocyte size, which together culminate into cardiac hypertrophy.

4.3 Cardiac hypertrophy

The innate reaction of the heart to increasing biomechanical stress dictates the development of cardiac hypertrophy with a set of pathological events. Elevated heart weight (with or without fluids) in the hypertrophic heart is referred to the enhanced mass of cardiomyocytes, which can be coupled together with various other parameters to interpret the tangible hypertrophic conditioning (Dorn et al., 2003). Initially, cardiac hypertrophy is a physiological reaction, similar to the heart-growth condition observed in athletes or pregnant women (Li et al., 2012). Here, adaptive hypertrophy inducing muscle growth is beneficial, helping to increase the blood pressure and volume ejection, overall favoring cardiac function. However, enduring pressure overload and subsequent biomechanical stress progressively turn this adaptive compensation into a maladaptive condition, severely affecting the mechanical properties of the heart. This maladaptive response is harmful and needs to be treated, in turn, to avoid heart tissue remodeling followed by myocardial infarction, chronic hypertension or other cardiovascular diseases (Pfeffer and Braunwald, 1990); (Zwadlo and Borlak, 2005); (Frantz et al., 2009).

To study the mechanistic features of cardiac hypertrophy, cell culture systems are widely used, allowing observation of the adverse effects that various proteins and signaling molecules impose on the disease outcomes, prior to the investigation in animal models and ultimately in humans. Increase in cell size, measured by the cell surface area is the primary indicator of hypertrophy in cultured cells. The increase in cell surface area is typically accompanied by the elevated expression of the hypertrophic fetal gene program, which is activated during development and stress, and encodes natriuretic peptides like *nppa* (atrial natriuretic peptide) and *nppb* (brain natriuretic peptide) (Sergeeva et al., 2016). Several other genetic factors and protein expression patterns can also be employed to investigate cardiac hypertrophy, possibly by tracing the symptoms of the hypertrophy induction.

4.3.1 Dysbindin is a potent inducer cardiac of hypertrophy

The genetic and mechanistic factors associated with the specific type of cardiac hypertrophy observed, provide valuable information about the involved proteins and signaling pathways. Cardiac hypertrophy is a complex process with the association of multiple signaling pathways that either alone or in tandem lead to the disease condition. Some of the major signaling pathways associated with cardiac hypertrophy are calcineurin-NFAT, PI3K/Akt/GSK-3, G-protein coupled receptors (GPCRs), MAPKs, and RhoA-SRF-mediated pathways (Molkentin et al., 1998); (Sotiropoulos et al., 1999); (Naga Prasad et al., 2000); (Frey and Olson, 2003). An intercalated disc protein, Myozap, was earlier reported to activate RhoA-SRF signaling (Seeger et al., 2010). A yeast-two-hybrid assay with Myozap as bait and human cardiac cDNA library as prey suggested Dysbindin as one of the potential interactors of Myozap (Rangrez et al., 2013).

The name Dysbindin was coined more than a decade ago for a protein found to interact with α/β -dystrobrevins (Benson et al., 2001). Now, this ubiquitously expressed Dysbindin is well known as a schizophrenia susceptibility protein with a central role in the brain. It works by facilitating neurite outgrowth by promoting the transcriptional activity of p53; whereas its deletion leads to the activation of NF κ B in the nucleus (Owen et al., 2004); (Arnold et al., 2005); (Fei et al., 2010); (Ma et al., 2011); (Fu et al., 2015). In other tissues such as kidney and liver, Dysbindin has been characterized as a vital component of the BLOC-1 complex (biogenesis of lysosome-related organelles complex-1), which is associated with intracellular trafficking and the biogenesis of specialized organelles of the endosomal-lysosomal system (Li et al., 2003); (Starcevic and Dell'Angelica, 2004); (Larimore et al., 2014). Most recently, Dysbindin has been endorsed with the regulation of lysosomal degradation of GPCRs, supporting the notion of a role in signaling (Roscioglione et al., 2014). Of note, Dysbindin has also been linked to other disorders such as limb-girdle muscular dystrophy, and its homozygous point mutation is linked to Hermansky-Pudlak syndrome (Li et al., 2003); (Wakayama et al., 2010); (Shieh et al., 2011).

After the discovery of its significant cardiac presence and the possibility of activating hypertrophic signaling through Myozap, Dysbindin was characterized in cardiac aspect. It was found to be a direct interaction partner of the small GTPase RhoA through which Myozap induces cardiac hypertrophy. This direct interaction with RhoA allows Dysbindin to strongly

activate SRF signaling in the neonatal cardiomyocytes. Moreover, Dysbindin also activated MEK1-ERK1 dependent MAPK signaling, in combination leading to the robust activation of cardiac hypertrophy, evidenced by activation of the fetal gene program and increased cardiomyocyte cell surface area (Rangrez et al., 2013).

4.3.2 TRIM24 and TRIM32 are potential cardiac interaction partners of Dysbindin

To dissect further players in Dysbindin-RhoA-SRF associated cardiomyocyte hypertrophy axis and cardiac Dysbindin interactome, a yeast two-hybrid screening was performed using Dysbindin as bait against a human cardiac cDNA library. Among several putative binding proteins, we identified tripartite motif-containing protein 24 (TRIM24) as a potential interaction partner of Dysbindin in the heart (Borlepawar et al., 2017).

TRIM24, in addition to signature RING-both B-boxes-coiled coil conserved structure at the N-terminal, has bromo and PHD domains at the C-terminal end. This transcriptional intermediary factor (TIF α) was well studied in the context of transcriptional activation of various nuclear receptors via activation function 2 (AF2), owing to its nuclear presence and its capacity to indulge with histones. TRIM24 interacts with coactivators GRIP1 and CARM1 by forming a stable ternary complex and further enhancing the AF2 of either one or both of them (Teyssier et al., 2006). TRIM24 was also found to be associated with the protector of genome stability, tumor protein 53 (p53, (Allton et al., 2009). It ubiquitinates p53 and thus prompts tumorous growth by affecting genomic stability, cell cycle arrest, and apoptosis. Through interaction with p53, TRIM24 plays a critical role in the progression of various carcinomas and gliomas, and differentially regulated in various cancers, for example breast cancer (Ma et al., 2016), gastric cancer (Fang et al., 2017), cervical cancer (Lin et al., 2017), and prostate cancer (Groner et al., 2016). With such credentials, TRIM24 has established itself as a novel marker in cancer-related studies and is targeted in regards to inhibiting tumor growth as a therapeutic strategy.

Another TRIM protein, TRIM32, has earlier been reported as an E3 ubiquitin ligase for Dysbindin in skeletal muscle. TRIM32 harbors tripartite motif at the N-terminus and a FIL domain with six NHL repeats at C-terminus. TRIM32 has been subject of various skeletal muscle dystrophy studies where two independent mutations in this gene were reported for various muscular

dystrophies like, Limb-girdle muscular dystrophy with mutation: 1459 G>A (D487N), Bardet-Biedl syndrome with mutation in B-box, sarcotubular myopathy, and dystrophic myopathy (Shieh et al., 2011). This ubiquitous protein has been reported to be associated with skeletal muscle thick filaments by binding myosin but targeting actin for degradation, upregulating skeletal muscle remodeling (Kudryashova et al., 2005). It has also been reported to bind with Dysbindin and PIASy, further ubiquitinating them for degradation via UPS and thus serving as a regulator of Dysbindin in skeletal muscle and PIASy in keratinocytes (Albor et al., 2006); (Locke et al., 2009). With available evidence of TRIM32-Dysbindin interaction in skeletal muscle, we hypothesized similar interaction between them in the heart.

As stated above, both TRIM24 and TRIM32 proteins are important members of the tripartite motif (TRIM) family and likely play an important role in ubiquitin-mediated protein degradation and thus protein homeostasis in the heart.

4.4 Proteostasis is essential for normal heart functioning

Proteins play a central role in maintaining steady cardiac function by participating in critical tasks for cardiac signaling and homeostasis. Total protein composition of the cell at any given time is coined as its proteome, and maintenance of protein homeostasis or proteostasis is the state of a cell when its proteome is in functional balance (Balch et al., 2008); (Korovila et al., 2017). Polypeptide chains undergo specific folding and modifications, termed post-translational modifications and are trafficked to the prerequisite cellular location. Misfolded proteins and non-useful native proteins undergo intracellular proteolysis, which in turn becomes a critical step for protein homeostasis; with any aberrations in proteolysis further ascending towards the disease conditions (Rodrigo-Brenni and Hegde, 2012). Various components of the proteostasis machinery mediate the functions of synthesis and disposal of native proteins along with detoxification by removal of damaged and misfolded proteins. Heat shock proteins (HSPs or chaperones), autophagy and the UPS are some of the most essential components of the proteostasis machinery (Korovila et al., 2017); (Borlepawar et al., 2018).

Cellular levels and functions of key proteins in the cardiomyocytes, like any other cells, are altered by various stress, stimuli, diseases, and age. Any changes in the intracellular environment can affect protein's synthesis-folding-degradation trio culminating into disturbed

protein pool and impaired proteostasis, and furthermore influencing organ functions. These alterations in protein quality control (PQC) subsequently reflect in the impairment of total proteome and compromise cellular functions ensuing senescence (Henning and Brundel, 2017). Aging of cells is linked with the accumulation of damaged and misfolded proteins after dented PQC machinery; accumulating oxidative stress proteins and in turn, affecting cell viability. Such protein misfolding has been reported to prevail in terminal neurodegeneration diseases like Alzheimer’s and Huntington’s (Gavilan et al., 2009), diabetes-type II (Sciarretta et al., 2015), cancers (Wallace, 2005) and cardiovascular diseases (Dai et al., 2012); (Ortega et al., 2014).

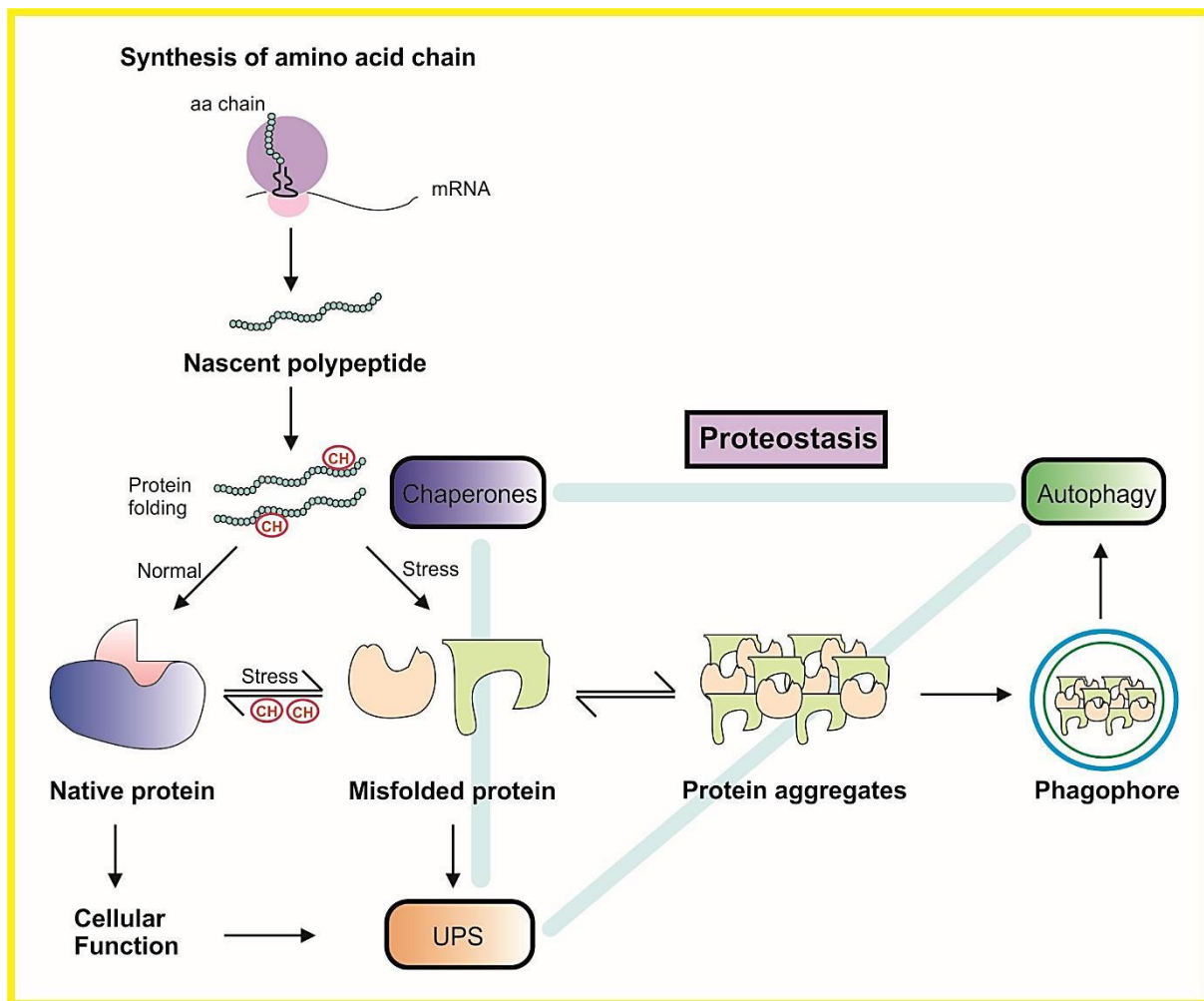


Figure 2: Major protein Homeostasis processes. Role of chaperones, autophagy and the ubiquitin-proteasome system (UPS), and their interactions with each other is presented diagrammatically. aa, amino acid; CH, chaperone; mRNA, messenger RNA. (Borlepawar et al., 2018, Copyright © Elsevier)

Metabolic pathways (like insulin/IGF-1 signaling), dietary restriction, and reduced mitochondrial function are capable of reducing cellular stress and thus have been implied to maintain the

lively proteome (Taylor and Dillin, 2011). Proteome imbalance is often linked with aging, which can result in altered stoichiometry causing proteostasis stress. However, protein aggregates comprising both misfolded proteins and hoisted levels of chaperones have been suggested to augment proper PQC response, enabling isolation of potentially harmful protein oligomers and thus can be prospective protective strategy against cell death (Walther et al., 2015). This, in turn, suggests that a healthy proteome can be maintained by both presences of upregulated proteostasis machinery induced by some protein misfolding and reduced stress, constantly upholding a youthful proteome.

4.5 Components of the cellular proteostasis machinery

4.5.1 Component 1: Heat shock proteins

HSPs, also known as chaperones (for some members), are highly conserved stress proteins that were first detected to cope with thermal stress (Ritossa, 1962), resulting in a serendipitous nomenclature. They are present in all cell types with roles in the protein folding-transport apparatus, cell cycle, cellular protection from stress and apoptosis, and antigen presentation to the major histocompatibility complexes. HSPs represent a large family of proteins that were often classified based on their molecular weight (Li and Srivastava, 2004). With increasing members, many inconsistencies had risen in their nomenclature. To avoid these discrepancies Kampinga (2009) have proposed new guidelines for classification emulating their HUGO nomenclature system (Kampinga et al., 2009). HSPs are now categorized into HSPA (HSP70, 13 members), HSPH (HSP110, 4 members), DnaJ (HSP40, 49 members), HSPB (small HSPs, 11 members), HSPC (HSP90, 5 members), and Chaperonins and related proteins (14 members).

Cells constantly undergo challenging conditions responsible for acute and chronic stress. Transcriptional activation with preferential translation is the instinctive way to achieve upregulation of specific proteins. Diverse environmental and biological stressors like infection, disease, UV-light, inflammation, toxins, exercise, starvation, hypoxia, N₂-deficiency, water deprivation, etc. induce production of HSPs; making them universal stress reaction proteins (Santoro, 2000). Heat shock factors (HSF1, HSF2, HSF3, and HSF4) regulate the synthesis of HSPs throughout growth and adaptation. Although, they are not sole factors responsible for

upregulation of *HSP* transcription as similar upregulation happens during cell cycle progression and primitive proliferation (Gomez-Pastor et al., 2018). In unstressed cells, HSF through its interactions with hsp70 is maintained in a monomeric form. Upon introduction of stress, HSF assembles into a trimer via binding through specific sequence elements in heat shock gene promoters and gets phosphorylated. Phosphorylation induces transcriptional activation of the heat shock genes by increasing levels of hsp70 with the escalated formation of an HSF-hsp70 inactive complex. Finally, HSF dissociates from DNA and is eventually converted to non-DNA-binding monomers (Morimoto, 1993).

Post-synthesis, nascent proteins are stabilized and folded accordingly to enact function in their active conformation and then transported to cellular compartments for their purpose through interaction or binding with others (Yahara, 1996). Furthermore, chaperones bind to active proteins reducing their mutual interaction and thus preventing them from the aggregate formation. *hsp60*, *hsp70*, and *hsp90* are involved in ATP-dependent folding and refolding, singularly or by even forming multicomponent complexes of *de novo* proteins. In brief, HSP70 folds budding polypeptides and releases them in the cytoplasm after HSP90 mediated conformational changes, where HSP60 supports in final folding of proteins. This folding apparatus is further assisted by the small HSPs, which function as ‘holdases’ involving binding of unfolded proteins and assisting its delivery to the ‘foldases’ (Henning and Brundel, 2017).

4.5.2 HSPs in cardioprotection

Cardiomyocytes express relatively high levels of HSPs; specifically members of HSPBs. Myocardial ischemia originating from rupture of an unstable plaque or congestive heart failure involves upregulation of some of HSPs. These include HSPB1 (HSP27), HSPB5 (α -crystallin B chain), HSPB6 (HSP20), HSPB7 (cardiovascular HSP), and HSPB8 (HSP22), which protect cardiomyocytes from proteotoxicity by stabilizing the contractile apparatus (Benjamin and McMillan, 1998). Small HSPs like α B-crystallin, MKBP, Hsp25, Hsp20, and cvHsp were found to translocate from the cytoplasm to myofibrils after cardiac ischemia (Golenhofen et al., 2004).

When hsp70 was overexpressed in stably transfected embryonal rat heart-derived H9c2 (2-1) cells, they displayed more resistance to ischemia-like stress (Mestril et al., 1994) and improved

recovery after heat-shock pretreatment before the prolonged ischemia-reperfusion (IR) (Hutter et al., 1994), indicating protective role. Free radical scavengers import oxidative stress after ischemic injuries and increased ROS ameliorates ventricular dysfunction, arrhythmias, and progressive cell damage. Catalases like superoxide dismutase and glutathione peroxidase are established to be protective against such oxidative stress. Many HSPs are speculated to act as chelators, cooperating in a synergistic way with the catalases for cardioprotection (Mocanu et al., 1993). For example, HO-1 (hsp32) was found to be upregulated in hypertensive rat aortas by mechanisms unique to AngII introduction and inhibited vasodilation of vascular SMCs after hemodynamic stress (Ishizaka et al., 1997). Hsp27 gets phosphorylated after physical stimuli like perfusion in IR rats and play a vital role in actin filament dynamics through p38-MAPKs and ERKs signaling (Bogoyevitch et al., 1996).

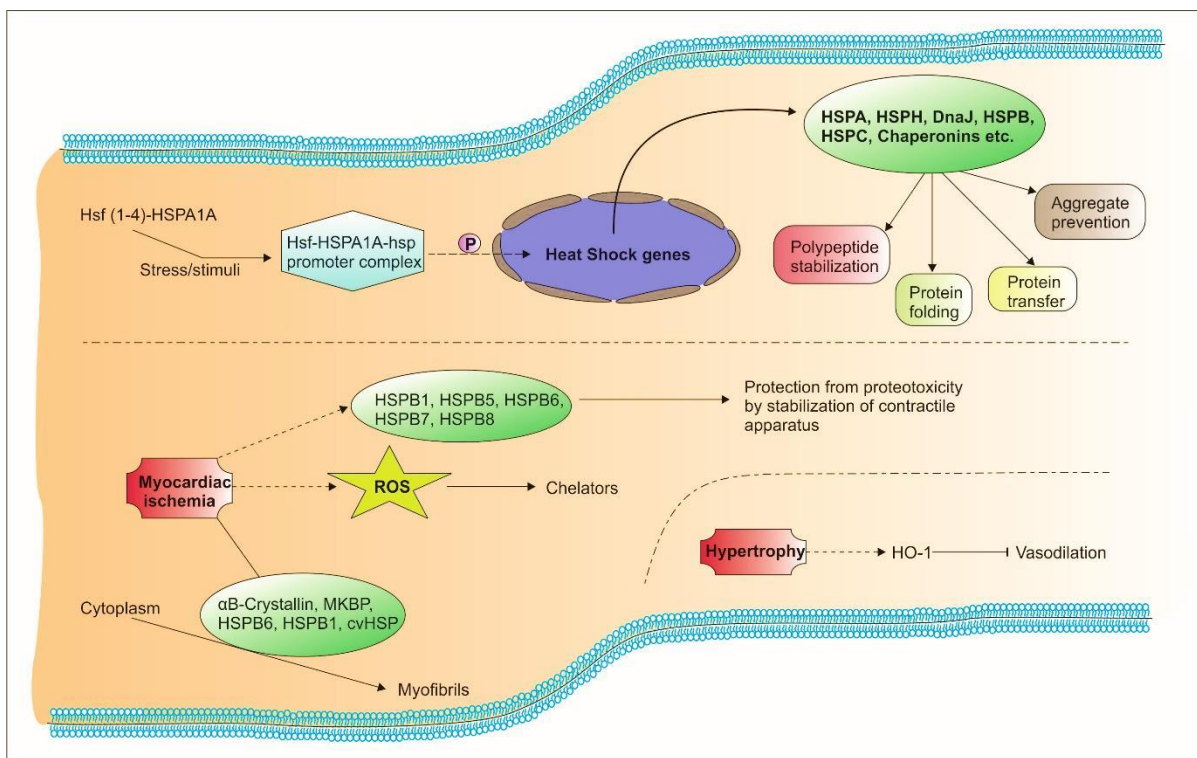


Figure 3: Heat shock proteins and their functions in the heart.

Another interesting member of chaperones is striated muscle-specific hsp22 or α B crystallin. The 20kD protein localizes to the Z-band, specifically with desmin filaments in cardiomyocytes. It was reported to bind to actin filaments after heat shock, preventing them from aggregate formation, thus playing a cardioprotective role in stress conditions (Bennardini et al., 1992). A

R120G mutation in α B crystallin causes aberrant desmin and α B crystallin aggregation in mice hearts inducing severe desminopathy (Wang et al., 2001); (Sanbe et al., 2004). It was also found to reduce elevated stiffness in failing human myocardium by relieving titin aggregation (Franssen et al., 2017).

With roles from ubiquitous hsp70 and hsp90 to striated muscle-specific α B crystallin, HSPs play vital roles in cardioprotection by maintaining a healthy proteome regardless of various ischemic injuries, oxidative stresses, aggregate formations, arrhythmias, atrial fibrillation, and CMPs.

4.5.3 Component 2: Autophagy

Cellular life is under constant change with elements being recycled and reconstructed. The recycled elements are then used as building blocks for the generation of new. Eukaryotic cells carry out recycling via two major degradation systems: lysosomal and proteasomal. While the proteasomal system remains energy dependent and highly specific; lysosomes provide an all-inclusive approach, even capable of degrading cytoplasmic components and cellular organelles. Autophagy is thus, a fundamental, essential and cell regulated degradative-mechanism that eliminates dysfunctional components with the help of degradative enzymes known as lysozymes (Mizushima and Komatsu, 2011). The word 'autophagy' was invented by Christian de Duve, whose pioneering experiments also provided biochemical proof of the lysosomal involvement in autophagy (Klionsky, 2008). After its description in the 1960s, autophagy had been a neglected subject; until the discovery of *atg*, autophagy-related genes in *S. cerevisiae* boosting collective interest in autophagy, making it one of the most studied mechanisms in later decades, which culminated in Nobel Prize for physiology in 2016 to Yoshinori Ohsumi (Brokstad, 2016).

The process of vacuolar proteolysis was explained after starvation initiated the formation of spherical bodies in vacuoles, having thinner membranes than cell organelles in *S. cerevisiae*. Isolation of these spherical bodies displayed the existence of cytosolic components like ribosomes, mitochondria, and lipid & glycogen granules. These 400-900 nm diameter spheres were named 'autophagic bodies' and considered as an intermediate step before the autophagic process (Takeshige et al., 1992). Autophagic bodies undergo fusion with vesicles containing

lysozymes and carry out the destruction of cellular material. Autophagy is responsible for the significant turnover of proteins in a nonselective manner, resulting in pronounced protein degradation at a rate of 3-4 % of the total cellular proteins per hour (Kopitz et al., 1990).

This adaptive cell survival response is conducted in three different ways. One is macroautophagy, enclosing a substantial segment of cytoplasm including organelles by an isolating membrane to form an autophagosome. The outer membrane of the autophagosome blends with the lysosome and internal material is then degraded by this autolysosome. Macroautophagy that is responsible for the degradation of mitochondria is called mitophagy and is in fact controlled by the E3 ubiquitin ligase Parkin through the Sirtuin3-Foxo3A-Parkin complex in cardiomyocytes (Yu et al., 2017). A second mechanism is a microautophagy, engulfing smaller pieces of the cytoplasm by the development of the lysosomal membrane around them. And the third mechanism is chaperone-mediated autophagy, specific for certain protein degradation, translocating substrate proteins containing a KFERQ-like pentapeptide sequence to the lysosomal lumen after binding via Lamp-2A (Mizushima and Komatsu, 2011).

4.5.4 Autophagy in the heart

Autophagy controls vital physiological functions mediating degradation and recycling of cellular components. It is also necessary for providing energy and building blocks for the formation of new cellular components, eliminating invaders like bacteria & viruses after infection, elimination of damaged proteins & organelles, PQC in aging, etc. and thus, is an essential mechanism in combating against various stresses. Aberration of autophagy has been linked to various diseases like Parkinson's disease, Diabetes mellitus, cancer, and cardiovascular diseases (Brokstad, 2016). Thus, currently, autophagy remains one of the vital targets for therapeutic actions against cardiovascular diseases that result from the accumulation of needless components.

In cardiac *Atg5* deficient mice, the cardiac function remained normal up to 12 weeks; however, chronic loss of autophagy resulted in death after 6 months of age due to increased left ventricular dimensions and decreased fractional shortening. Moreover, disturbed sarcomeric structures and collapsed mitochondria supplemented age-related cardiomyopathy, suggesting a cardioprotective role of constitutive autophagy in the heart (Taneike et al., 2010). Histone

deacetylases (HDACs) regulate cardiac plasticity and HDAC inhibitors (HDACi) are suggested to control PE-hypertrophy and autophagy. Knockdown of autophagy effectors Atg5 and Beclin1 have similar effects, showing HDACs to be autophagy essentials. When HDACi were subjected to pre-hypertrophy mice, near normal cardiac function was maintained, implicating autophagy to be an obligatory process in pathological cardiac remodeling where HDACs are essential autophagy effectors (Cao et al., 2011). With the help of autophagy-reporter mice, pressure overload was found to impart autophagy along with hypertrophy, after 48 h of TAC and both remained elevated for 3 weeks. Deletion of Beclin1, which is necessary for early autophagosome formation, lowered autophagy and hampered cardiac remodeling after TAC; while its overexpression had completely opposite effects. These findings suggest increased autophagy under hemodynamic stress to be maladaptive (Zhu et al., 2007); with constitutive autophagy in the non-failing heart being an intrinsic mechanism for maintaining overall cardiac structure (Nakai et al., 2007). Interestingly, Atg13- and FIP200-knockout mice died embryonically because of growth retardation and myocardial growth defects; indicating that these proteins are essential for both autophagy and cardiac development in mice (Kaizuka and Mizushima, 2016).

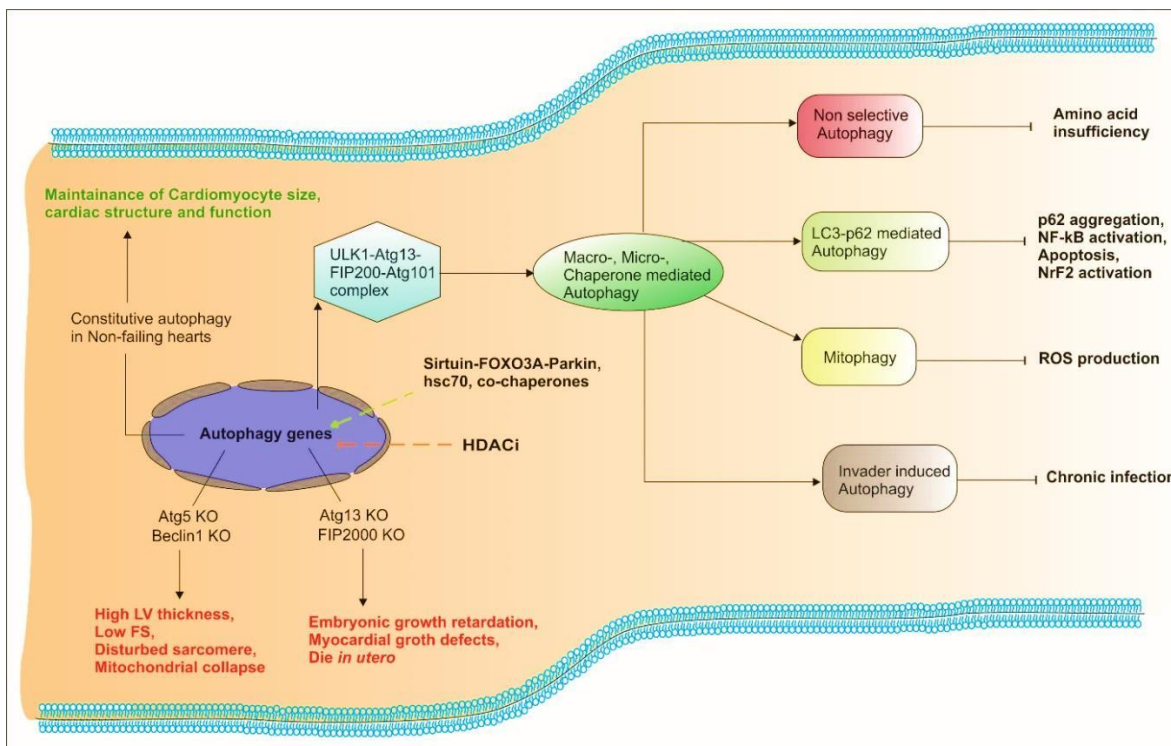


Figure 4: Autophagy in the heart.

4.5.5 Component 3: Ubiquitin-Proteasome system (UPS)

UPS is the next vital cog in the process of proteostasis, operating through degradation of proteins in a selective manner via the proteasome. A handful of non-specific E1 and E2s, as well as numerous substrate specific E3 proteins, work in tandem to activate, conjugate and ligate ubiquitin to target proteins, facilitating their degradation by proteasomes (Figure 5). Following intensified research in targeted protein degradation during the late 1970s and 1980s, a landmark paper on 'The Ubiquitin System' (Hershko and Ciechanover, 1982) gave exciting insights into this vital protein degradation mechanisms in eukaryotes. From the presence of proteolysis pathways like lysosomal degradation, the role of ubiquitin-mediated degradation was found to be separate, specifically controlling the new energy-dependent mechanism resulting in targeted protein degradation. With time, UPS also has now been found to be essential for numerous processes like cell-cycle progression, signal transduction, transcriptional regulation, receptor down-regulation, endocytosis, immune response, development, and programmed cell death. Ciechanover, Hershko and Rose were awarded the Nobel Prize in Chemistry in 2004 for 'the discovery of ubiquitin-mediated protein degradation'.

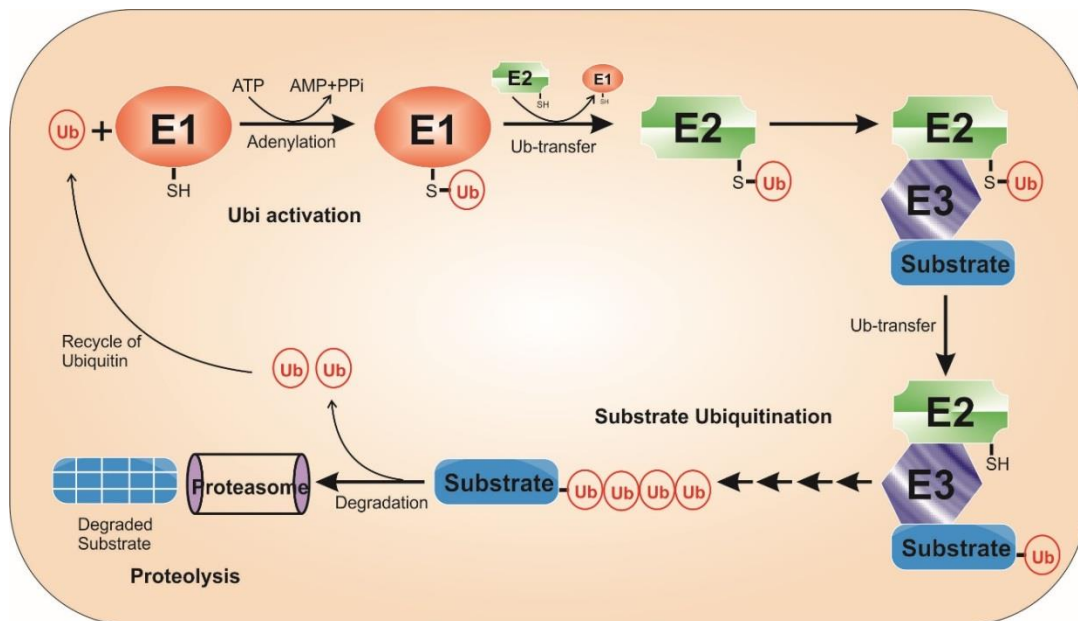


Figure 5: The process of Ubiquitination. It is accomplished by the concerted action of three enzymatic steps involving E1 activating, E2 conjugating enzymes, and E3 ligases. (Borlepawar et al., 2018, Copyright © Elsevier)

The key enzymatic steps in the ubiquitin proteolytic pathway include ATP-dependent activation of ubiquitin with the formation of a high-energy thiol ester bond with enzyme E1; transfer of

this activated ubiquitin to enzyme E2 and finally the binding of enzyme E2 to an already formed 'substrate protein-specific enzyme E3' complex. Covalent ligation of ubiquitin to its substrate via lysine-48 (K-48) residue is followed by the formation of a poly-ubiquitin chain leading to ATP-dependent degradation of the protein into smaller peptides by 26S proteasome complex (Figure 5), where free ubiquitin residues are made available by de-ubiquitinating enzymes for reuse (Hershko, 1996); (Su and Wang, 2010). However, K-48 mediated ubiquitin tagging is not the sole possible way leading to proteolysis. Ubiquitin contains in total of seven lysine residues and all of them are reported to be able to bind target proteins. M-1 and K-6 ligations also result in protein degradation in the non-canonical way. Branched poly-ubiquitin chains linked via K-11 have been found to enhance substrate recognition resulting in amplified proteolysis of cell cycle regulators after eukaryotic cell division; while K-27, K-29, and K-33 branched chains have been found to delay proteolysis (Meyer and Rape, 2014), suggesting a behavior-driven development. Poly-ubiquitin chains linked via K-63 play a central role in various cellular processes like signal transduction, endocytosis, kinase activation, and DNA damage control, *etc.* presenting a multifocal scenario of ubiquitination. Furthermore, mono-ubiquitination and multi-ubiquitination have been reported to be responsible for DNA repair and altered subcellular distribution of substrate proteins respectively (Sadowski and Sarcevic, 2010).

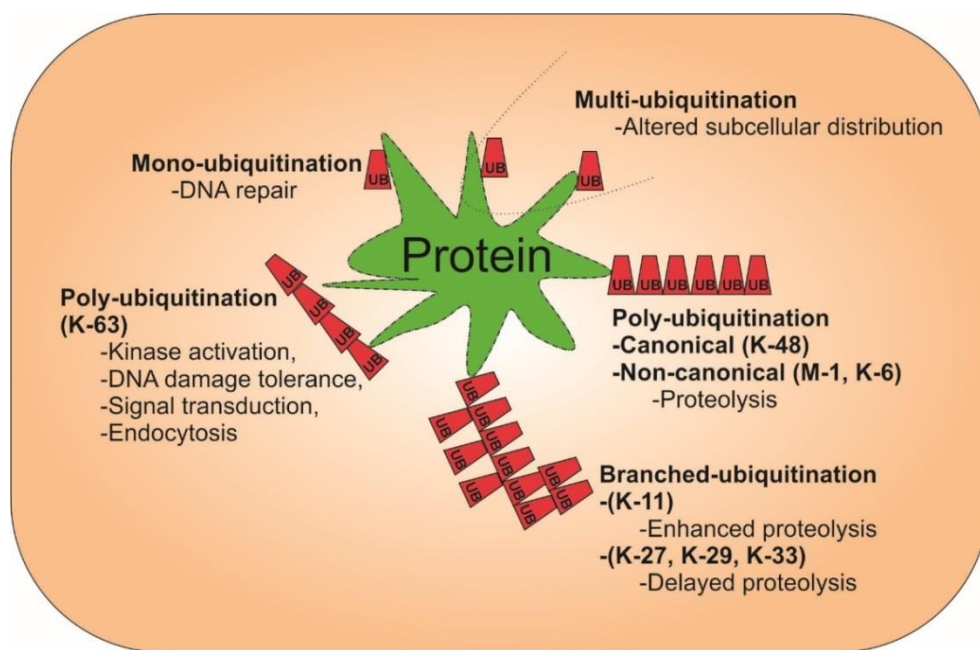


Figure 6: Fate of ubiquitinated proteins.

4.5.6 E3 ligases provide substrate recognition specificity

Targeted protein degradation by UPS has been established as a principal mechanism by which cells regulate protein levels and functions. The diversity of ubiquitin binding and substrate specificity is achieved by the existence of ~600 E3 ubiquitin ligases that catalyze the final step of ubiquitination, compared with only one E1 and very few E2 enzymes in mammals (Mearini et al., 2008). Based on their structural properties and domain structure, E3 ubiquitin ligases are classified as RING (Really Interesting New Gene), HECT (homologous to E6AP C- terminus) and RBR (RING-between-RING) ligases (Morreale and Walden, 2016). HECT and RBR E3 ligases carry a catalytic Cys that accepts ubiquitin from the E2-ubiquitin complex to form an E3-ubiquitin thioester intermediate, which subsequently transfers this ubiquitin to the substrate. In contrast, RING E3 ligases, which constitute the most abundant ubiquitin ligases, catalyze the direct transfer of ubiquitin from the E2-ubiquitin complex to the substrate (Buetow and Huang, 2016). Given the crucial role UPS plays in cardiac homeostasis, it is not surprising that several E3 enzymes have been implicated in various processes and pathologies like heart development, signaling cascades, ion channel regulation, autophagy regulation, protein degradation, congenital heart diseases and cardiomyopathies (Zolk et al., 2006); (Willis et al., 2014a).

4.5.7 E3 ubiquitin ligases in the heart

In higher eukaryotes, UPS mechanism revolves around the specific covalent binding of ubiquitin to label target proteins for proteolysis (Freemont, 2000). Many proteins have emerged to be playing this particular role and are known as E3 ubiquitin ligases. The UPS system is very essential in cardiac aspect, where cells undergo constant aging without duplication and thus have increasing stress of maintaining a healthy proteome. Various E3 ligases have been reported to play vital roles in cardiac processes like heart development, signaling cascades, ion channel regulation, autophagy regulation, protein degradation, cardiovascular disease progression, congenital heart diseases, cardiomyopathies, *etc.* Through intensive data mining and literature search in PubMed, several E3 ligases were identified with an assigned cardiac function. The majority of these E3 ligases belong to either single- or multi-subunit RING-type E3 ligases. In appendix 1, these sixty E3 ligases are summarized including their proposed function, protein targets, affected biomolecules and pathways, and the respective literature.

A major class of E3 ubiquitin ligase proteins, Tripartite motif family (TRIM), containing a highly conserved tripartite motif has been reported recently in various publications with vital roles in cardioprotection in cardiomyopathies.

4.6 TRIM E3 ubiquitin ligases

The tripartite motif family is a famed metazoan subfamily of E3 ubiquitin ligases, containing RING finger-B-Box-Coiled-coil domains at the N-terminus. These three motifs are highly conserved in a sequential manner, throughout all cell types. The remaining sequences, however, have evolved to acquire possible organ-specific physiological functions. The RING domain is one of the most prominent domains bestowing property of covalently tagging ubiquitin to specific proteins; as all of the TRIMs contain RING domain, they participate in ubiquitin ligation. The coiled-coil domain allows TRIMs to establish an interaction with the target protein, facilitating the transfer of the ubiquitin moiety.

In *Homo sapiens*, KEGG database classifies TRIM proteins into the Single Ring-Finger type E3 proteins class. With the idea of similar structures performing similar functions at the biochemical level, the width of the TRIM family grew significantly along with an exploration of the human genome (Short and Cox, 2006). This superfamily now containing more than 65 members is studied significantly for its multifocal functions in diverse tissues and species. The classification of TRIM proteins into eleven different subclasses depend mostly on the type of domains present at their C-terminus (Ozato et al., 2008). Beyond conserved N-terminal domains mediating interaction and ubiquitin ligation roles; it is the C-terminus domains that provide specificity of differential functions. Subclass IV forms almost two-third of TRIM/RBCC family possessing RFP- like B30.2 (PRY and SPRY) domains at the C-terminus in vertebrates. As in humans, in fishes also the B30.2 containing subclass is most prominent, although other human TRIMs have limited orthologs (Boudinot et al., 2011). In invertebrates, however, the total TRIMs number goes down to almost twenty members (Meroni and Diez-Roux, 2005).

Class	N-terminal domains	C-terminal domains	TRIM proteins
C-I			TRIM1, TRIM9, TRIM18, TRIM36, TRIM46, TRIM67
C-II			TRIM54, TRIM55, TRIM63
C-III			TRIM42
C-IV			TRIM4, TRIM5, TRIM6, TRIM7, TRIM10, TRIM11, TRIM15, TRIM17, TRIM21, TRIM22, TRIM25, TRIM26, TRIM27, TRIM34, TRIM35, TRIM38, TRIM39, TRIM41, TRIM43, TRIM43B, TRIM47, TRIM48, TRIM49, TRIM50, TRIM58, TRIM60, TRIM62, TRIM64, TRIM65, TRIM68, TRIM69, TRIM72, TRIM75
C-V			TRIM8, TRIM19, TRIM31, TRIM40, TRIM52, TRIM56, TRIM61, TRIM73, TRIM75
C-VI			TRIM24, TRIM28, TRIM33
C-VII			TRIM2, TRIM3, TRIM32, TRIM71
C-VIII			TRIM37
C-IX			TRIM23
C-X			TRIM45
C-XI			TRIM13, TRIM59
			TRIM-like proteins
1			TRIM51, TRIM77
2			TRIML1
3			TRIM14, TRIM16
4			TRIM29, TRIM44
5			TRIM66
6			TRIM16L (TRIM70)

Figure 7: Classification of Tripartite motif family proteins into 11 subclasses. The classification mainly depends on the C-terminal domain structure. (Borlepawar et al., 2018, Copyright © Elsevier)

4.6.1 N-terminal invariable domains in TRIM24 and TRIM32

Identification of protein domains plays a crucial role in recognizing the function and localization of a particular protein. As per titular implication, TRIM/RBCC family contains the rigidly conserved tripartite motif, namely: a RING domain, one or two B-box domains (BB1, BB2) and a coiled-coil (CC) region. The Cys and His residues responsible for RING and B-box domain patterns are also highly conserved along with β -sheets of the CC domain, suggesting conservation of domain sequence. The ability of the RING domain to carry conjugation of ubiquitin, SUMO or IFN-stimulated protein of 15 kDa (ISG15) to the target proteins provides a multifocal activity to TRIMs. B-boxes are bona fide domains for TRIM family members, while CC domains allow TRIMs to interact with target proteins, as well as to homo-dimerize resulting in protein-super complexes occupying various cell compartments (Reymond et al., 2001).

The RING finger is a zinc-binding domain that characteristically provides the ubiquitin ligation property. It was firstly identified in 1991 as the protein product of the gene RING1 (Really

Interesting New Gene 1) (Freemont et al., 1991) and was named A-box domain. The 40-60 residues long domain binds two zinc ions in a unique "cross-brace" arrangement through a defined motif of Cys and His residues. This arrangement provides the RING domain with a globular conformation, where an alpha-helix is positioned centrally to loops of variable lengths, which are separated by various small beta-strands forming finger-like protrusions (Chasapis and Spyroulias, 2009). This domain is typically present after the first 10-20 amino acids in TRIM proteins. (Borden and Freemont, 1996). Although the domain was identified in very few functionally distinct proteins, the number of such proteins has grown enormously, and now Hugo Gene Nomenclature Committee (HGNC) identifies ~ 275 proteins with a Ring finger.

B-boxes are another kind of zinc finger domains with ~40 residues in length that strictly succeed RING finger domains in the tripartite motif. They are divided into two groups B-box 1 (BB1) and B-box 2 (BB2), containing similar pattern but different consensus sequences of cysteine and histidine residues (Lovering et al., 1993). Both B-boxes have a ternary structure to similar RING domains, suggesting a common ancestry. Several TRIMs possess both BB1 and BB2, implying some level of cooperativity, with BB1 always preceding in case of mutual presence. They are found in over 1500 proteins in a variety of organisms. All human TRIMs certainly possess a BB2 domain, while BB1 shows sporadic presence among TRIMs. B-boxes are famous for their role in innate immunity against various genetic disorders with Mendelian inheritance and HIV. The BB2 domain in TRIM5 α has been shown to influence C-terminal PRY-SPRY domains to recognize HIV capsid (Li et al., 2007), and in TRIM15 to mediate HIV restriction (Brass et al., 2008). Moreover, mutations in B-box of TRIM18 cause Opitz G/BBB syndrome (Ferrentino et al., 2007), suggesting a multifocal role of B-boxes and asserting TRIMs with functional importance.

In 1953 Pauling and Corey, and Crick separately described the CC domain in a large class of fibrous proteins like keratin, myosin, and fibrinogen. The 100 residues long region is usually fragmented in many separate CC-motifs (Torok and Etkin, 2001). The name coiled-coil originates from its structure, as it is a bundle of α -helices that are wound into a superhelix by knobs-into-holes packing. They have variable sequences in many TRIMs but have strictly conserved hydrophobic areas that are responsible for the knob-in-hole structure with a characteristic repetitive pattern of seven hydrophobic and hydrophilic residues, called heptad

repeats. The CC domains are responsible for mediating homomeric or heteromeric interactions. Various TRIMs e.g. TRIM6, 8, 11, 18, 19, 23, 27, 28, 30, *etc.* have been reported to form high molecular weight complexes through homomeric interactions (Reymond and Brent, 1995) defining specific subcellular structures (Reymond et al., 2001). Many of these subcellular structures play central roles in cellular defense, for example, TRIM19s that are assigned to the nucleus to induce antiviral defense (Everett and Chelbi-Alix, 2007) and trimerization of TRIM5 α is vital for the restriction against viral infection (Javanbakht et al., 2005).

4.6.2 C-terminal variable domains occurring in TRIM24/32

When the invariable presence of tripartite motif at one end imparts interaction and presents ubiquitin to target proteins, the other end is responsible for variable physiological properties. A diverse range of C-terminal domains has prompted the TRIMs classification in various subclasses over the years (Short and Cox, 2006); (Ozato et al., 2008). The prominent domains are COS, FN3, PRY & SPRY, PHD, BR, FIL, NHL, MATH, ARF, TM *etc.* among others. Presence of these domains in solo or in combination has resulted in 11 subclasses, dividing TRIMs by their functional properties (Figure 7) (Ozato et al., 2008); (Borlepawar et al., 2018).

Association of the two domains; PHD (50-80 residues) and Bromo (110 residues) is specific for TRIM24, TRIM28 and TRIM33 belonging to class VI of TRIM family. They are widely known as transcriptional intermediary factors (TIF) α , β , and γ respectively. The PHD was first reported in *A. thaliana* and found to have structural similarity with other zinc fingers such as RING finger (Schindler et al., 1993). It is one of the vital domains responsible for DNA binding via interaction with chromatin (Histone H3) and mediates transcriptional regulation of various genes by virtue of its nuclear presence (Aasland et al., 1995). Haynes (1992) first reported sequence motif called bromodomain in human, *Drosophila*, and yeast (Haynes et al., 1992). Its secondary structure revealed to have two amphipathic α -helices with reverse turns, suggesting their role in intra- and inter-molecular interaction. In TRIM24 they occur as a single copy per protein and along with PHD domain mediate transcriptional repression by recognizing acetylated lysine residues present on N-terminal tails of histones (Ozato et al., 2008). Through their ability to bind DNA, they also act as transcriptional activators via activation function 2 (AF2) (Teyssier et al., 2006).

FIL domains appear in association with NHL repeats in subclass VII of TRIMs comprising of cytoskeletal TRIMs 2, 3, 2, and 71, but singularly in TRIM45. These domains of ~100 residues tandem repeats are rich in Gly and Pro and form a rod-like structure in the actin-binding cytoskeleton protein Filamin. They are speculated to be involved in homo-dimerization and crosslinking between TRIMs and cytoskeletal proteins through actin binding globular domains (Fucini et al., 1997). NHL repeats (~40 residues) are named after Ncl-1, HT2A (human proteins that bind to HIV Tat), and Lin-41 (a translational regulator in *C. elegans*) in which it was first identified. They are widely believed to be involved in various protein-protein interactions because of their structural similarity to WD repeats (Slack and Ruvkun, 1998). Subclass VIII of human TRIMs possesses this abundant pro- and eu-karyotic domain. The sequence repeats (2-6) that comprise NHL domains lead to β -propeller-like structures connected by loops. The deletion of the NHL domain in brain tumor protein (brat) has been shown to cause excessive growth of larval tissue in *Drosophila*, causing neoplasm in the larval brain (Arama et al., 2000).

4.6.3 Roles of TRIM family in cardiac proteostasis

Cardiomyocytes barely undergo cellular differentiation and thus there is constant need to maintain their cellular integrity throughout the lifespan. Proteostasis machinery plays a central role in discarding non-essential and harmful components through targeted proteolysis. With HSPs and autophagy being more constructive and destructive respectively, UPS is essential in nurturing youthful proteome by degrading proteins after their native function. With more than 70 members present in *Homo sapiens*, not many TRIM proteins have been studied in a cardiac perspective. But with increasing scientific input, some TRIMs have been established as essential players in cardiac function and diseases, e.g. muscle Ring Fingers (MuRFs TRIM63, TRIM55, and TRIM54), TRIM8, and TRIM72, which are discussed in detail below.

4.6.3.1 Muscle Ring Fingers (MuRFs)

MuRFs, namely MuRF1 (TRIM63), MuRF2 (TRIM55) and MuRF3 (TRIM54) are members of class II TRIM proteins (Figure 7). They characteristically lack B-box 1 and have COS domain at the C-terminus. MuRF2 is expressed at the early onset of mouse cardiac differentiation, specifically at embryonic day 8.5, emerging as a sensitive marker for differentiating myocardium. In

contrast, MuRF1 displays strong upregulation postnatally, whereas MuRF3 is expressed only after birth (Perera et al., 2011).

MuRF1 has been shown to mediate skeletal muscle atrophy along with MAFbx, where mice deficient in either of them were resistant to muscle atrophy (Bodine et al., 2001). In cardiac atrophy, MuRF1 $-/-$ mice were found challenging to return to baseline (70% less than WT mice) after the release of TAC (Willis et al., 2009a). Adult MuRF1-tg mice contain thinner LV walls with worsened cardiac functioning, leading to heart failure upon TAC (Willis et al., 2009b). MuRF1 also regulates cardiac ROS production in mitochondria, contemplating a further cardioprotective role in IR injuries (Mattox et al., 2014). The degradation of MHC β /slow and MHCIIa by MuRF1 and MuRF3 via UPS is an essential function to avoid muscle myopathy and hypertrophic cardiomyopathy, as evidenced in MuRF1 $-/-$ and MuRF3 $-/-$ mice, which developed an elevation of sub-sarcolemmal MHC accumulation and myofiber fragmentation (Fielitz et al., 2007a).

In younger HCM patients, MuRF1 and MuRF2 were found to have rare variants leading to higher penetrance and more severe clinical manifestation of cardiomyopathy (Su et al., 2014). MuRF1 and MuRF2, the closely related proteins are known to heterodimerize with each other, thus, displaying a high degree of functional redundancy; while the absence of both the proteins resulted in abrupt cardiac development with massive spontaneous hypertrophic cardiomyopathy and heart failure. MuRF1 alone has been reported to regulate pathologic cardiac hypertrophy (Willis et al., 2014b). Study with labeling MuRF2 in microtubules of cardiac sarcomeres have demonstrated its vital contribution as a transient adaptor between microtubules, titin, and nascent myosin filaments, suggesting that it is playing a key role in sarcomere to nucleus signaling (Pizon et al., 2002).

MuRF2 and MuRF3 also share considerable functional redundancy for binding to microtubules and lead the sarcomere formation in striated muscles. The double knockout mouse resulted in protein aggregate myopathy in striated muscles with decreased systolic and diastolic functions and increased MHC β /slow, affecting calcium handling in sarcomere (Lodka et al., 2016). In another instance, MuRF2 $-/-$ and MuRF3 $-/-$ mice were subjected to 60% fat diet for 26 weeks, where both MuRF2 (He et al., 2015) and MuRF3 (Quintana et al., 2015) knockout mice

demonstrated exaggerated diabetic cardiomyopathy and enhanced activation of peroxisome proliferator activating receptors (PPAR) transcription factors, suggesting a role in resistance against the development of diabetic cardiomyopathy. MuRF3 interacts with FHL2 and γ -filamin proteins leading to their degradation via UPS, which was confirmed after abnormal aggregation of these proteins in mice lacking MuRF3. Additionally, MuRF3^{-/-} mice display normal cardiac function but are more prone to cardiac rupture after acute myocardial infarction (AMI) (Fielitz et al., 2007b). Recently, a clinical study aimed to identify cardiac specific E3 ubiquitin ligases for early prognosis of AMI found MuRF3 and MuRF1 to be upregulated in the blood plasma of rats and AMI patients (Han et al., 2015). The knockdown of MuRFs in combination with GC/MS and non-targeted metabolomics analysis suggested that all MuRFs possibly have overlapping substrate specificities with similarly altered metabolome (Banerjee et al., 2015).

4.6.3.2 TRIM8 (RNF27)

TRIM8, also known as Ring finger 27 (RNF27), is a 551 residues long protein characteristically having both B-boxes but lacking any C-terminal domain. It has been confirmed by interaction-mating and co-IP to bind with itself, demonstrating homo-interaction in the nuclear region (Reymond et al., 2001). Its genetic location has been mapped at a specific locus where genetic mutations have resulted in various glioblastoma, suggesting a role in gliomas and other malignancies (Vincent et al., 2000). Recently, (Chen et al., 2017) provided a detailed scenario for the cardiac role of TRIM8 after it was found to be upregulated in human DCM patients and hypertrophied mice. TRIM8 KO mice showed characteristics similar to WT mice without any abnormalities and reversed pressure overload effects after TAC, avoiding heart failure. On the other hand, TRIM8-tg mice exaggerated pressure overload hypertrophy after TAC and induced heart failure. Similarly, AngII mediated pro-hypertrophic effects were also exacerbated by TRIM8 *in vitro*. These pro-hypertrophic effects of TRIM8 are mediated via poly-ubiquitination of TAK1 which further activates p38 and JNK1/2 hypertrophic signaling. Thus, TRIM8 has been suggested as a prospective therapeutic agent for pathological hypertrophy and heart failure.

4.6.3.3 TRIM72 (MG53)

TRIM72, also widely known as Mitsugumin53 (MG53) possesses the most common structure of the TRIM family, with RING-BB1-CC-PRY/SPRY domains conservatively aligned from N-terminus to C-terminus (Figure 7). It is noted to play a central role in insulin resistance and thus metabolic disorders such as obesity and diabetes, with possible involvement in cardiovascular diseases like diabetic cardiomyopathy. MG53 has been reported to mediate degradation of both insulin receptor and insulin receptor substrate 1 (IRS1), causing dyslipidemia and hypertension; while its ablation has been credited with preserving IRS1. This mechanistic role of MG53 has been suggested as a therapeutic agent for targeting metabolic disorders and cardiovascular complications (Song et al., 2013).

MG53 is reported to be a vital player in both preconditioning and post-conditioning of IR by activating PI3K-Akt-GSK3 β and ERK1/2 cell survival signaling pathways (Zhang et al., 2016). Myocardial injury resulting from IR in dysferlin KO murine strongly correlated with myocardial muscle impairment, prompting a clinical trial in pediatric patients with corrective heart surgery. But strangely, human myocardium was found to be completely sans of MG53, proposing rhMG53 to be an effective tool in skeletal and cardiac muscle repairs (Lemckert et al., 2016). Furthermore, MG53 (TRIM72) has been reported to have beneficial roles in phosphatidylserine-dependent prevention of skeletal muscle damage, protection of heart against IR injury, and protection of other vital organs by membrane repair; as well as adverse roles leading in development of skeletal muscle insulin resistance, pathogenesis of diabetic cardiomyopathy in the heart and negatively regulating myogenesis with skeletal muscle stiffness and relaxation (Zhang et al., 2016). This 'Janus-faced' nature renders TRIM72 a 'double-edged sword' for human diseases, questioning its use as a therapeutic agent.

5 Aims of the study

Recent discoveries related to RhoA-SRF axis of cardiac hypertrophy have led to the establishment of Dysbindin, a schizophrenia susceptibility protein, to be a robust inducer of cardiomyocyte hypertrophy *in vitro*, by virtue of interactions with hypertrophic proteins like Myozap and RhoA. A yeast two-hybrid screen performed with the aim of finding novel cardiac binding partners of Dysbindin, suggested an E3 ubiquitin ligase TRIM24 to be one of the potential interaction partners. A thorough literature search revealed TRIM32, another TRIM family member to interact with Dysbindin in skeletal muscle and leading its degradation via UPS. The TRIM protein family, known for promoting selective proteolysis to maintain proteostasis, also plays central roles in cellular life regarding the regulation of cell cycle, cell differentiation, and cellular defense. In regard to the above-stated observations, the following aims were proposed in the current thesis:

1. Establishment of the cardiac interaction between Dysbindin and TRIM24, thereby elucidating the cardiac role of TRIM24 in the context of Dysbindin mediated hypertrophy.
2. Confirmation of the Dysbindin-TRIM32 interaction in the heart, thereby characterizing functional aspects of UPS-mediated Dysbindin degradation by TRIM32 and its implications on Dysbindin-mediated hypertrophic SRF signaling.
3. Determination of the roles TRIM24 and TRIM32 play in overall cardiomyocyte homeostasis and cell life.

6 Materials

6.1 Hardware and consumables

Amersham™ Protran NC membrane	GE Healthcare
Axiovert 40 C Microscope	Zeiss
Cell Scraper 16cm 2-position blade	Sarstedt
Cellstar cell culture dishes 6-, 12-, 24-well, 6cm-, 10cm dishes	Greiner Bio one
Centrifuge 5810	Eppendorf
CFX96 Real-Time PCR System	BioRad
Coverslips 18 mm diameter	Karl Hecht KG
Duomax 1030 horizontal rotator	Heidolph
DynaMag-2 Magnet	Invitrogen
ECX-F26.M UV-trans illuminator	Peqlab
Electroporation cuvette	Peqlab
Filter paper 110 mm diameter	Schleicher & Schuell
FluorChem Q Camera (Western Blot)	Alpha Innotech
Galaxy MiniStar Microcentrifuge	VWR
Heraeus Fresco 21 Centrifuge	Thermo Scientific
Heraeus Pico 21 Centrifuge	Thermo Scientific
Horizon 11x14 Gel-electrophoresis	Life Technologies
Infinite M200Pro microplate reader	Tecan

Mini PROTEAN Tetra System	Bio Rad
Mr. Frosty™ Freezing Container	Thermo Fisher Scientific
MyCycler Thermal Cycler	Bio Rad
NanoDrop 2000 spectrophotometer	Thermo Fisher Scientific
Neubauer- cell counter	Assistant
Slide 76x26x1 mm	MARIENFELD
Olympus BX53 microscope	Olympus
Olympus DP72 camera	Olympus
Parafilm	BEMIS
Pasteur pipettes, glass	ROTH
Pipettes Eppendorf-Reference	Eppendorf Research
Pipette tips Biosphere Filter Tip	Sarstedt
Pipette tips, with filter	Sarstedt
Pipetus	Hirschmann Laborgeräte
Power Pac HC	Bio Rad
PP-Microplate 96-well	Greiner-Bio One
RCT Basic magnetic stirrer	IKA
Tubes 0.5 mL, 1.5 mL, 2 mL, 5 mL	Sarstedt
Tubes 15 ml, 50 ml	Sarstedt
Pipettes 2 mL, 5 mL, 10 mL, 25 mL	Sarstedt
Precellys 24 homogenizer	Peqlab

qRT-PCR plates, 96-well, multiply	Sarstedt
Seven Easy pH-meter	Mettler-Toledo
Stemi 2000-C microscope	Zeiss
Steril-Cult 200 incubator	Labotect
Sterile filter 0.2µm Pore Size	Nalgene Labware
SterilGARD Hood	The Baker Company
TE1502S precision scale	Sartorius
Thermomixer Comfort	Eppendorf
Titan PCR-working station	ScanLaf
Vacusaft ventilation	Integra Biosciences
Variomag Poly magnetic stirrer	Thermo Fisher Scientific
Vortex-Genie 2	Scientific Industries
Cell culture flasks 75cm ² , 175cm ²	Sarstedt

6.2 Chemicals

Agarose	Biozym Scientific GmbH
Albumin fraction V, bovine	Merck KG
Carbenicillin	Sigma-Aldrich
DAPI	Sigma-Aldrich
DEPC	Sigma-Aldrich
DMEM	PAA Laboratories
DMSO	Sigma-Aldrich

DNA Loading Dye 6x	Fermentas
Collagen I – solution, bovine skin	BD Biosciences
DreamTaq 10x green buffer	Thermo Scientific
DynaBeads Protein G sepharose	Novex by Life Technologies
EDTA	Serva Electrophoresis
Ethanol	Carl Roth
Ethidiumbromide	Invitrogen
FCS Gold	PAA Laboratories
Fluor Preserve Reagent	Calbiochem
Formamide	Sigma-Aldrich
GeneRuler 1kb Plus DNA Ladder	Fermentas
HEPES	Carl Roth
Hygromycin B	Invitrogen
Ionomycin	Sigma-Aldrich
iQ PowerMix Reagent, multiplex qRT	Bio-Rad
Kanamycine	Sigma-Aldrich
Lipofectamine 2000 Reagent	Invitrogen
Methanol	Carl Roth
NCS (Newborn Calf Serum)	PAA Laboratories
PageRuler Plus prestained Protein Ladder	Thermo Fisher Scientific
Penicillin/Streptomycin	Invitrogen/GIBCO

Phenol/Chloroform/Isoamylalcohol	Carl Roth
Phenylephrine	Sigma-Aldrich
PMA (Phorbol-12-myristat-13-acetat)	Sigma-Aldrich
Protein-Assay dye-concentrate (Bradford)	Bio-Rad
QIAzol Lysis Reagent	Qiagen
Sodium chloride	AppliChem
Sodium hydroxide	AppliChem
SDS	Serva Electrophoresis
Spectinomycin	Sigma-Aldrich
TEMED 99% p.a. Electrophoresis	ROTH
Tris-Base	Carl Roth
Tris-HCl	Carl Roth
Triton X 100	Serva Electrophoresis
Trypan blue	Sigma-Aldrich
Tween 20	Sigma-Aldrich
Vectashield HardSet Mounting Medium	Vecta-Labs

6.3 Enzymes

Collagenase type 2	Worthington/Cellsystems
Complete-Proteinase Inhibitor Cocktail	Roche Diagnostics
Desoxyribonuclease I (DNase I)	Sigma-Aldrich
DreamTaq DNA-Polymerase (GreenTaq)	Thermo Fisher Scientific

LR-Clonase™ II	Invitrogen
Pac I	BD Biosciences Clontech
BP-Clonase™ II	Invitrogen
Phusion HF DNA polymerase	Invitrogen
Proteinase K	Invitrogen
Trypsin-EDTA-solution	Invitrogen/GIBCO

6.4 Antibodies

6.4.1 Primary Antibodies

Table 1: List of primary antibodies. IF=Immunofluorescence, WB=Western Blot, IP=Immunoprecipitation.

Antibody anti-	Species	Clonality	Company	Description
α-actinin	Mouse	mono	Sigma	IF (1:200)
α-actinin	Rabbit	poly	Abcam	IF (1:400)
α-tubulin	mouse	mono	Sigma	WB (1:8,000)
Actin	goat	poly	Santa Cruz Biotechnology	WB (1:3,000)
Caspase3	rabbit	poly	Cell Signaling Technology	WB (1:1,000)
Caspase7	rabbit	poly	Cell Signaling Technology	WB (1:1,000)
Cleaved Caspase3	rabbit	poly	Cell Signaling Technology	WB (1:1,000)
Dysbindin	mouse	mono	Santa Cruz Biotechnology	WB (1:500)
FLAG tag	mouse	mono	Sigma	IP, WB (1:500)
GAPDH	mouse	mono	Sigma	WB (1:20,000)
p53	mouse	mono	Novus Biologicals	WB (1:1,000)
TRIM24	rabbit	poly	Proteintech	IP, WB (1:1,000)
TRIM32	rabbit	poly	Sigma	IP, WB (1:500)
ubiquitin	mouse	mono	Millipore Upstate	WB (1:1,000)
V5 tag	mouse	mono	Biozol	IP, WB (1:500)
XIAP	rabbit	poly	Cell Signaling Technology	WB (1:1,000)

6.5.3 Viruses

Table 4: Adenoviral constructs. Used for the overexpression of the depicted constructs in neonatal rat ventricular cardiomyocytes.

#	Virus Name	Description
1	Ad-LacZ	Overexpression control
2	Ad-HA-Dys	Overexpression of HA-Dysbindin
3	Ad-Dys	Overexpression of Dysbindin
4	Ad-TRIM24	Overexpression of TRIM24
5	Ad-TRIM32	Overexpression of TRIM32
6	Ad-Ubi	Overexpression of Ubiquitin
7	Ad-SRF-Luc	Overexpression of Firefly luciferase
8	Ad-Renilla-Luc	Overexpression of Renilla luciferase
9	Ad-miRNeg	Knockdown control
10	Ad-miRTRIM24	Knockdown of TRIM24
11	Ad-miRTRIM32	Knockdown of TRIM32

6.6 Kits

Block-iT™ Pol II miR RNAi Expression Vector Kit	Invitrogen
ECL-Select detection system	GE Healthcare
Nucleo Spin Plasmid Kit	Macherey-Nagel
Platinum SYBR Green qPCR SuperMix	Invitrogen
Qiagen PLUS Plasmid Midi Kit	Qiagen
QIAquick Gel Extraction Kit	Qiagen
Superscript III First Strand Kit	Invitrogen
Cell Proliferation Kit I	Sigma-Aldrich
In Situ Cell Death Detection Kit, Fluorescein (TUNEL Kit)	Sigma-Aldrich

6.7 Buffers and solutions

ADS-Buffer 10x

1.16 M	NaCl
197 mM	HEPES
94 mM	NaH ₂ PO ₄ .H ₂ O
55.5 mM	Glucose
53.6 mM	KCl
8.3 mM	MgSO ₄ , pH 7.4, sterile filtration

RIPA lysis buffer

50 mM	Tris-HCL
pH 7.5	titrate with 1 M NaOH
150 mM	NaCl
0.5 % (w/v)	Sodium Deoxycholate
1 % (v/v)	NP-40
0.2 %	SDS

Addition of Inhibitors to 1 ml of lysis buffer prior to harvest:

40 µl	25x Proteinase-Inhibitor-Cocktail
10 µl	Phosphatase-Inhibitor 2
10 µl	Phosphatase-Inhibitor 3
1 µl	1 M DTT

Running buffer, SDS-PAGE (10x)

250 mM	Tris
1.9 M	Glycine

1 % (w/v)	SDS
PBS	
137 mM	NaCl
2.7 mM	KCl
4.3 mM	Na ₂ HPO ₄
1.47 mM	KH ₂ PO ₄ , pH 7.4, autoclaved
Laemmli buffer (4x)	
250 mM	Tris pH 6.8
5 % (w/v)	SDS
40 % (v/v)	Glycerin
0.005 % (w/v)	Bromophenole blue
10 % (v/v)	2-Mercaptoethanol
Collecting gel buffer	
0.5 M	Tris-HCl, pH 6.8
TBS	
100 mM	Tris-HCl, pH 7.5
0.9 % (w/v)	NaCl
Transfer buffer	
20 % (v/v)	Methanol
25 mM	Tris
192 mM	Glycine
0.037 % (w/v)	SDS
Separating gel buffer	
1.5 M	Tris, pH 8.8

Trypsin-EDTA solution (in PBS)

0.25 % (w/v)	Trypsin
0.53 mM	EDTA

6.8 Media

LB-Medium (Luria-Bertani)

1 % (w/v)	Tryptone
0.5 % (w/v)	Yeast-extract
1 %	NaCl

Titration to pH 7.0 with NaOH

Growth medium (NRVCM)

DMEM with 4.5 g/l Glucose and 110 mg/l Sodium pyruvate

10% (v/v)	FCS Gold (No FCS in media starting from 24 h of culture)
100 µg/ml	Penicillin G
100 µg/ml	Streptomycin
2 mM	L-Glutamine

Growth medium (HEK293-A)

DMEM with 4.5 g/L Glucose and 110 mg/l sodium pyruvate

4 % (v/v)	FCS Gold
100 µg/ml	Penicillin G
100 µg/ml	Streptomycin
2 mM	L-Glutamine

6.9 Bacteria

E. coli DH10B, electro-competent Life-Technologies

7 Methods

7.1 Microbiological methods

7.1.1 Generation of electro-competent bacteria

For the bacterial transformation via electroporation, bacteria are required to uptake plasmid from the culture media after application of high voltage. *E. coli* DH10B strains were pre-incubated overnight at 37°C at 200 rpm in 50 ml LB medium. The pre-warmed LB medium (1 liter) was added and culture was further incubated until an OD₆₀₀ between 0.4 and 0.8 was obtained (~12-14 h). The culture was centrifuged at 4°C for 15 min at 11000X g to pellet down the bacteria. The pellet was washed twice in ice-cold, sterile ddH₂O. After the second washing, the bacterial pellet was re-suspended in 250 ml 10% (v/v) glycerol and centrifuged. The pellet was further re-suspended in 1.5 ml 10% (v/v) glycerol, aliquoted (50 µl), snap frozen using liquid nitrogen, and stored at -80°C. Transformation efficiency was determined by transforming three random stocks, which were spread (1/100 of the reaction) onto a 100 µg/ml antibiotic containing LB-agar plate. After overnight cultivation at 37°C, the clones were counted to determine the transformation efficiency.

7.1.2 Electroporation

For electroporation, electro-competent DH10B *E. coli* bacteria were thawed on ice. About 5-10 ng of DNA material (plasmid/linearized oligo) was added directly to the bacteria and the suspension was mixed well by pipetting up and down. The mix was transferred into a pre-chilled (-20°C) electroporation-cuvette (Cell projects Ltd., UK) and an electric pulse at 2.5 kV, 200 Ω and 25 µF was given. 1 ml of LB-medium was added to the electroporated bacteria and the mixture was transferred to a sterile reaction tube. The transformed bacteria were incubated at 37°C for ~1 h in a thermomixer at 750 rpm. A portion of the incubated bacteria was then spread on LB-agar plates containing appropriate antibiotic for selection of transformed *E. coli*.

7.1.3 Agar plate preparation

LB medium was prepared by mixing LB agar powder and ddH₂O (1.5% w/v). The mixture was autoclaved and cooled down to 55°C in a water bath. The respective antibiotics were added at this lower temperature to prevent the structural breakdown of antibiotics. Ampicillin was substituted by Carbenicillin and used at a concentration of 100 µg/ml; while, Kanamycin, and

Spectinomycin were added at concentrations of 50 µg/ml. The antibiotic-containing warm solution was cast into 10 cm Petri dishes under a sterile hood. After cooling down, the agar plates were stored at 4°C until the next use.

7.1.4 Spreading of bacterial cultures

Sterile glass beads were used for spreading of transformed bacteria onto agar plates under the sterile hood. The plates were shaken vigorously to allow glass beads to distribute culture evenly. The volume of electroporation mix to be spread was considered according to respective copy numbers of plasmid, typically between 100-300 µl. Agar plates with transformed bacteria were incubated at 37°C overnight. Individual colonies were picked with a pipette tip for colony PCR or culture inoculation for further experiments.

7.1.5 The growth of the bacteria in liquid-culture

The appropriate antibiotics were added to the LB-medium (5 ml) at the above-mentioned concentrations. Single bacterial colonies were picked from agar plates with a pipette tip and added to the medium separately and incubated overnight at 37°C, 200 rpm with horizontal shaking. In some cases, low volume (5 µl) of liquid bacterial culture was also inoculated in the LB-medium. The growth cultures were used for plasmid isolation after ~12-16 h incubation.

7.1.6 Storage of positive clones as glycerol stocks

The culture tubes were stored at 4°C following the plasmid harvest. After confirmation of positive clones by sequencing, 5 ml LB-medium was incubated in the same culture tubes along with the respective antibiotic. The incubated culture was centrifuged at 4200 rpm and 1:1 amount (500 µl) of fresh media and 60% glycerol was added to the pellet. These components were mixed well and transferred to a new 2 ml tube with screw-top lids and stored at -80°C.

7.1.7 Plasmid DNA extraction: Mini preparation

The NucleoSpin® Mini-Preparation-Kit (Macherey-Nagel) was used for extraction of plasmid DNA from smaller *E. coli* DH10B cultures (5 ml). The bacterial cultures were pelleted at 4°C and 4200 rpm for 5 min in a benchtop centrifuge. The bacterial pellet was re-suspended in 125 µl of buffer A1 (resuspension buffer, with RNase A added) and transferred to a 1.5 ml tube. 250 µl of buffer A2 (lysis buffer) was added, mixed well by inverting the tube 5-6 times and incubated at

RT for 5 min. The neutralization buffer (buffer A3, 300 μ l) was added to stop the lysis reaction. The mixture was centrifuged for 7 min at 16200X g; the supernatant was loaded onto the silica-membrane columns. Centrifugation for 30 sec at 6200X g allows the plasmid DNA to bind to the column, which was purified after addition of ethanol-containing washing buffer A4 (700 μ l). The columns were dried by centrifugation at 7800X g for 2 min. Pre-warmed EB-buffer (35 μ l) was used to elute the plasmid DNA by brief centrifugation for 1 min at 16200X g.

7.1.8 Plasmid DNA extraction: Midi preparation

For extraction of Plasmid DNA from higher volumes of liquid culture, Plasmid Plus Purification Midi-Kit (Qiagen) was used. Post incubation, bacteria were pelleted in 50 ml Falcon tubes at 4°C and 4200 rpm for 15 min. The pellet was resuspended in buffer P1 containing RNase A, to which lysis buffer P2 (2 ml each) was added and incubated at RT for 5 min. For neutralization of the alkaline lysis conditions, 2 ml of buffer P3 was added and the mixture was placed into a filter cartridge. After 10 min of incubation, a plunger was inserted into the cartridge to filter the cell lysate through the membrane for removal of cell debris. To the flow through, 2 ml of DNA binding buffer BB was added allowing plasmids to bind to membranes of the spin column after pressure application by a vacuum generator. The solution was then sucked through the spin columns by applying a pressure of ~300 millibars. Endotoxins were removed by addition of ETR buffer to the columns, followed by washing with ethanol-containing washing buffer PE (700 μ l). To remove all buffer residues, the columns were centrifuged at 11000X g for 2 min. The plasmid DNA was eluted with pre-warmed EB-buffer (200 μ l) by centrifugation at 11000X g for 1 min.

7.1.9 Agarose gel electrophoresis

Agarose gel electrophoresis was utilized to separate DNA fragments, based on the size of the fragments. Agarose powder (1% w/v) was dissolved in TAE buffer by boiling the solution in a microwave until the powder was dissolved completely. The solution was cooled down to ~60°C and 0.5 μ g/ml ethidium bromide was added to the solution. The agarose solution was cast into the gel-chamber, a comb was inserted to create wells in the gel for the sample loading and the gel was allowed to polymerize at RT for ~20 min. After polymerization and solidification, the gel was transferred to the electrophoresis chamber containing TAE buffer. DNA-containing samples were loaded into the wells and samples were allowed to run by application of an electric field

(~100 V). Here the negatively charged DNA travels through the gel towards the anode and is separated based on the size of the fragments: with larger fragments traveling slower than smaller fragments. Finally, DNA bands were imaged with the help of UV-light that illuminated ethidium bromide bound DNA.

7.1.10 DNA extraction from agarose gels

DNA that was separated via agarose gel electrophoresis was isolated and purified from the gel. The QiaQuick® Gel-extraction system was used. Therefore the ethidium bromide-stained DNA in the gel was visualized under UV-light, cut out with a scalpel and transferred into a 1.5 ml reaction tube. The sample was then weighed and thrice the volume of the gel-slice, QG-buffer was added to the tube (e.g. 300 µl for every 0.1 g of gel). The gel slice was then incubated at 55°C for 10 min with intermittent vortexing until the gel was dissolved completely. This solution was transferred into a spin-column containing a silica-membrane for DNA binding at 500 µl portions at a time and subsequently centrifuged at 11000X g for 1 min each. Finally, another 500 µl of fresh QG-buffer was added to the column and centrifuged. The flow-through was discarded in each of the steps. The columns were then washed with 600 µl of ethanol containing PE buffer by centrifugation. The residual buffer was removed by centrifuging at 11000X g for 2 min. Addition of 25 µl EB-buffer allowed for elution of the membrane-bound DNA in final centrifugation step.

7.1.11 DNA and RNA concentration measurement

DNA and RNA concentrations were determined with the NanoDrop™ photometer. Optical density was measured at 260 nm and 280 nm and concentrations were automatically calculated for DNA or RNA. Measurements were carried out in duplicates and the mean concentration was considered as the reliable measurement.

7.2 Cell culture methods

7.2.1 Culturing of immortalized HEK293A cell line

Immortalized cryo-conserved HEK293A cells were stored in big liquid nitrogen chambers. For culturing, cells were thawed rapidly in a 37°C water bath and added with 1 ml pre-warmed growth medium. This cell solution was transferred into a T75 cell culture flask containing 8 ml of

warm growth medium. HEK293A cells grow in a monolayer on non-coated plastic surfaces. The generation time of HEK293A is 36h under optimal conditions. Cells were passaged at 70-80 % of confluency. Cells were dissociated from the plastic surface by addition of 2 ml Trypsin-EDTA solution and incubation for 1-2 min at 37 °C until single cells were visible under the microscope. 10 ml of growth medium was added to the cell-solution to stop the trypsin activity. The cells were then centrifuged at 1000X g at RT for 5 min. The supernatant consisting of Trypsin and media was discarded and the cells were resuspended in the warm growth medium. The cells were counted in a Neubauer chamber and seeded in the respective culture plates or, without counting, seeded at a ratio of 1:10 into new T175 flasks for maintenance of the cell line. All cell culture operations like cell splitting and seeding were performed under sterile hood and cells were incubated in a 37 °C incubator with 5% CO₂ until next use.

7.2.2 Cell Transfection in HEK293A cells

The transfection procedure was started after achieving almost 80% confluency of the cells on the plates. Volumes of plasmid DNA intended to overexpress the particular protein, lipid reagent (Lipofectamine 2000) to allow entry of plasmids into mammalian cells and advanced DMEM media (without antibiotics and without FCS) were scaled up as per the need. An equal amount of media was used for the addition of plasmid DNA and Lipofectamine 2000 separately in reaction tubes. Separately, particular amounts of DNA and lipid reagent were added to media for all conditions. After incubation of media and Lipofectamine 2000 mixture for 5 min at RT, it was added to DNA containing media conditions. This plasmid DNA, Lipofectamine 2000 and media mixture was incubated for a further 20 min at RT and transferred to cell plates uniformly in a dropwise manner. The plates were shaken gently in round wise manner to mix up all ingredients uniformly and incubated further.

7.2.3 Cryo-conservation of the HEK293A cell line

To generate cryo-stocks of the HEK293A cells, one T175 flask was passaged as described but finally resuspended in media containing 20 % FBS and 10 % glycerol. Cell density was $1-2 \times 10^{12}$ cells/ml. 1 ml of the cell-solution was pipetted into a cryo-vial and cooled down at 1 °C per minute in a freezing-container to -80 °C overnight. On the next day, cells were transferred into liquid nitrogen for long-term storage.

7.2.4 Isolation of neonatal rat ventricular cardiomyocytes

All culture plates, dishes, and flasks used for the culturing of NRVCM needed to be coated with collagen I to provide cell adherence on the plastic surface prior to seeding of the cells. Hence, collagen I stem-solution (3.1 mg/ml) was diluted to a concentration of 50 µg/ml. Dishes were coated with 5-10 µg/cm² collagen I solution for at least 4 h or overnight at RT. After two washing steps with sterile ddH₂O the plates were air-dried and stored at 4 °C until usage. If not used, plates were stored for no longer than 7 days.

This protocol describes the procedure for the purification and culturing of 40 rat-pup hearts (1-2 day old Wistar rats, Charles River). For the generation of primary cultures from neonatal rat left ventricles, about 40 neonatal rat pups were sacrificed per preparation. The rat pups were decapitated with scissors after quickly dipping in 75% ethanol solution. A small incision of ~1-2 cm into the thorax was made to the left side of the sternum. With the application of mild pressure on the abdomen, the heart was pushed out, cut off and immediately placed in ice-cold ADS buffer. The atria were removed and only ventricles transferred into fresh ice-cold ADS buffer. The ventricles were minced with scissors to obtain finely chopped mass and were transferred into a digestive solution. This digestion solution was a mix of 0.5 mg/ml collagenase type 2 and 0.6 mg/ml pancreatin in ADS-buffer (containing 120 mmol/liter NaCl, 20 mmol/liter HEPES, 8 mmol/liter NaH₂PO₄, 6 mmol/liter glucose, 5 mmol/liter KCl, and 0.8 mmol/liter MgSO₄, pH 7.4) and was sterile-filtered and heated to 37°C prior to use. Digestion also took place at 37°C in a water bath at 40 rpm horizontal shaking. After 20 min single cells started to accumulate in the supernatant, which was taken out to be processed further. To the remaining tissue, fresh digestion-solution was added. Similarly, five to six enzymatic digestion steps were performed until the tissue was digested completely. The supernatants were pipetted through a cell-strainer into a 50 ml reaction tube and 8 ml of newborn calf serum (NCS) were added to inactivate collagenase and pancreatin activity. The solution was then centrifuged at 1000X g, the supernatant was discarded and the cells were resuspended in 5 ml NCS and stored at 37°C in an incubator until further use. After four to five of these digestion steps, the supernatants were pooled together and in NSC resuspended cells were centrifuged, pelleted down and resuspended in 50 ml ADS buffer.

At this stage, the cell solution contains cardiomyocytes along with various cell-types found in the heart like fibroblasts, blood cells, and others. Therefore, it needs to be purified to isolate the cardiomyocytes only. The cells can be separated by their density using a percoll-gradient column (GE Healthcare) (Iwaki et al., 1990). A percoll stem-solution was made from 27 ml percoll and 3 ml 10x ADS buffer. From this stem-solution, two solutions with high (13 ml of stem-solution + 7 ml ADS buffer) and low (9 ml of stem solution + 11 ml ADS buffer) density were generated. First, 4 ml of the low density-solution was pipetted into a 15 ml reaction tube and high-density solution was added later by carefully pushing the pipette through the low-density solution and pipetting it to the bottom of the tube. For column-integrity, it is crucial to pipette the solution very slowly and avoid pipetting air-bubbles into the mixture. Addition of phenol-red dye to the low-density solution allowed for visualization of gradient-phase separation. Each time 500 μ l of cell-solution was carefully pipetted onto gradient and centrifuged at 3000X g and 4°C for 30 min with slow acceleration and deceleration without breaks. Cells were thus separated by their density after three phases of the columns were visible. Cardiomyocytes travel through column until the phase-border between low and mid-phase and were segregated with a transfer pipette. Fibroblasts are less dense and do not travel as far, whereas erythrocytes pellet at the bottom. The cardiomyocytes were resuspended and washed twice with ADS buffer and centrifuged at 1000X g for 5 min. After two washing steps, cells were resuspended in growth medium and counted in a Neubauer Chamber with Trypan-blue staining. Cells were seeded onto different plates at various densities for the respective experiments as depicted in the Table 5.

Table 5: Cell seeding density for NRVCMs.

NRVCMs cell seeding (cells/well)		
Immunocytochemistry	12 well plates with coverslips	0.2×10^6
RNA	6 well plates	0.8×10^6
Protein	6 well plates	1×10^6
	10 cm dishes	10×10^6
Luciferase assay	12 well plates	0.35×10^6
MTT assay	24 well plates	0.15×10^6
	96 well plates	0.03×10^6

NRVCM were seeded and incubated in growth medium containing 10% FCS for the first 18h of culture. For all experiments with NRVCMs mentioned in this thesis, the cells were washed with warm PBS on the next day and were supplemented with FCS-free growth medium for the remaining time of culture.

7.3 Generation of mammalian vectors

7.3.1 Open reading frame (ORF) PCRs using target specific and attB site-specific primers

For the cloning of ORFs (open reading frame) and micro-RNAs, the Gateway®-System that uses a recombination-system from the bacteriophage λ was employed to enzymatically integrate the genomic material into the genome of *E. coli*. These reactions are site-specific and reversible. For the amplification of the gene of interest (GOI), a thermocycler employing polymerase chain reaction was used. The PCR was performed using artificially generated primers specific for particular genes, where primers also contained partial attB1 and attB2 flanking sequences. Depending on the length of the construct, the annealing temperature and the GC-content of the primers, different DNA polymerases can be used. For the experiments shown in this thesis, the high fidelity Phusion DNA polymerase, a DNA-dependent DNA-polymerase with 5'→3' polymerase and 3'→5' exonuclease activity ("proofreading") was used to avoid mutations in the amplified construct. The standard-reaction mix according to the manufacturer's manual was modified if needed, by varying either the salt concentration (MgSO₄) or addition of DMSO for an increase of the primer-annealing temperature range. Typically the PCR was carried out in a 20 μ l scale to yield amplified DNA fragments. This yields cDNA copies of the ORF of interest flanked by the specific parts of the attB-sequences. This reaction mixture was loaded on agarose gel for confirmation of product length. In a second PCR, the first PCR product was used as a template and amplification was carried out with primers containing the full attB1- and attB2-sequences using the exact same conditions as the ORF-PCR. Thus copies of the ORF of interest flanked by the full-length attB-sites were generated.

Table 6: ORF cloning primers.

Primer name	Sequence	Purpose
Dysbn_fw	5'-GCTGGCACCATGCTGGAGACCCTGCGC-3'	Full length Dysbindin
Dysbn_rv	5'-GCTGGGTCGCCAATGTCCTGAGTTGAGTC-3'	
Dys-coil-fw	5'-GCTGGCACCATGTCTGCCCACTGGGAGAAG-3'	Coiled-coil domain
Dys-coil-rv	5'-GCTGGGTCGCCCAGCTTCAGTTGCTGGGT-3'	
Dys-dom-fw	5'-GCTGGCACCATGCAGAAGGCCCTGGAAATG-3'	Dysbindin domain
Dys-dom-rv	5'-GCTGGGTCGCCATCAGCAGTGTCAGGTC-3'	
Dysbn_fw	5'-GCTGGCACCATGCTGGAGACCCTGCGC-3'	N terminus + coiled-coil domain
Dys-coil-rv	5'-GCTGGGTCGCCCAGCTTCAGTTGCTGGGT-3'	
Dys-dom-fw	5'-GCTGGCACCATGCAGAAGGCCCTGGAAATG-3'	Dysbindin domain + C terminus
Dysbn_rv	5'-GCTGGGTCGCCAATGTCCTGAGTTGAGTC-3'	
TRIM24_gw_fw	5'-GCTGGCACCATGGAGGTGGCGGTGGAG-3'	TRIM24
TRIM24_gw_rv	5'-GCTGGGTCGCCTTATTTAAGCAACTGGCG-3'	
TRIM32_gw_fw	5'-GCTGGCACCATGGCTGCGGCTGCAGCA-3'	TRIM32
TRIM32_gw_rv	5'-GCTGGGTCGCCCTAAGGGGTAGAGTATCT-3'	
attB_gw_fw	5'-GGGGACAAGTTTGTACAAAAAAGCTGGCACC-3'	Gateway attB product
attB_gw_rv	5'-GGGGACCACTTTGTACAAGAAAGCTGGGTCGCC-3'	
Luc_firefly_fw	5'GGGACAAGTTTGTACAAAAAAGCTGGCTAGTATGTCC ATATTAGGACATCTACC-3'	Firefly luciferase
Luc_firefly_rv	5'GGGGACCACTTTGTACAAGAAAGCTGGGTTTTACCAC ATTTGTAGAGGTTTTACTTG-3'	
Luc_renilla_fw	5'GGGGACAAGTTTGTACAAAAAAGCTGGCTAAATGAG TCTTCGGACCTCG-3'	Renilla luciferase
Luc_renilla_rv	5'GGGGACCACTTTGTACAAGAAAGCTGGGTTTTACCAC ATTTGTAGAGGTTTTACTTG-3'	

7.3.2 Recombination using BP and LR clonase from Gateway® technology

The GOI is amplified via ORF-PCR from a cDNA pool of the desired species (e.g. mouse, human or rat tissue). These flanked constructs were then recombined into the specific donor (DONR221) vector with the BP Clonase II by incubating 150 ng of PCR-product along with 150 ng of pDONR221 vector and 1 µl of BP Clonase II in a reaction volume of 10 µl overnight at RT. This enzyme is able to cut out regions flanked by specific regions called attP and replace them with attB flanking sequences. This step allows the integration of the generated ORF sequences into the pDONR 221 vector. The generated flanking sites are called attL-sites (attB-insert + attP-vector = attL vector). Similar to this step, the shuttling of the sequence of interest from pDONR to a destination (DEST) vector was carried out with another enzyme, the LR Clonase II. This enzyme catalyzes the recombination between attL and attR sites. The insert-carrying pDONR and the destination vector are recombined by the LR Clonase in the same way as the BP Clonase reaction and this reaction was used to yield destination vector constructs which contained the sequence of interest. The destination vectors employed for cloning of full-length V5-Dysbindin and V5-Dysbindin fragments were pDest40; while pcDNA3.1 was used for cloning of Flag-TRIM32. The plasmid for Flag-tagged pDest40 TRIM24 expression vector was a generous gift from Dr. Barton, University of Texas, Houston. The empty vectors contained a resistance for specific antibiotics for selection of plasmid-carrying bacteria after transformation as well as a ccdB-gene (suicide cassette) that is only removed when the gene of interest or micro RNA is recombined into the plasmid. All generated plasmid-constructs were amplified in *E. coli*; DNA was isolated and sequenced to assure insertion of correct and non-mutated sequences.

7.3.3 Generation of artificial micro-RNA constructs using the Gateway®-compatible Block-iT system

For the cloning of TRIM24 and TRIM32 microRNAs, the Block-iT RNAi-designer by Invitrogen was used. The gene-specific miRNAs flanked by specific sequences allow the formation of hairpin-structures and are subsequently degraded in the mammalian cell. For the purpose, digitally generated oligonucleotides as top and bottom oligo strands with 3' and 5' overhangs were annealed in 10x oligo-annealing buffers and ligated into the linear pcDNA6.2-GW/miR vector with the help of T4 DNA ligase (1 U/µl). This insertion of annealed diploid oligo next to a

polymerase II promoter sequence of the vector is flanked by the attB1 site from the gateway system, generating an attB site flanked Pol II promoter and miRNA sequence. The newly generated plasmid is then transformed into *E. coli* DH10B bacteria and spread on Spectinomycin (50 µg/ml) containing agar plates. Plasmids were amplified in bacteria as described before. The shuttling into a donor and subsequent destination vector was carried out by BP Clonase® II and LR Clonase® II as described.

Table 7: Synthetic oligo sequences for microRNA generation.

Name	Sequence	Purpose
miRTRIM24_top	TGCTGTGAATTTGGTGACTGCACGGTGTTTTGGCCA CTGACTGACACCGTGCACACCAAATTCA	TRIM24 knockdown in NRVCMs
miRTRIM24_bottom	CCTGTGAATTTGGTGTGCACGGTGTCAGTCAGTGG CCAAAACACCGTGCAGTCACCAAATTCAC	
miRTRIM32_top	TGCTGACATCTTGCAGGGTAAGCTCCGTTTTGGCCA CTGACTGACGGAGCTTACTGCAAGATGT	TRIM32 knockdown in NRVCMs
miRTRIM32_bottom	CCTGACATCTTGCAGTAAGCTCCGTCAGTCAGTGGC CAAAACGGAGCTTACCCTGCAAGATGTC	

7.3.4 Generation of adenoviruses for recombinant protein or miRNA expression

The adenoviruses used for overexpression or knockdown of proteins in NRVCMs were generated using the ViraPower™ Adenoviral Kit. A cDNA (for overexpression) or microRNA peptide (for knockdown) that had been previously cloned into the pDONR 221 vector was shuttled into the pAd/CMV/V5-DEST Gateway vector and then *PacI* digested. For digestion, 10 µg of vector-DNA was incubated with *PacI* enzyme (1.5 µl, 10 U/µl) and CutSmart buffer (1x) in a total volume of 70 µl at 37°C to obtain linear DNA. *PacI* restriction enzyme digested pAd/CMV/V5-DEST constructs were transfected into HEK293A cells to produce specific adenoviruses. For this purpose, HEK293A cells provide the genes encoding for the packaging of the adenoviruses and allow for lytic virus-production. The HEK293A cells (~70% confluent in 6 well plates) were then transfected with 2 µg of the linear pAd/CMV/V5-DEST vector. Post 24 h

of transfection, cells were transferred into a T75 flask containing 12 ml of growth media. The cells were microscopically checked for virus production twice a day; with the addition of 3 ml media every 2 days. After a week, the dead cells started displaying chain-like structures in cell-layer because of the detached cells. This showed that the virus started to lyse the cells and is present in the supernatant. The cells were incubated further until complete lysis occurred. This lysate is then stored at -80 °C until further usage. 3-5 ml of this lysate were added into 100% confluent HEK293A-T175 flasks for the generation of greater amounts of virus particles and incubated until the cells showed first signs of lytic virus production. Based on the assumption, that every cell has been infected by the adenoviruses from the lysate cells were harvested before they were detached from the flask bottom. The cells with still intact membranes and filled with virus particles were centrifuged; the supernatant was discarded and the pellet was resuspended in 1-2 ml of PBS and underwent three freeze-thaw cycles to break open the membranes. After centrifuging for 10 min at 12000X g and 4 °C, the supernatant was aliquoted into fresh PCR tubes in 20-30 µl portions. One of these aliquots was then used for the determination of the number of infectious viruses per µl (ifu/µl) - the virus particles titration.

7.3.5 Virus particle titration

Virus titration for adenoviruses was performed by staining the adenovirus-infected HEK293A cells with the FITC-labeled anti-Hexon antibody. HEK293A cells were seeded in 24 WPs at 3×10^5 cells/well. Cells were then infected with the adenoviruses diluted at different concentrations in duplicates. For this purpose, various serial dilutions of 10 µl of the virus aliquot were prepared from 10^{-2} to 10^{-7} with ten-fold dilution in every step, resulting in 6 different dilutions. One well was not infected, serving as a negative control; whereas the first dilution of 10^{-2} served as a positive control and was pipetted only into one well. The remaining dilutions were pipetted 50 µl per well for two wells each as stated. The infected cells were incubated at 37°C for 48 h. Post incubation, media was removed and the cells were fixed with 500 µl cold methanol for 10 min at -20°C. After the three washing steps with PBS containing 1% BSA, the cells were incubated with 150 µl of the FITC-coupled anti-Hexon antibody for each well for ~1 h at 37°C in the dark. After three more washing steps with PBS containing 1% BSA, the number of infected cells was counted under the microscope. For the purpose, FITC was excited under UV-light and

the emitted green fluorescence was microscopically observed. Infected cells thus emitting green fluorescence were counted in ten randomly chosen fields of view with the 10x or 20x objectives for each well. The mean cells per field of view were calculated. For the 10x objective 79 'fields of view' and for the 20x objective, 313 'fields of view' can be expected to cover the whole well. Thus, a mean number of infected cells was then multiplied by 79 or 313 to approximate the total number of infected cells per well. Division of this number by the manifold of dilution and subsequent multiplication with the amount of virus pipetted into each well result in the infectious units per ml (ifu/ml) and this unit was used to maintain a constant amount of infectious particles between individual viruses and controls in each experiment.

7.4 Interaction studies

7.4.1 Co-immunoprecipitation in HEK293A cells

HEK293A cells were maintained in DMEM containing 4% FCS, 2 mM L-glutamine, and Penicillin/Streptomycin. Dysbindin was cloned with the C-terminal V5 tag, whereas both TRIM24 and TRIM32 were cloned with the N-terminal FLAG tag in mammalian expression plasmids. For establishing interaction between dysbindin and TRIM proteins, HEK293A cells (2.5×10^6 /dish) were co-transfected with 10 μ g of TRIM expression plasmids with or without dysbindin (10 μ g) using Lipofectamine 2000 (Life Technologies, Inc.). Empty vector pcDNA3.1 was used as a negative control. 48 h after transfection with an intermittent media change at 24 h intervals, cells were washed and harvested with warm PBS, pelleted down, and resuspended in RIPA buffer (50mM Tris, 150mM NaCl, 1% Nonidet P-40, 0.5% sodium deoxycholate, and 0.2% SDS) supplemented with phosphatase and protease inhibitor mixtures (Complete; Roche Applied Science) as needed. Cells were subsequently lysed by three successive freeze-thaw cycles followed by centrifugation at 18000X g at 4°C for 20 min. The supernatant containing cellular proteins was used for immunoprecipitation using anti-V5 or anti-FLAG affinity gels in two separate setups following the manufacturer's guidelines. In brief, 1 mg of protein in a total volume of 1 ml of lysis buffer was mixed with 50 μ l of equilibrated beads, and V5- and FLAG-tagged proteins were then allowed to bind to the respective antibody on the beads for ~4 h at 4°C atop a rotating shaker. Protein lysate was removed carefully after centrifugation at 8000X g, and magnetic beads were washed 4-5 times with lysis buffer. Precipitated proteins from the

beads were eluted with 50 μ l of Laemmli sample buffer. 10 μ l of this eluted protein was immunoblotted with SDS-PAGE followed by transfer to nitrocellulose membranes and developing with anti-Flag-tag (MBL International Corporation, #M185-11) or anti-V5-tag (MBL international corporation, #M167-11) antibodies for checking two-way interactions between Dysbindin and TRIMs. All the co-IP experiments were performed twice. A similar methodology was also performed to check the interaction between Flag-TRIM24 and various V5-tagged Dysbindin fragments namely, N-terminal + coiled-coil domain, coiled-coil domain, Dysbindin domain, and C-terminal + Dysbindin domain. Here, IP was carried out using anti-V5-tagged magnetic beads (MBL International Corporation, #M167-11) and immunoblotting was performed using nitrocellulose membranes against Flag-tag-antibody (Sigma-Aldrich, #F1804) to establish the domain-specific interaction between dysbindin and TRIM24.

7.4.2 Co-immunoprecipitation in NRVCMs

Cultured NRVCMs (6×10^6 /dish) were co-infected with adenoviruses for HA-tagged dysbindin (Ad-HA-dysbindin, 50 ifu), TRIM24 (Ad-TRIM24, 100 ifu), and TRIM32 (Ad-TRIM32, 100 ifu) in several setups in DMEM containing 2 mM penicillin/streptomycin and L-glutamine but lacking FCS. Adenovirus expressing β -galactosidase (Ad-LacZ) was used as a negative control as well as adenovirus quantity filler for all the co-IP experiments. 72 h after infection with intermittent media change after the first 24 h, cells were washed with PBS and scraped using cell scraper and RIPA cell lysis buffer (50 mM Tris, 150 mM NaCl, 1% Nonidet P-40, 0.5% sodium deoxycholate, and 0.2% SDS) supplemented with phosphatase and protease inhibitor mixture (Complete; Roche Applied Science). Cardiomyocytes were lysed by three cycles of freeze and thaw, and debris was removed by centrifugation at 18000X g for 20 min. Protein containing supernatant was used for the immunoprecipitation using 50 μ l anti-HA tagged antibody beads (MBL International Corporation, #M132-11) following the manufacturer's guidelines. In brief, 1 mg of protein in a total volume of 1 ml of RIPA lysis buffer was applied to 50 μ l of equilibrated beads, and HA-tagged proteins were allowed to bind to the anti-HA antibody on the beads for ~4 h at 4°C atop a rotating shaker. Protein lysate was removed carefully after centrifugation at 8200X g, to remove flow-through and beads were subsequently washed thrice with lysis buffer to remove unbound-protein impurities. Precipitated proteins from the beads were released by boiling at

95°C for 5 min with 50 µl of Laemmli buffer. 10-15 µl from eluted protein was immunoblotted with SDS-PAGE followed by transfer to nitrocellulose membranes and incubation with various antibodies, including anti-TRIM24, anti-TRIM32, anti-Dysbindin, anti-HA, etc. All co-IP experiments were performed twice to confirm the interaction between specific proteins.

7.4.3 Co-localization in NRVCMs: Confocal immunofluorescence microscopy

Co-localization studies for Dysbindin with TRIM24 and TRIM32 were carried out in NRVCMs. Cells were seeded in a 12-well plate on collagen-coated coverslips. Following the adenovirus infection and incubation phase, NRVCMs were fixed with 4% paraformaldehyde for 10 min at RT, permeabilized, and blocked with 0.1% Triton X-100 in 2.5% BSA in PBS for 1 h at RT. Cells were then incubated for ~2 h with various primary antibodies using the following dilutions: monoclonal mouse anti-dysbindin (1:100; Santa Cruz Biotechnology), monoclonal mouse anti- α -actinin (Z-disc specific, 1:200; Sigma), polyclonal rabbit anti- α -actinin (Z-disc specific, 1:400; Abcam), polyclonal rabbit anti-TRIM24 (1:200; Acris), and polyclonal rabbit anti-TRIM32 (1:200, Sigma) for co-localization. Respective secondary antibodies conjugated to either Alexa Fluor-488 (AF488, green, Thermo Fisher Scientific) or Alexa Fluor-546 (AF546, red, Thermo Fisher Scientific) were incubated for ~2 h, all at a dilution of 1:200 in 2.5% BSA in PBS, along with nuclear stain DAPI (1:500). FluorPreserve reagent (Merck Millipore) was used as a mounting medium to preserve the fluorescence, as well as to fix coverslips on glass slides. Images were taken with a Zeiss LSM800 laser-scanning confocal microscope with a Plan-Apochromat X40/1.4 oil differential interference contrast (UV)-visible IR objective at room temperature. The image pixel size was set to optimal for individual acquisitions. The pinhole was adjusted to 1 airy unit or less for each individual laser line. AF546 and DAPI channels were acquired via GaAsP-Pmt detectors and AF488 channel with a Multialkali-Pmt detector with gain settings between 600 and 700 V. The laser power for excitation ranged from 0.2 to 0.8%. Cropped regions from the overviews are not digital magnifications of the areas but separately acquired images.

7.4.4 Co-localization in NRVCMs: Analysis

The co-localization analyses were carried out using the Zeiss co-localization method using ZEN-blue software package. Individual cells from three different overview images were taken into account for the measurement to maintain the integrity of co-localization coefficient calculation.

For setting the scatter plot boundaries and to automatically identify the threshold value to be used to identify background values, we utilized the method of Coste *et al.* which was automatically implemented by the software. To assess the particular fraction of a protein that co-localizes with another protein, we utilized the Mander's colocalization coefficients (MCC), which are metrics that are widely used in biological microscopy analyses and have been implemented in all biological image analysis software packages. MCC measures co-occurrence independent of signal proportionality and ranges from 0 to 1, where an MCC of 0 represents 0% and of 1 represents 100% colocalization of the respective dyes.

7.5 Animal experiments

7.5.1 Transverse Aortic Constriction (TAC)

Sham (control) and TAC operations were performed in 8-weeks old Charles River C57BL/6 mice. For the purpose, mice were anesthetized by using isoflurane 4% (v/v) per mask and then orally intubated with a 20-gauge tube and ventilated (Harvard Apparatus) at 120 breaths per min (0.2 ml tidal volume). The aortic constriction was accomplished via a lateral thoracotomy through the second intercostal space. A suture (Prolene 6-0) was placed around the transverse aorta between the brachiocephalic and left carotid artery. The suture was ligated against a 27-gauge needle and the needle was removed leaving discrete stenosis. The chest was finally sutured with the pneumothorax evacuated. Sham-operated animals underwent the exact same procedure except for the suture ligation. Cardiac function was examined by echocardiography, and the animals were killed 2 weeks post-operation to extract the heart for downstream analysis of RNA and proteins. All the animal experiments were approved and performed as per the guidelines of the local ethical committee (Ministerium für Energiewende, Landwirtschaft, Umwelt und Ländliche Räume Schleswig-Holstein).

7.5.2 Phenylephrine osmotic pump implantation

This was another attempt to generate cardiac hypertrophy related phenotype in mice, other than TAC, and induces biochemical hypertrophy. To stimulate hypertrophy in mice, osmotic mini-pumps filled with the α -adrenergic agonist phenylephrine (PE, 25 g/kg body weight/min) prepared in PBS with 1 mg/ml L-ascorbate (Sigma) were implanted subcutaneously in 8-weeks old WT C57BL/6 mice. Control group in this study received the vehicle L-ascorbate in saline PBS

in the exact same amount. 2 weeks post-implantation of osmotic pumps, cardiac function was examined via echocardiography and the animals were subsequently sacrificed to extract the heart and lung, for phenotypic measurements and for RNA and protein related analysis.

7.6 Cellular assays

7.6.1 SRF reporter gene assay

All SRF reporter gene (SRF-RE) assays shown in this study were performed in NRVCMs. Cells were infected with several combinations of adenoviruses expressing Dysbindin (50 ifu), TRIM24 (100 ifu), TRIM32 (100 ifu), and LacZ (as control or a filler virus to maintain equal count of viruses) along with adenovirus for ad-SRF-RE-luciferase (20 ifu) carrying a firefly luciferase and ad-Renilla-luciferase (5 ifu) carrying Renilla luciferase (for internal normalization of the measurements). For TRIM24 and TRIM32 knockdown experiments, NRVCMs were transfected with ad-miRTRIM24 and ad-miRTRIM32 where ds-mimic microRNA (ad-miRNeg) was used as control or filler in addition to adenovirus infection. After 72 h incubation period with intermittent media change after first 24 h post-infection, cells were washed twice with warm PBS and passive lysis buffer (PLB, Promega, 5X, and diluted using ddH₂O) was added to each well. Plates were then stored in -80°C to induce cellular lysis in the presence of PLB for 15 min. After subsequent thawing at RT for 20 more min on a shaker, 20 µl of the sample from each well was transferred to opaque 96 well plates to allow analysis using a photometer. Experiments were performed using a dual-luciferase reporter assay kit (Promega), according to the manufacturer's guidelines. Chemiluminescence was measured photometrically with an Infinite M200 PRO system (Tecan, Life Science). All the experiments were performed in quadruplicates or sextuplicates, repeated three times, analyzed and plotted relative to respective control.

7.6.2 MTT assay for cell viability in NRVCMs

NRVCMs (0.15×10^6 cells/well) cultured in 24-well plates were infected 24 h after the seeding with respective adenoviruses and incubated for additional 72 h with a media change after the first 24 hours of infection. MTT labeling reagent (cell proliferation kit, MTT I, Roche Applied Science) was added at 10% concentration of total DMEM to each well. Plates were incubated for 4 h in a humidified atmosphere (37 °C, 5% CO₂). After this incubation phase, MTT solubilization solution (cell proliferation kit, MTT I, Roche Applied Science) was added to each well with a

quantity of 10 times the initially added MTT labeling reagent volume and incubated overnight under the conditions mentioned above. After complete solubilization of purple formazan crystals, spectrophotometric absorbance was measured using a microplate reader on an Infinite M200 PRO System (Tecan, Life Science). The percentage of viable cells was plotted relative to control. Samples were then compared by Student's t-test. All the experiments were performed in sextuplicates or octuplicates and repeated three times.

7.7 Immunofluorescence studies

7.7.1 Immunofluorescence microscopy

Microscopic visualization based cellular experiments requiring the assistance of fluorescent stainings like cell size measurement, TUNEL, cleaved caspase-3 (CC3), and Propidium iodide (PI) staining were studied in NRVCMs by immunofluorescence microscopy. Cell preparation and seeding were performed as described above. Monoclonal mouse anti- α -actinin (1:200; Sigma) antibody was used for cell size measurements, whereas polyclonal rabbit anti-CC3 (1:400, Cell Signaling Technology) antibody was used for activated caspase-3 staining. Respective secondary antibodies conjugated to either Alexa Fluor-488 or Alexa Fluor-546 (Thermo Fisher Scientific) were incubated for 2 h at a dilution of 1:200 in 2.5% BSA in PBS along with the nuclei specific stain DAPI. TUNEL and PI stainings were performed as described in this section. FluorPreserve reagent (Merck Millipore) was used as a mounting medium. Fluorescence micrographs were taken with Keyence microscope BZ 9000, at 10x objective (Plan Aplanachromat, NA: 0.45) with the help of BZ-II viewer (Keyence, version 2.1) using a built-in camera at room temperature. Images were processed and analyzed by BZ-II Analyzer (Keyence, version 2.1) as detailed below.

7.7.2 Cell surface area measurement using BZ-9000 microscope

After staining NRVCMs with cardiomyocyte-specific α -actinin antibody and nuclear stain DAPI, immunofluorescence pictures were taken using the Keyence BZ-9000 microscope. For each coverslip with fluorescence-stained cells, 10 pictures were taken at 10X magnification (objective: CFI Plan Aplanachromat λ X10; Nikon) with BZ-II Viewer (version 2.1). Images were further processed and analyzed using the BZ-II Analyzer (version 2.1), where cell size was measured using 'Hybrid Cell Count' software module (Keyence) with the fluorescence intensity single-extraction mode. First, fluorescence intensity thresholds were set for a reference picture

thereafter, α -actinin (cardiomyocyte-specific, to avoid any impurities with fibroblasts) whole-cell staining was set as the target area, and the DAPI-stained nuclei were then extracted from each target area to determine the number of nuclei per target area and were set as a condition picture. Then 'Macro Cell Count' was performed, applying the settings from the reference condition picture to each micrograph in the experiments. Results were manually filtered using a macro for the following filtering criteria: (a) $150 \mu\text{m}^2 < \text{target area in micrometers squared} < 2,500 \mu\text{m}^2$ (size filter); (b) extraction from target area = 1 (filter for number of nuclei); and (c) area ratio $1 < 30\%$ (cell surface to nucleus ratio filter). Statistical analysis was performed using GraphPad Prism (version 5). Equal distributions of the data were tested by the Shapiro-Wilk test.

7.7.3 TUNEL assay

NRVCMs were seeded in a 12-well plate on collagen-coated coverslips. Following the adenovirus infection and 72-h incubation phase, NRVCMs were fixed with 4% paraformaldehyde for 10 min and permeabilized/blocked with PBS containing 2.5% BSA and 0.1% Triton X-100 for 1 h at RT. An enzyme mixture was prepared by adding TUNEL mix into labeling solution at 1:10 ratio (In situ-Cell death detection kit, Roche Applied Science). The positive control was treated with DNase enzyme for 10 min, as TUNEL employs cleaved DNA as a marker of apoptosis; while the enzyme mixture for negative control lacked TUNEL mix. All coverslips were incubated at 37 °C for 1 h along with positive and negative controls in their respective enzyme mixtures. Nuclear staining was performed with DAPI for 15 min after incubation phase followed by three washing steps with PBS. Coverslips were mounted on glass slides with the aid of Fluor-Preserve reagent (Merck Millipore). Acquisition of fluorescent micrographs was performed as described earlier for cell size imaging. Images were further processed and analyzed using the BZ-II Analyzer (version 2.1). Processing was executed using 'Hybrid Cell Count' software module (Keyence) with the fluorescence intensity single extraction mode. First, fluorescence intensity thresholds were set for a reference picture. Thereafter, DAPI nuclear staining was set as the target stain, and the TUNEL-stained nuclei were then extracted from each target nuclei to determine the number of TUNEL/DAPI-stained nuclei per coverslip. Then, 'Macro Cell Count' was performed, applying the settings from the reference picture to overlay images from each set of

experiments. Statistical analyses were performed using GraphPad Prism (version 5), and samples were compared by Student's t-test.

7.7.4 Cleaved Caspase3 staining

NRVCMs seeding and infection were performed as described under "Immunofluorescence microscopy". Post-incubation, cells were fixed on coverslips with cold methanol at -20 °C for 10 min and stained using an antibody specific for a cleaved fragment of Caspase3 (1:400, Cell Signaling Technology; Alexa Fluor-546, 1:200, Thermo Fisher Scientific), where DAPI served as a nuclear stain. Coverslips were mounted using Fluor-Preserve reagent (Merck Millipore) and fluorescent micrographs were taken at 10X objective as explained above. Images were then analyzed with the BZ-II analyzer separately for DAPI and cleaved Caspase3 by keeping off the extraction mode. The total number of nuclei was counted using 'Hybrid Cell Count' protocol and plotted by taking the percentage of cleaved Caspase3-positive nuclei over DAPI-stained nuclei for individual coverslips. All these experiments were repeated twice in triplicates. The samples were then compared via Student's t-test.

7.7.5 Propidium Iodide (PI) staining

NRVCMs seeding and infection were performed as described under "Immunofluorescence microscopy". After 72 h incubation, coverslips were washed twice with warm PBS. PI (1 mg/ml) diluted in PBS at 1:2000 was added to coverslips (500 µl/well) at RT for 10 min. This was followed by two times washing and fixation of cells on coverslips with methanol for 10 min at 20°C. Post fixation, cells were blocked and permeabilized with BSA (2.5%) in PBS + TritonX-100 (0.1%). Nuclear stain DAPI (diluted in BSA-PBS 1:500) was added and the coverslips were incubated at RT for 15 more min. After three times washing, the coverslips were transferred on glass slides using Fluor preserve mounting medium (Merck Millipore). Acquiring fluorescent micrographs and analysis was exactly similar as described above for cleaved Caspase3.

7.8 Molecular biology methods

7.8.1 RNA isolation and qRT-PCR

Total RNA was isolated from NRVCMs, mouse heart (and other tissues), or human heart samples using TRIzol lysis reagent (QIAzol; Qiagen) following the manufacturer's instructions. 1 µg of

DNA-free total RNA was transcribed into cDNA using the first strand cDNA synthesis kit (SuperScript III; Life Technologies, Inc.). For qRT-PCR, the EXPRESS SYBR GreenER reagent (Life Technologies, Inc.) was used in a real-time PCR system (CFX96; Bio-Rad). Rpl32 or 18S ribosomal RNA genes were used as internal standards for normalization of reverse transcription. All experiments with NRVCMs were performed in triplicate/sextuplicate and repeated two times.

7.8.1.1 RNA extraction from cultured cells

Total RNA was isolated from cultured cells using QIAzol lysis reagent. After incubation period media was removed from the cells and two washes were given with PBS. Then 1 ml of TRIZOL was added to each well, cells were flushed with the help of a pipette and the cell mass was collected into 1.5 ml reaction tubes. Chloroform (200 μ l) was added to each tube by vigorous shaking and incubation at RT for 2 min to induce phase separation where DNA, protein and RNA get separated in the lower phenol/chloroform phase, in the interface, and in the upper aqueous phase respectively. The reaction was then centrifuged at 12000X g for 15 min in a 4°C cooling centrifuge to separate the phenolic and the aqueous phase. The supernatant was transferred carefully to new RNase and DNase free reaction tube, without disturbing the interphase or lower phase. 500 μ l isopropanol was added to the supernatant to chelate salts and induce RNA precipitation, followed by shaking by inverting tubes, incubation at RT for 5 min and centrifugation at 12000X g for 10 min. The supernatant was discarded and 1 ml 75% ethanol was added to concentrate the pellet by desalting of RNA and centrifuged further at 14000X g for 5 min. Finally, the supernatant was discarded carefully and the RNA containing pellet was air dried by keeping tubes upside down for ~10 min at RT. To elute RNA along with getting rid of any DNA impurity, following components of DNase I mix were added to the tubes.

Table 8: Re-suspension mix for RNA isolation with DNase I enzyme.

#	Particulars	Amount per sample
1	DNase I	1.5 μ l
2	DNase buffer	2 μ l
3	Water	16.5 μ l

The tubes were flicked well to mix DNase I solution to RNA pellets and were incubated at 300 rpm for 30 min in a thermomixer at 30°C to allow proper mixing. DNase I enzyme was heat inactivated by first heating tubes at 70°C for 10 min and then snap cooling on ice for 5 min. The samples were stored at -80°C until further use.

7.8.1.2 RNA extraction from the heart and other tissue samples

For isolating total RNA from mouse hearts or other organs, the tissue had to be broken down beforehand, which was achieved by using the Precellys24 homogenizer. The tissues were placed in 2 ml tight capped tubes and 1 ml QIAzol lysis solution was added along with big (2.8 mm) and small (1.4 mm) ceramic beads and placed in the homogenizer. The homogenizer program used was dependent on the size of the tissue, either 2 x 20 s at speed 5000 or 2 x 15 s at speed 6500 until complete dissociation of the tissue. The dissociated tissue lysate was then centrifuged at 12000X g for 20 min and the supernatant containing nucleic acids was transferred into a fresh 1.5 ml reaction tube. The RNA-extraction was carried out as described for cell-culture based RNA extraction above.

7.8.1.3 cDNA synthesis from RNA

For cDNA synthesis, 1 µg of RNA was used as starting material using the Superscript III first strand cDNA synthesis kit, where ddH₂O was added to make up the volume to 12 µl in 500 µl PCR tubes. A RNA-dependent DNA polymerase master mix of 8 µl, containing a mixture of following ingredients was added to all PCR tubes.

Table 9: Contents for cDNA synthesis master mix.

#	Particulars	Amount per tube
1	Random hexamer primer (250 ng)	0.5 µl
2	dNTPs (10 mM)	1 µl
3	First strand RT buffer (5X)	4 µl
4	DTT (0.1 mM)	1 µl
5	RNase out enzyme	1 µl
6	Superscript III RT	0.5 µl

The tubes were spun down in a table top centrifuge and the PCR reaction was started in a thermocycler with the following protocol:

Table 10: cDNA synthesis conditions.

Step	Temp.	Time	Purpose
1	25°C	10 min	Primer binding
2	50°C	60 min	Enzyme activation, DNA synthesis
3	70°C	15 min	Enzyme inhibition
4	4°C	∞	Cooling down, only after the last cycle

After synthesis, cDNA samples were diluted to achieve a final concentration of 5ng/μl to facilitate their use in real-time PCR analysis and were stored at -20°C until further use.

7.8.1.4 Quantitative real-time PCR

For the real-time quantification of gene copies, the Platinum SYBR Green qPCR SuperMix-UDG (Thermo Fisher Scientific) was used. SYBR Green binds to the novel amplified DNA and thus emits a signal proportional to the amount of cDNA in the reaction. The SYBR Green dye is excited with a laser and its emission is detected and measured by the PCR-cycler. For this purpose, 18 μl of a master mix for each sample was prepared, containing 10 μl Platinum SYBR Green qPCR Supermix, 0.5 μl of forward + reverse primer (10 μM each) and 7.5 μl of DNase-free H₂O. First, 2 μl of cDNA (10 ng) was added into the wells of the real-time PCR plate, followed by the SYBR Green master mix. After sealing the plate with adhesive foil, the samples were spun down and a polymerase chain reaction was started in the qRT-PCR cycler. The protocol for PCR reaction is given in Table 11.

Table 11: Quantitative real-time PCR protocol

Step	Temp.	Time	Purpose	Repeats
1	95°C	3 min	Initial denaturation	-
2	95°C	15 sec	Denaturation	39
3	60°C	45 sec	Primer annealing and extension	

In the common step for annealing and extension, the fluorophore is excited and the emission is recorded by thermocycler. Specifically designed synthetic primers were employed for quantification of particular genes; while Rpl32 or 18S ribosome was used as an internal normalization control (Frank et al., 2008). Samples were prepared in triplicates/sextuplicates and real-time measurement was carried out in duplicates for each sample. For the quantification, the principle of threshold-cycling was utilized where the threshold is the first value that is significantly higher than the background.

Table 12: Quantitative real-time PCR primers.

Name	Sequence	Purpose
mr_dys_rt-F	5'-CGCATCCTCATACTGCTAAGT-3'	Mouse, Rat Dysbindin
mr_dys_rt-R	5'-GCAGGATTTACCCGGG-3'	
hs_trim24_rt-F	5'-AGCCTAGCTCAATTACGGCTC-3'	Human TRIM24
hs_trim24_rt-R	5'-GCGGTTGCTGATGAGAGATGG-3'	
mmu_trim24_rt-F	5'-GCCACCCAAGTTGGAGTCAT-3'	Mouse TRIM24
mmu_trim24_rt-R	5'-GGAAGTTCAGTGGTGTCTTC-3'	
rno_trim24_rt-F	5'-AAACCCTAGAATGCAGGGGC-3'	Rat TRIM24
rno_trim24_rt-R	5'-CTGGTCCATTGGGCTTAGGG-3'	
hs_trim32_rt-F	5'-CAGCCCCAGTGGCATTGATA-3'	Human TRIM32
hs_trim32_rt-R	5'-TCAGTCACACCAATCAGCCC-3'	
mr_trim32_rt-F	5'-AAGTGTTCAACCGCAAAGGC-3'	Mouse, Rat TRIM32
mr_trim32_rt-R	5'-AGTGAGATTGGGCAAGTCGG-3'	

7.8.2 Protein isolation and Western blotting

7.8.2.1 Protein extraction from tissue samples

To harvest protein from whole mouse hearts and other organs, the tissue was broken down using the Precellys 24 homogenizer. The tissue was placed in reaction tubes consisting 1ml RIPA lysis buffer (50mM Tris, 150mM NaCl, 1% Nonidet P-40, 0.5% sodium deoxycholate, and 0.2% SDS) and big (2.8 mm) and small (1.4 mm) ceramic beads were added and placed in the

Precellys. The homogenization program used depended on the size of the tissue and was either 2 x 20 s at speed 5000 or 2 x 15 s at speed 6500. The dissolved tissue was then centrifuged at 12000X g for 20 min and the supernatant was transferred into a fresh 1.5 ml reaction tube. The protein concentration was measured by the DC™-Protein concentration measurement assay.

7.8.2.2 Protein extraction from cultured cells

Post-incubation, NRVCMs were washed twice with ice-cold PBS prior to addition of the RIPA lysis buffer containing protease and phosphatase inhibitor cocktails. Plates containing both cells and lysis buffer were then frozen in a -80°C freezer for half an hour to accelerate membrane lysis. After thawing on ice, the cells were scraped off with a cell scraper and transferred into a reaction tube. NRVCMs were further lysed by 3 freeze-thaw cycles from -80 °C freezing to on-ice thawing. The cell lysate was then centrifuged at 18000X g for 20 min and the supernatant was carefully transferred to a fresh reaction tube without disturbing the pelleted cell-debris. The protein concentration was measured by the DC™-Protein concentration measurement assay.

7.8.2.3 Protein concentration measurement using DC protein-assay kit

For determination of the protein concentration from the cell lysate as mentioned above, the DC Protein assay kit (Bio-Rad) was used. To analyze the concentration of a given protein sample, a standard curve with known protein concentration had to be generated. The stock-solution of 2 mg/ml BSA (w/v) dissolved in the respective lysis buffer was serially diluted five times to obtain standard dilutions from 2 mg/ml to 0.0625 mg/ml in 20 µl of lysis buffer. The cellular protein mix was also diluted using the same lysis buffer so that its concentration fits into the range of 2 mg/ml to 0.0625 mg/ml. The stock dilutions and protein dilutions were pipetted into a 96 well plate in triplicates that allowed for measurement of the OD at 750 nm using a photometer TECAN M2000 pro. The proteins were added in quantity of 5 µl to each well, followed by addition of 25 µl of solution A' (mixture of solution A and solution S) and 200 µl of solution B. After gentle mixing and an incubation of 15 min at RT, the samples were measured photometrically and by linear regression of the standards, the protein concentration in the samples was measured against the standard BSA.

7.8.2.4 Protein loading and immunoblotting

NRVCMs were lysed by two to three freeze-thaw cycles in RIPA lysis buffer containing phosphatase inhibitor II, phosphatase inhibitor III, and protease inhibitor mixture (Roche Applied Science). Cell debris was removed by centrifugation, and protein concentration was determined photometrically by DC protein quantification assay method (Bio-Rad). Protein samples were resolved by SDS-PAGE, transferred to a nitrocellulose membrane, and immunoblotted with the target-specific primary antibodies. The overnight application of primary antibodies was followed by incubation with a suitable HRP-coupled secondary antibody (1:10,000; Santa Cruz Biotechnology) or fluorescent antibody Alexa Fluor 546. Finally, visualization was achieved using a chemiluminescence kit (GE Healthcare) and was detected with an imaging system (FluorChem Q; Biozym). Quantitative densitometry was performed using ImageJ version 1.46 software (National Institutes of Health).

7.8.2.5 SDS polyacrylamide gel electrophoresis (SDS-PAGE)

To separate proteins according to their molecular weight, the sodium-dodecyl-sulfate (SDS) polyacrylamide gel electrophoresis (PAGE) system was used. SDS is a molecule that stoichiometrically binds to protein chains by masking the protein's charges and creating an overall negative charge. This allows the proteins to travel in the same direction along an electrical field and get separated as per the molecular weight. For this purpose, an appropriate gel-casting-cassette was set up and filled up to 80% of total height with separating gel containing ~10 % polyacrylamide. Separating gel consisted of separating gel buffer and a 37.5:1 acrylamide: bisacrylamide solution along with water, while TEMED and APS (10%) were added to induce the polymerization. The mixture was vortexed and after pouring the solution in the cassette, it was immediately filled up with isopropanol on top of the separating gel to remove any air bubbles formed after mixing all ingredients by vortexing. After 15-20 min, the isopropanol was discarded and the collecting gel containing 4% polyacrylamide was poured on top of the separating gel. A comb, creating 10/15 pockets was inserted into the collecting gel. After polymerization, the gel-chamber was set up and the combs removed. The pockets were then flushed with running buffer and samples consisting of proteins, water, and Lämmli loading dye was loaded into the gel pockets. Alongside the samples, a pre-stained protein ladder was

also loaded, which acted as a marker of the molecular weights for proteins. An electrical field was applied at a constant voltage of 120 V and the proteins were allowed to separate until the loading dye from the samples reached the bottom of the gel-cassette.

7.8.2.6 Transfer of proteins to nitrocellulose membranes

To transfer the proteins from the polyacrylamide gel to a nitrocellulose membrane, a tank-transfer blotting chamber was used. The SDS-gel with separated proteins embedded into it was carefully taken out of the cassette and set up in the so-called “blotting sandwich”. The setup from bottom to top was: a sponge, three cellulose filter papers, the SDS-gel containing the separated proteins, a nitrocellulose membrane (pore size 0.2 μm), three cellulose filter papers, and another sponge fixed together in a cassette. The sandwich was set up in the transfer buffer after carefully removing air-bubbles to ensure high quality of transfer of the proteins along the membrane surface. The blotting sandwich-containing cassettes were then placed in the blotting-tanks that were filled up with transfer-buffer and cooled by the addition of -20°C cold ice-packs inside the tank. An electrical field was then applied at constant 4000 mA for 90 min. The transfer was visualized after blotting by assessing the transfer of the pre-stained protein ladder that ran alongside the samples and was visible on the white nitrocellulose membrane. The membrane containing the size-separated proteins was then placed in 5% (w/v) dry-milk powder solved in TBS-T buffer and thus blocked for 1-2 h. In this step, the unspecific protein binding sites of the membrane are saturated with the proteins of the milk powder.

7.8.2.7 Detection of specific proteins on a nitrocellulose membrane

The blocking of unspecific protein binding sites on the membrane was followed by incubation in the primary protein/tag specific antibody. Therefore, the appropriate antibody that binds to the protein of interest's epitope was diluted in 5% (w/v) dry-milk in TBS-T as stated in Table 1. The membrane was then placed in a 50 ml falcon tube, with the protein transferred-side facing the inside of the tube. ~ 5 ml of the diluted antibody + milk solution was pipetted into the tube. The membrane was incubated in the primary antibody solution overnight at 4°C on a roller. Post incubation, the membranes were washed three times for 10 min in TBS-T buffer and incubated with the secondary antibody, coupled to a horseradish-peroxidase (HRP) as stated in Table 2 for

2-3 h at RT. After washing the membrane thrice for 10 min in TBS-T at RT again, the membranes were developed using the Enhanced-chemiluminescence (ECL) system. ECL visualization method uses solutions of diacyl-hydrazine luminol and peroxide to obtain chemiluminescence specifically at those sites on the membrane, where the HRP-coupled secondary antibody is bound to the protein of interest through the primary antibody. The HRP catalyzes the oxidation of the luminol in the presence of hydrogen-peroxide resulting in chemiluminescence that can be detected with the help of a camera. Therefore the luminol-peroxide solutions were mixed in 1:1 ratio, pipetted onto the membrane and incubated for ~3 min in the dark. The membrane was then placed into the detection chamber of the Gel doc. The emitted chemiluminescence was detected using FluorChem Q software and proteins were densitometrically quantified using the ImageJ software.

7.9 Human DCH and HCM heart samples

The left ventricular myocardial tissue samples were acquired from explanted hearts of XX patients (HCM, n = 4; DCM, n = 10; NF, n = 7) with end-stage heart failure (New York Heart Association heart failure classification IV) undergoing heart transplantation. All procedures involving human volunteers were performed in compliance with the ethical committee of the medical school of the Georg-August-University, Göttingen, Germany. The explanted hearts were acquired directly in the operating room during surgical procedures and immediately placed in pre-cooled cardioplegic solution (in mmol/liter: NaCl 110, KCl 16, MgCl₂ 16, NaHCO₃ 16, CaCl₂ 1.2, glucose 11). Myocardial samples were frozen in liquid nitrogen and stored at -80°C immediately after excision. Further, they were utilized to perform Western blot and RT-qPCR analysis as described above.

7.10 Statistical analyses

All results are shown as the mean \pm S.E. for all experiments unless stated otherwise. Statistical analyses of the data were performed using the two-tailed Student's t-test. When necessary, two-way analysis of variance (ANOVA) followed by Student-Newman-Keuls post hoc tests was applied. p values of less than 0.05 were considered statistically significant, p < 0.05; **, p < 0.01; ***, p < 0.001; ns, non-significant.

8 Results

8.1 TRIM24 and TRIM32 are putative cardiac interaction partners of Dysbindin

SRF is one of the founding members of the MADS-box family of transcription factors. This family of transcription factors regulates expression of various genes by binding to their specific promoter sequence known as CarG box (Shore and Sharrocks, 1995); (Miano, 2010); (Kuwahara and Nakao, 2011). By virtue of CarG box binding, SRF modulates the expression of a major subset of cardiac-specific genes both during embryonic development and cardiac pathogenesis with increased fetal cardiac gene expression; while its deletion leads to lethal cardiac defects (Zhang et al., 2001a; Zhang et al., 2001b); (Parlakian et al., 2004); (Miano et al., 2004). In one of the previous papers from our lab, it has been established that Dysbindin, a well-known schizophrenia susceptibility protein, is also a robust inducer of RhoA-SRF-mediated cardiac hypertrophy (Rangrez et al., 2013).

In search of new cardiac-specific binding partners of Dysbindin and thus, further players in SRF-mediated hypertrophic signaling, a yeast two-hybrid (Y2H) screening was performed using Dysbindin as bait against human cardiac cDNA library as the prey. The Y2H assay is a genetic system wherein the interaction between two proteins is detected through the reconstitution of a transcription factor and the subsequent activation of reporter genes under the control of this transcription factor (Fields and Song, 1989). This Y2H screening with Dysbindin as bait revealed various well-known hypertrophic genes like *MYH6*, *MYH7*, *NPPA*, and *RhoA* as potential partners. Interestingly, TRIM24, a tripartite motif-containing family E3 ubiquitin ligase, was also identified as one of the potential interaction partners of Dysbindin (Table 13). In the literature TRIM32, which is another TRIM E3 ligase has earlier been reported to interact with Dysbindin in skeletal muscle cells through its coiled-coil domain (Locke et al., 2009). This established link with another TRIM family member prompted us to characterize the cardiac role of TRIM24, as well as to confirm the Dysbindin-TRIM32 cardiac interaction, and link it to Dysbindin and further RhoA-SRF mediated hypertrophic signaling.

Table 13: List of putative Dysbindin-binding partners. The proteins are arranged alphabetically, identified through a yeast two-hybrid screen performed using human Dysbindin as bait against human cardiac cDNA library. (Borlepawar et al., 2017, © the American Society for Biochemistry and Molecular Biology)

Prey	Description	Gene ID
ALDOA	Aldolase A, fructose-bisphosphate	226
ANKRD2	Ankyrin repeat domain 2	26287
APPL1	Adaptor protein, phosphotyrosine interaction, PH domain, and leucine zipper containing 1	26060
ATP5B	ATP synthase, H ⁺ -transporting, mitochondrial F1 complex, β -polypeptide	506
CTDNEP1	CTDNEP1 CTD nuclear envelope phosphatase 1	23399
CYB5R3	Cytochrome <i>b5</i> reductase 3	1727
EIF2B4	Eukaryotic translation initiation factor 2B, subunit 4 δ a, 67 kDa	8890
HADHB	Hydroxyacyl-coA dehydrogenase/3-ketoacyl-coA thiolase/enoyl-coA hydratase (trifunctional protein), β subunit	3032
LIMA1	LIM domain and actin binding 1	51474
MYH6	Myosin, heavy chain 6, cardiac muscle, α	4624
MYH7	Myosin, heavy chain 7, cardiac muscle, β	4625
NDUFB8	NADH dehydrogenase (ubiquinone) 1 β subcomplex subunit 8, mitochondrial precursor	4714
NLRP1	NLR family, pyrin domain containing 1	22861
NMNAT1	Nicotinamide mononucleotide adenylyltransferase1 (EC 2.7.7.1) (NMN adenylyltransferase 1)	64802
NPPA	Natriuretic peptide precursor A	4878
OPTN	Optineurin	10133
PES1	Pescadillo homolog 1, containing BRCT domain	23481
RARG	Retinoic acid receptor, γ	5916
RHOA	<i>ras</i> homolog gene family, member A	387
SHMT1	Serine hydroxymethyltransferase 1 (soluble)	6470
SNRPN	Small nuclear ribonucleoprotein polypeptide N	6638

SNURF	SNURF SNRPN upstream reading frame	8926
TNNT2	Troponin T type 2 (cardiac)	7139
TRIM24	Tripartite motif-containing protein 24 (TIF1-α, RNF82)	8805

8.2 TRIM24 and TRIM32 exhibit endogenous cardiac expression

Subsequently, for establishing the rationale of TRIM24 being a cardiac binding partner of Dysbindin, it was vital to observe if TRIM24 is endogenously present in the heart. With previous reports of TRIM32 being an interaction partner of Dysbindin in skeletal muscle, we studied both Dysbindin-TRIM24 interaction with Dysbindin-TRIM32 interaction, to elucidate the cardiac role of both these TRIMs together in regard with Dysbindin. Interestingly, the tissue distribution patterns of TRIM24 and TRIM32 in wild-type C57BL/6 mice showed ubiquitous expression with a significant cardiac presence at mRNA level; further strengthening the possibility of a cardiac role (Figure 8A). However, at the protein level, TRIM24 was maximally expressed in skeletal muscle, whereas TRIM32 was predominantly expressed in the brain (Figure 8B). Additionally, both the TRIMs showed significant expression levels in the heart tissue.

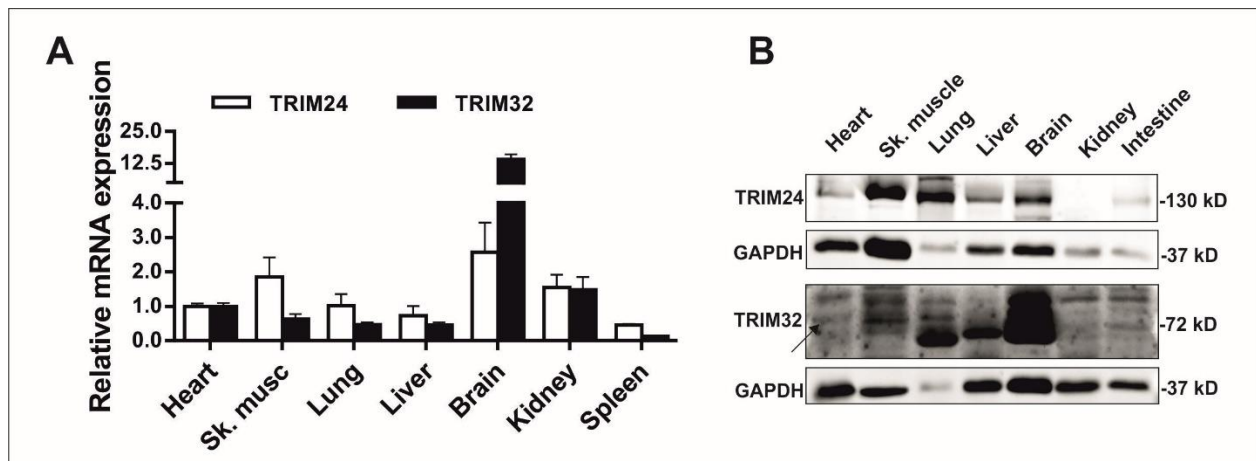


Figure 8: TRIM24 and TRIM32 are endogenously present in mouse heart. Mice used for multi-tissue expression monitoring were wild-type C57BL/6 mice. **(A)** Relative expression of TRIM24 and TRIM32 mRNA levels in different mouse organs, determined by qRT-PCR and normalized to expression in the heart (N=4). **(B)** Representative immunoblots indicating the tissue distribution of TRIM24 and TRIM32 in protein mixture isolated from various mouse organs. Sk. muscle, skeletal muscle. (Modified from: Borlepawar et al., 2017, © the American Society for Biochemistry and Molecular Biology)

8.3 TRIM24 and TRIM32 are differentially expressed after biochemical and biomechanical stress

We then analyzed the expression of TRIM24/32 in mouse models of cardiac hypertrophy induced either by biomechanical stress due to transverse aortic constriction (TAC) or by controlled infusion of the α -adrenergic agonist phenylephrine (PE) to determine the (patho)-physiological relevance, if any, of these TRIMs. Sham-operated and mice infused only with phosphate buffered saline (PBS) served as the respective control groups. At the protein level, TRIM24 was significantly up-regulated in PE-treated mice (Figure 9A-B), but its expression remained unchanged in TAC-operated mice (Figure 9D-E). However, TRIM24 transcript levels were unaffected in both of the mouse models (Figure 9C, 9F). TRIM32 also displayed no change in the mRNA levels (Figure 9C, 9F), but its expression at the protein level was significantly reduced in both hypertrophic models (Figure 9A, 9B, 9D, and 9E). This differential expression suggested a possible involvement of TRIM24 and TRIM32 in cardiac (patho)-physiology.

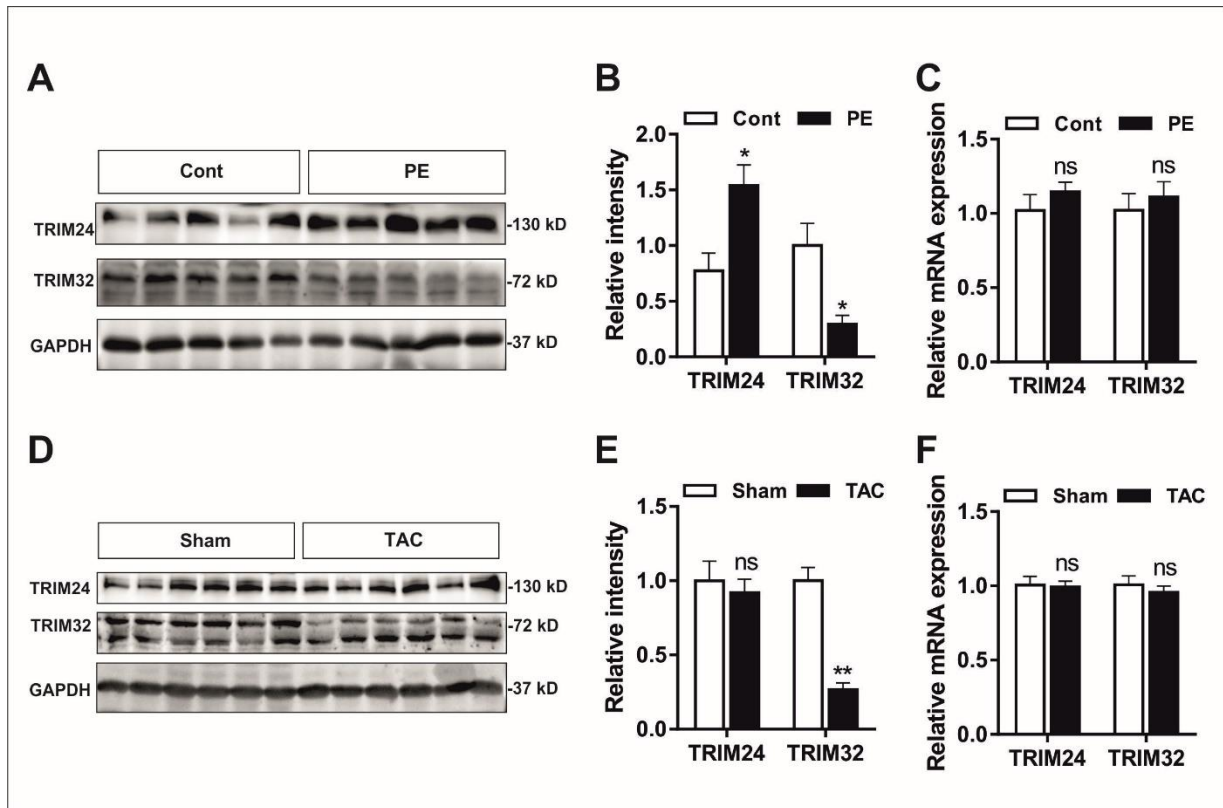


Figure 9: TRIM24 and TRIM32 are differentially regulated in biochemical and biomechanical stress in mouse heart. (A) Protein expression of TRIM24 and TRIM32 in control (PBS) and phenylephrine (PE)-treated mice. Osmotic mini-pumps filled with PE (25 μ g/kg body weight/min) prepared in PBS with 1 mg/ml L-ascorbate (Sigma) were

implanted subcutaneously in 8-week-old wild-type C57BL/6 mice and were housed for 2 weeks. Control mice received vehicle L-ascorbate in PBS. Post-2-week implantation, proteins isolated from the hearts of these mice were immunoblotted against respective TRIM antiserum. n = 5. Respective densitometry analysis is shown in **(B)**, with GAPDH as an endogenous control. **(C)** Quantitative real-time PCR was performed with mRNA to identify the transcript levels of TRIM24 and TRIM32 in PE-treated mice, compared with the control mice group. **(D)** Protein expression of TRIM24 and TRIM32 in TAC or sham-operated mice. 8-Week-old wild-type C57BL/6 mice were subjected to TAC operations, and heart samples were used for protein isolation 2 weeks post-operation. Protein samples were again immunoblotted against respective TRIM antiserum. n = 6. Respective densitometry analysis is shown in **(E)** with GAPDH as an endogenous control. **(F)** Transcript levels of TRIM24 and TRIM32 were determined with mRNA by qRT-PCR in sham versus TAC-operated mouse hearts. Statistical significance was determined using two-tailed Student's t-test. Error bars show mean \pm S.E. *, p < 0.05; **, p < 0.01; ***, p < 0.001; ns, non-significant. Cont, control; PE, phenylephrine; TAC, transverse aortic constriction. (Modified from: Borlepawar et al., 2017, © the American Society for Biochemistry and Molecular Biology)

8.4 TRIM24 and TRIM32 are differentially expressed in human cardiomyopathies

In the next step, we asked whether protein levels of TRIM24 and TRIM32 are altered in human patients suffering from hypertrophic or dilated cardiomyopathy (HCM/DCM). Similar to the effects observed in hypertrophic mice, TRIM24 displayed a striking increase in both HCM and DCM heart tissues, whereas TRIM32 again showed a significant reduction in protein levels compared with samples of non-failing (NF) heart (Figure 10 A, 10B, 10D and 10E). Thus, the consistent dysregulation of the TRIM24/32 expression in hypertrophic datasets obtained from animal models and human patients indicated the relevance of both TRIMs in the pathogenesis of cardiac hypertrophy and cardiomyopathy. This prompted us to further investigate their functional characteristics *in vitro*.

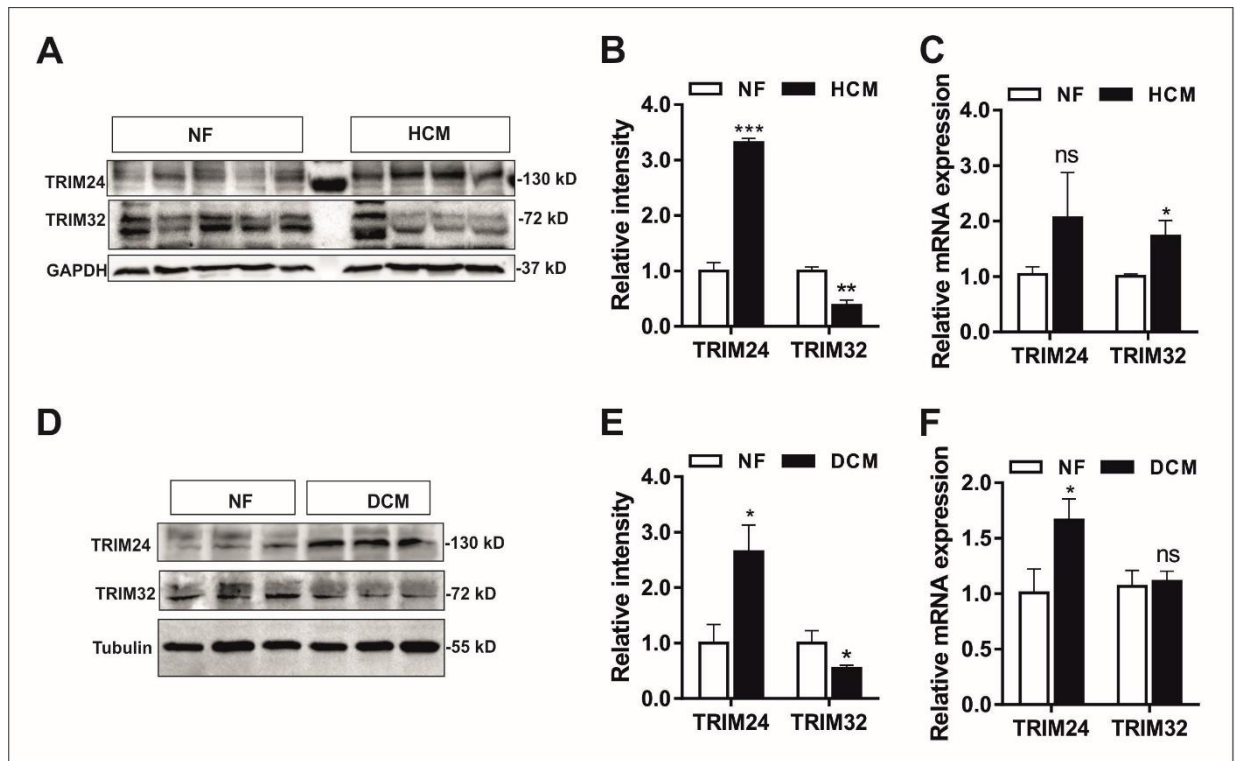


Figure 10: TRIM24 and TRIM32 are differentially regulated in human dilated and hypertrophic cardiomyopathies. (A) Protein expression of TRIM24 and TRIM32 in non-failing (NF, n = 7) and hypertrophic cardiomyopathy (HCM, n = 4)-affected human hearts. (B) Densitometric analysis was performed for respective immunoblots from A, with GAPDH as an endogenous loading control. (C) Quantitative real-time PCR was performed to identify the transcript levels of TRIM24 and TRIM32 in NF versus HCM patients. (D) Protein expression of TRIM24 and TRIM32 in non-failing (NF, n = 7) and dilated cardiomyopathy (DCM, n = 10) affected human hearts. (E) Densitometric analysis was performed for respective immunoblots from D, with tubulin as an endogenous loading control. (F) Quantitative real-time PCR was performed to identify the transcript levels of TRIM24 and TRIM32 in NF versus DCM patients. Statistical significance was determined using two-tailed Student's t-test. Error bars show mean \pm S.E. *, $p < 0.05$; **, $p < 0.01$; ***, $p < 0.001$; ns, non-significant. Cont, control; PE, phenylephrine; TAC, transverse aortic constriction. (Modified from: Borlepawar et al., 2017, © the American Society for Biochemistry and Molecular Biology)

8.5 TRIM24 and TRIM32 interact with Dysbindin in HEK293A cells

Protein-protein interactions define the modulation of protein functions and thus the biological activity of proteins. Such interactions can be predicted using biological and genetic methods like protein probing, the two-hybrid system, phage display, isolation of extragenic suppressors, synthetic mutants, and unlinked non-complementing mutants, etc. The predictions can be confirmed with the help of various biochemical methods like protein affinity chromatography, affinity blotting, co-immunoprecipitation and cross-linking (Phizicky and Fields, 1995). Co-immunoprecipitation (co-IP) is a frequently used biochemical technique to identify physiologically relevant protein-protein interactions by using target protein-specific antibodies.

Specific antibodies indirectly capture proteins that are bound to a specific target protein from a protein lysate. These protein complexes can then be analyzed using western blotting to identify new binding partners of the target protein.

For establishing interactions between Dysbindin and TRIM24/32, mammalian overexpression vectors were generated using Gateway cloning technology. Dysbindin was cloned into pDest40 with C-terminal V5 tag and TRIM24/32 were cloned into pcDNA3.1 with N-terminal Flag-tag. Subsequently, TRIM24 was co-transfected using Lipofectamine2000 with or without V5-Dysbindin in HEK293A cells. A co-IP was performed using Flag-tagged (for TRIM24) monoclonal antibody beads, where proteins having an affinity for TRIM24 can be pulled down. A western blot was performed using this pulled down protein mixture and was developed against V5 (for Dysbindin) antibody (Figure 12A). This showed successful pulldown of Dysbindin by TRIM24. To confirm this interaction via reversal of strategy, Dysbindin was coexpressed with or without Flag-TRIM24. Proteins were pulled using V5 tagged monoclonal antibody beads and immunoblotted against Flag antibody (Figure 12B). This two-way co-IP confirmed Dysbindin-TRIM24 interaction. A similar strategy was applied to confirm the interaction between V5-Dysbindin and Flag-TRIM32 (Figure 12C-D). Together, the potential interaction of these two TRIM family member proteins with Dysbindin was verified by co-IP in HEK293A cells, where, Dysbindin was successfully pulled down with TRIM24/32 and vice versa.

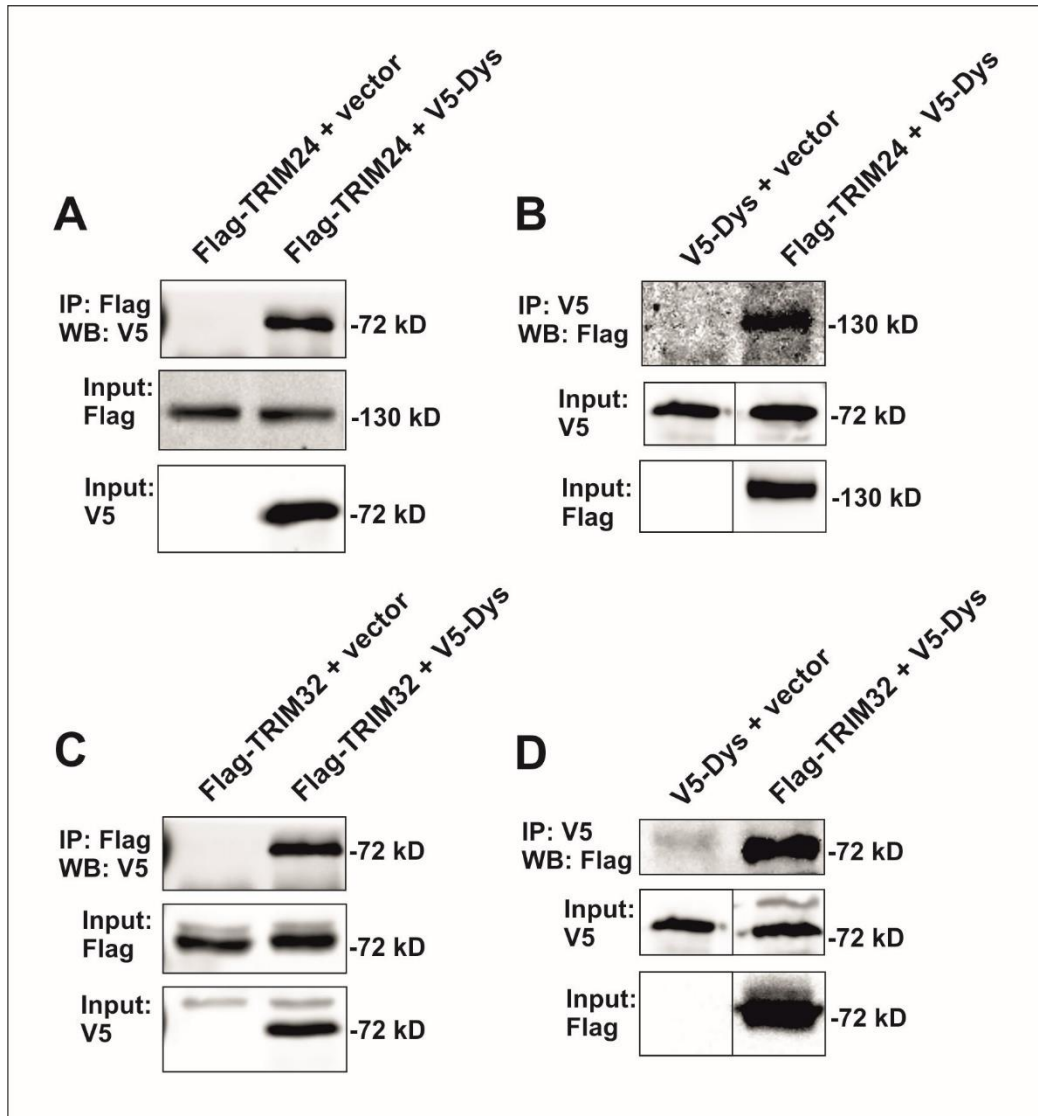


Figure 11: TRIM24 and TRIM32 are interaction partners of Dysbindin. HEK293A cells were co-transfected with V5-tagged Dysbindin and FLAG-tagged TRIM24 or TRIM32. Empty vector co-transfected with Dysbindin, TRIM24, or TRIM32 was used as a filler plasmid. Input immunoblots against V5 antibody show expression of V5-Dysbindin, while immunoblots against Flag antibody show expression of the respective Flag-TRIM protein. Immunoprecipitation was performed using anti-V5 or FLAG tag cross-linked magnetic beads. Precipitated proteins were immunoblotted with respective antibodies. Dysbindin was found to be co-precipitated with TRIM24 (**A**) and vice versa (**B**). Similarly, TRIM32 and Dysbindin pulled down each other (**C** and **D**, respectively), although no interaction was seen in control IP (lane 1 in each blot), confirming the interaction between Dysbindin and TRIM24/32. IP, immunoprecipitation; WB, western blot; vector, empty vector control; Dys, Dysbindin. (Modified from: Borlepawar et al., 2017, © the American Society for Biochemistry and Molecular Biology)

8.6 Dysbindin interacts with TRIM24 via its coiled-coil domain

Dysbindin is known to bind with other proteins through its coiled-coil domain. Most notably, it binds with various dystrobrevins in muscles and brain via this domain (Benson et al., 2001). To validate if the interaction between Dysbindin and TRIM24 is assisted by coiled-coil domain too,

we fragmented Dysbindin into four segments and cloned them into pDest40 with C-terminal V5-tag via gateway cloning technology. These segments were N-terminal + coiled-coil domain, coiled-coil domain, Dysbindin domain and C-terminal + Dysbindin domain (Figure 13A). All Dysbindin fragments were co-transfected with or without Flag-TRIM24 with full-length Dysbindin serving as a positive control in HEK293A cells. The protein lysate was pulled using V5-tagged monoclonal antibody beads and immunoblotted against anti-Flag antibody to seek out domain specific binding of Dysbindin with TRIM24. Anti-Flag immunoblot after IP did successfully pull Flag-TRIM24 by Dysbindin full length, N-terminal + coiled-coil domain and coiled-coil domain segments (Figure 13B) confirming that the coiled-coil domain is a sufficient and necessary domain for the Dysbindin-TRIM24 interaction.

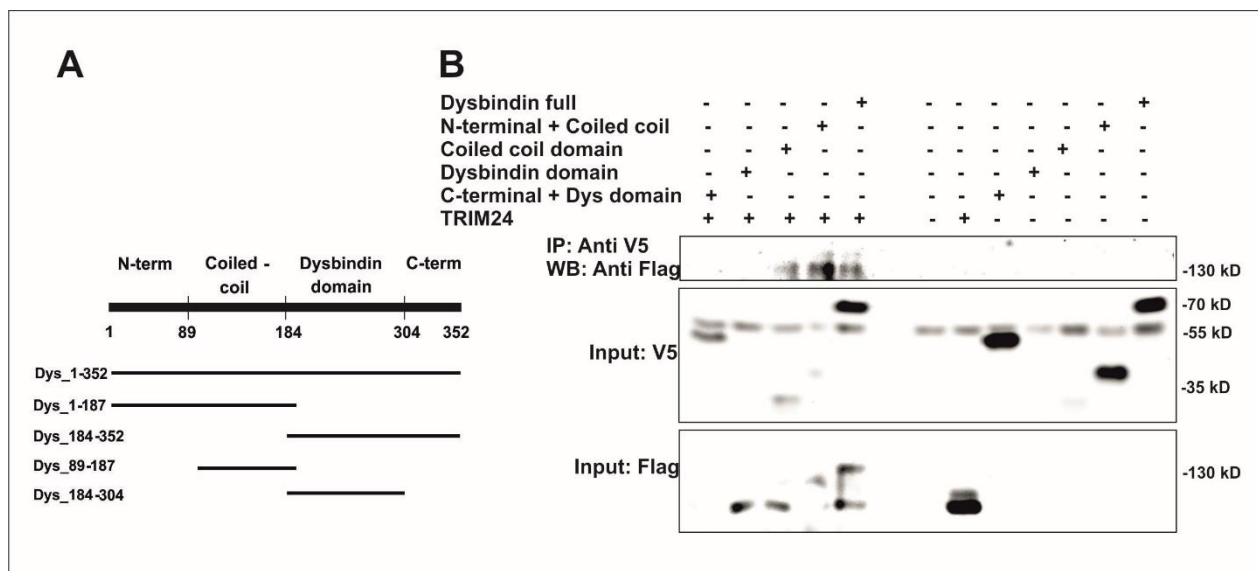


Figure 12: Dysbindin interacts with TRIM24 through the coiled-coil domain. (A) Schematic diagram representing different domain fragments of Dysbindin, to check the domain-specific interaction of TRIM24 with Dysbindin. (B) Co-IP of TRIM24 and various Dysbindin fragments. HEK293A cells were co-transfected with plasmids encoding V5-tagged Dysbindin fragments and Flag-tagged TRIM24 as depicted in the figure. Input immunoblot against V5 antibody show expression of V5-Dysbindin fragments, while immunoblotting against Flag antibody show expression of Flag-TRIM24. Immuno-precipitation was performed using anti-V5-tagged magnetic beads. Empty vector was used as a negative control. Precipitated proteins were immunoblotted with Flag-antiserum. TRIM24 was co-precipitated with Dysbindin full-length protein along with N-terminal + Coiled-coil and Coiled-coil domain containing fragments of Dysbindin, suggesting the Coiled-coil domain of Dysbindin is sufficient for interaction with TRIM24. IP, immunoprecipitation; WB, western blot; vector, Dys, Dysbindin. (Modified from: Borlepawar et al., 2017, © the American Society for Biochemistry and Molecular Biology)

8.7 Validation of vector expression efficiency in cardiomyocytes

The differential cardiac regulation of TRIM24 and TRIM32 in various hypertrophic and cardiomyopathy mouse & human samples presented a strong case for the functional characterization of TRIM proteins in the heart. For this purpose, we generated various adenoviral expression vectors to induce altered expression of these proteins in the presence or absence of Dysbindin. The major emphasis was on establishing the interaction between Dysbindin and TRIM24/32 proteins, and further characterization of hypertrophic parameters like cell size measurement and SRF-signaling.

8.7.1 Dysbindin, TRIM24 and TRIM32 overexpression in cardiomyocytes via adenoviruses

For overexpression of Dysbindin, TRIM24, and TRIM32 in cardiomyocytes adenoviral vectors were generated from mouse/human cDNA via gene targeted gateway cloning as stated in methods part of this thesis. The optimum overexpression at the protein level was observed for Dysbindin with 50 ifu (Figure 14A-B), while both TRIM24/32 were added at 100 ifu (Figure 14C-F) concentration throughout this work, unless and otherwise mentioned, to induce a prominent effect on Dysbindin.

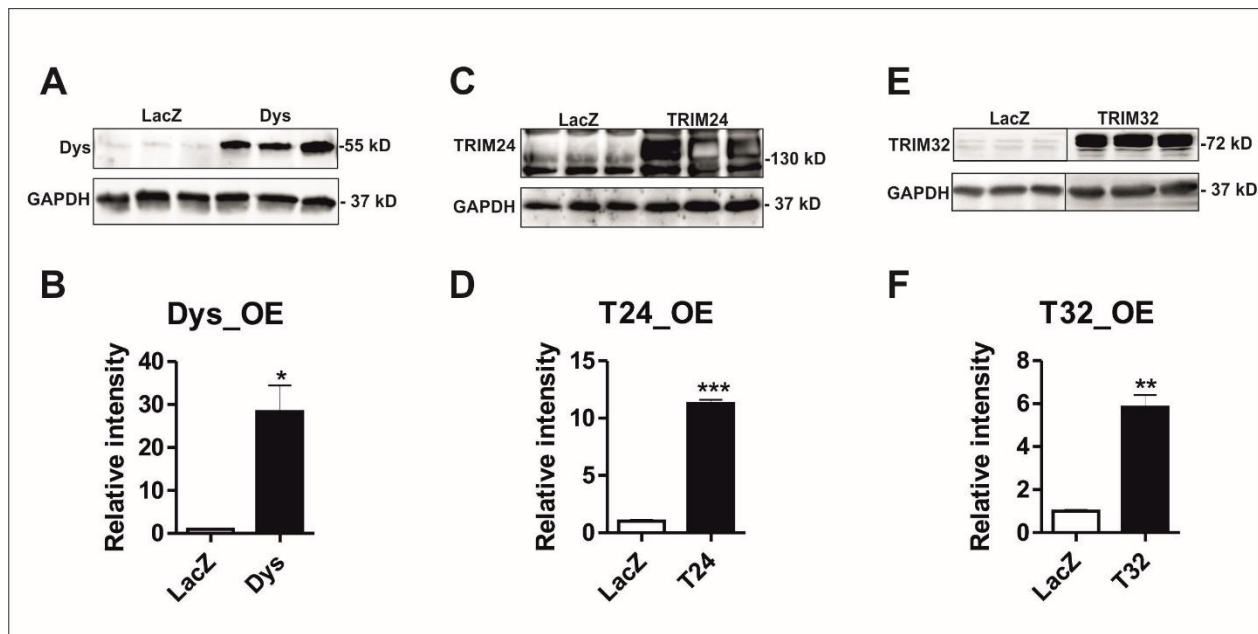


Figure 13: Validation for the efficiency of adenoviral overexpression vectors. (A) Dysbindin with densitometry analysis (B), (C) TRIM24 with densitometry analysis (D) and (E) TRIM32 with densitometry analysis (F). Statistical significance was determined using two-tailed Student's t-test. Error bars show mean \pm S.E. *, $p < 0.05$; **, $p < 0.01$; ***, $p < 0.001$; ns, non-significant. Dys, Dysbindin; T24, TRIM24; T32, TRIM32; OE, overexpression.

8.7.2 Dysbindin, TRIM24 and TRIM32 knockdown in cardiomyocytes via siRNA and microRNAs

Knockdown of Dysbindin in NRVCMs was achieved using a siRNA mixture specific for rat Dysbindin from Santa Cruz Biotechnology (#sc-106988). According to user guidelines, a specific dose of siDysbindin was established that lead to a ~70-80 % knockdown of endogenous Dysbindin (Figure 15A-B). For knockdown of TRIM proteins adenoviruses consisting of synthetic micro-RNAs specific for rat TRIM24 (miRTRIM24) and TRIM32 (miRTRIM32) were developed using Block-it microRNA synthesis kit and gateway cloning strategy, as stated in methods part. A knockdown of ~90% for TRIM24 (Figure 15C-D) and ~60% for TRIM32 (Figure 15E-F) was achieved with the help of microRNA-containing adenoviruses (200 ifu). Equal ifu concentrations were maintained for respective TRIMs in all prospective experiments of this thesis.

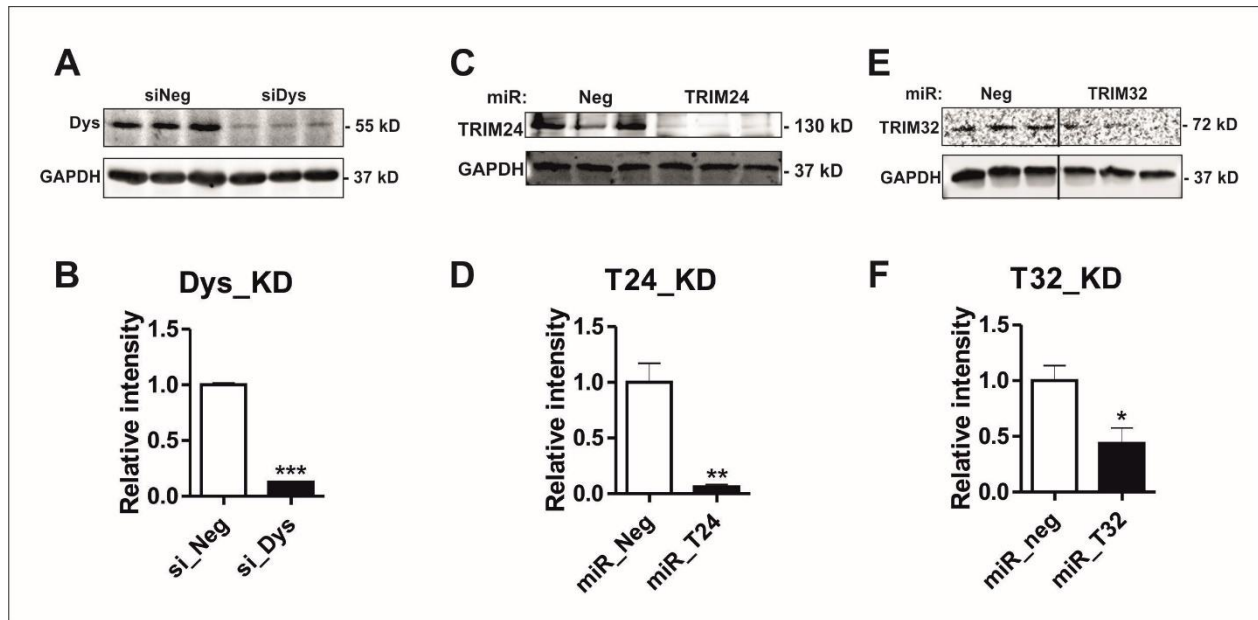


Figure 14: Validation for knock-down of native Dysbindin, TRIM24, and TRIM32 in NRVCMs. (A) Dysbindin by siRNA with densitometry analysis (B), (C) TRIM24 by miRNA with densitometry analysis (D) and (E) TRIM32 by miRNA with densitometry analysis (F) at the protein level. Statistical significance was determined using two-tailed Student's t-test. Error bars show mean \pm S.E. *, $p < 0.05$; **, $p < 0.01$; ***, $p < 0.001$; ns, non-significant. siRNA, small interfering RNA; miR, microRNA; neg, negative; Dys, Dysbindin; T24, TRIM24; T32, TRIM32; KD, knockdown.

8.8 Dysbindin interacts with TRIM24 and TRIM32 in cardiomyocytes

Our next aim was to validate Dysbindin interaction with TRIM24 and TRIM32 in cardiomyocytes. Neonatal rat ventricular cardiomyocytes (NRVCMs) were infected with the adenoviruses expressing HA-Dysbindin (50 ifu), TRIM24 (100 ifu) and TRIM32 (100 ifu) in various combinations

for TRIM24/32. Co-IP was performed using NRVCM protein lysate with anti-HA magnetic beads (Dysbindin) to pulldown proteins interacting with Dysbindin and samples containing pulled down proteins were separately immunoblotted against anti-TRIM24/32 antibodies. Distinct immunoblots after co-IP did successfully display HA-Dysbindin interacting with both TRIM24 (Figure 16A) and TRIM32 (Figure 16B).

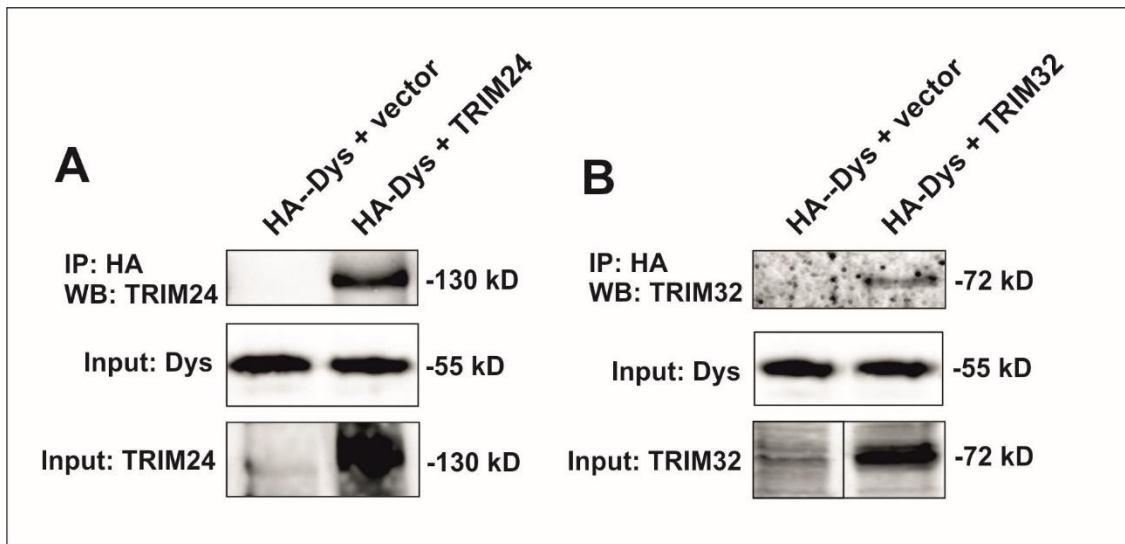


Figure 15: TRIM24 and TRIM32 are cardiac interaction partners of Dysbindin. We also performed co-IP by overexpressing HA-tagged Dysbindin in NRVCMs and precipitated using anti-HA tag cross-linked magnetic beads. Precipitated proteins were immunoblotted with TRIM24 (**A**) and TRIM32 (**B**) antiserum and the interaction between Dysbindin and TRIM24 or TRIM32 was further validated. Vertical black lines in the blots indicate that the intervening lanes have been spliced out. IP, immunoprecipitation; WB, western blot; vector, empty vector control; Dys, Dysbindin. (Modified from: Borlepawar et al., 2017, © the American Society for Biochemistry and Molecular Biology)

8.9 Dysbindin localizes with TRIM24 and TRIM32 in cardiomyocytes

To facilitate interaction with each other, it is essential for the proteins to be present in close proximity or in a similar subcellular compartment. Immunostaining of proteins with the help of specific antibodies against them gives an idea of their (co)localization in the cell. Subcellular localization of both TRIMs and their co-localization with Dysbindin were thus determined by high-resolution confocal imaging in NRVCMs by co-immunostaining Dysbindin with either TRIM24- or TRIM32-specific antibodies. Similar to Dysbindin, endogenous TRIM24 was found to be predominantly located in the nuclear and perinuclear region (Figure 17A, upper panel). On the one hand, endogenous TRIM32 was localized throughout the cell, but on the other hand, it was concentrated in the perinuclear region (Figure 17A, lower panel). Robust Mander's

colocalization coefficients (MCC) were measured for endogenous TRIM proteins after they co-localize with Dysbindin (~ 93% co-localization, Figure 17A) in NRVCMs. Furthermore, co-immunostaining of Dysbindin, TRIM24, or TRIM32 with α -actinin indicated that these proteins only partially co-localize with sarcomeric α -actinin (Figure 17B), asserting their strong cytoplasmic and nuclear presence.

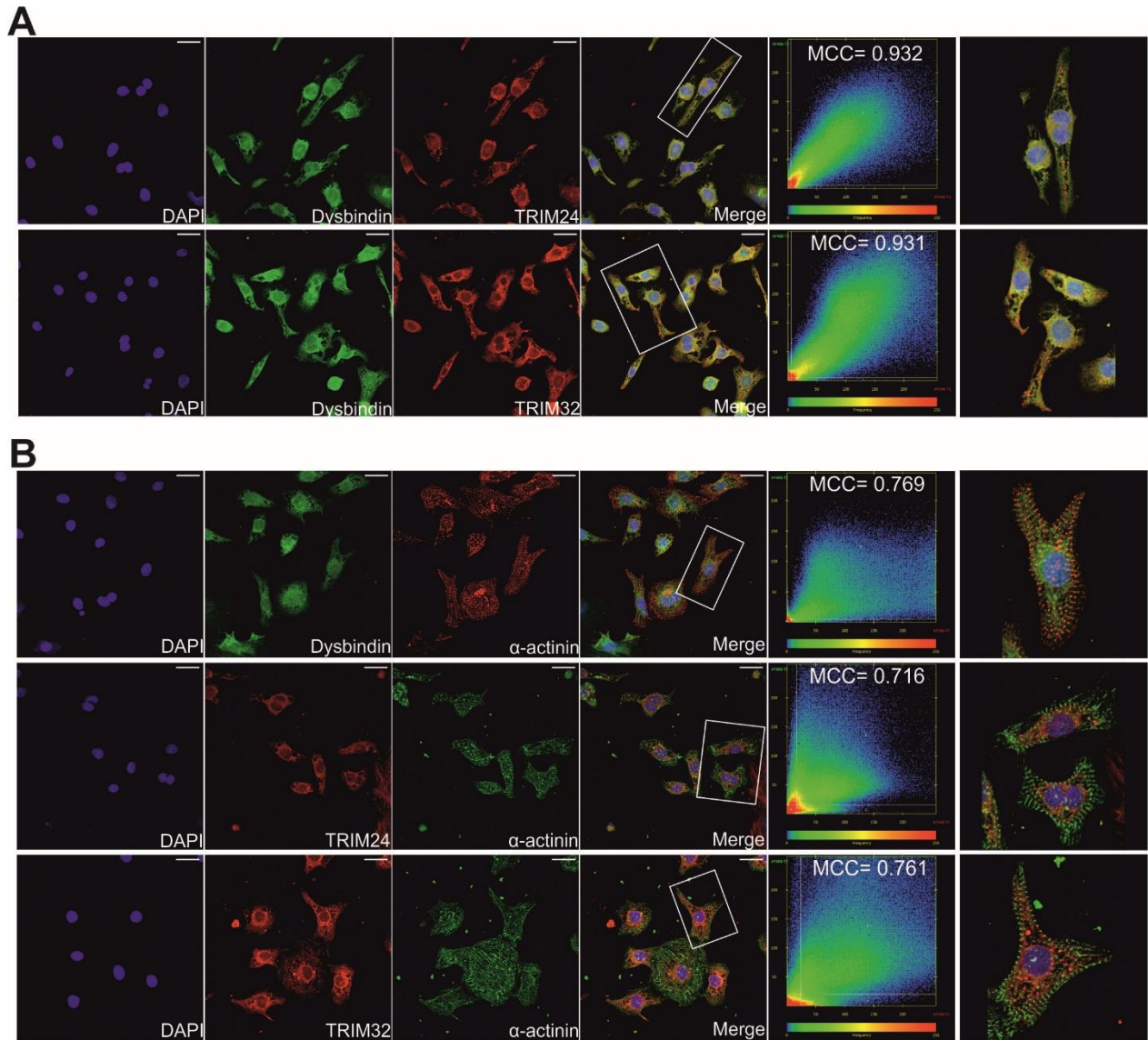


Figure 16: Dysbindin co-localizes with TRIM24 and TRIM32 in NRVCMs. (A) Confocal micrographs representing the co-immunostaining of endogenous Dysbindin with either TRIM24 (upper lane) or TRIM32 (lower lane). **(B)** Co-immunostaining of native Dysbindin (upper panel), TRIM24 (middle panel), or TRIM32 (lower panel) with α -actinin. Nuclei were stained with DAPI, and images were captured with a Zeiss LSM800 laser-scanning microscope. Scatter plots show the analysis of co-localization as described under “Experimental Procedures.” White rectangles represent cropped areas for detailed re-acquisition. MCC = Mander’s colocalization coefficient. Scale bar

(shown with a white line) represents 20 μm . (Modified from: Borlepawar et al., 2017, © the American Society for Biochemistry and Molecular Biology)

8.10 Expression of TRIM24 and TRIM32 discordantly affects cellular levels of

Dysbindin

TRIM24 and TRIM32 are members of the TRIM protein superfamily, mainly consisting of E3 ubiquitin ligases. They contain a Ring finger domain, which is responsible for the transfer of ubiquitin moiety to the target protein. This transfer of ubiquitin is responsible for post-translational ubiquitination of cellular proteins deciding their functional fate, most notably being degraded by the 26s proteasome (Ozato et al., 2008). TRIM24 and TRIM32 were expressed in NRVCs with or without Dysbindin to conclude the fate of its endogenous or overexpressed cellular presence. As expected, the presence of TRIM32 robustly downregulated levels of cellular Dysbindin (Figure 18A-D), while adenovirus-mediated knockdown of TRIM32 using synthetic microRNA resulted in un-altered Dysbindin levels (Figure 18E-F). Interestingly, cellular levels of Dysbindin remained unaffected by either overexpression or knockdown of TRIM24 (Figure 18A-F). The differential fate of Dysbindin levels in NRVCs after expression of TRIM24/32 instigated contradictory effects of these TRIM proteins on Dysbindin suggesting that TRIM32, but not TRIM24, potentially acts as an E3 ubiquitin ligase of Dysbindin in cardiomyocytes.

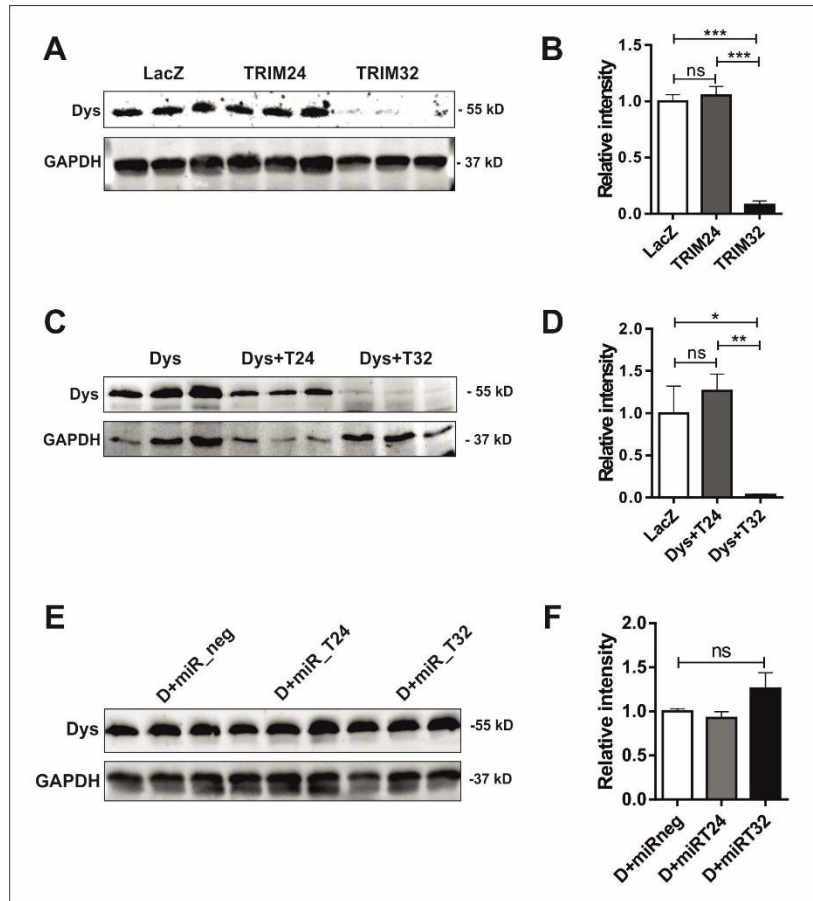


Figure 17: TRIM24 and TRIM32 have an antagonistic effect on Dysbindin protein levels in NRVCs. Effect of adenovirus-mediated overexpression of TRIM24 (Ad-TRIM24, 100 ifu), and TRIM32 (Ad-TRIM32, 100 ifu) on endogenous (A) or overexpressed (B) (Ad-Dysbindin, 50 ifu) Dysbindin protein level indicates that TRIM24 does not, whereas TRIM32 does actively degrade Dysbindin; respective densitometry data are presented as graphs in (C) and (D). (E) Infection with synthetic microRNAs targeting either TRIM24 or TRIM32 did not alter Dysbindin protein levels (densitometry in F). $n = 3$. Statistical significance was determined using two-tailed Student's t-test. Error bars show mean \pm S.E. *, $p < 0.05$; **, $p < 0.01$; ***, $p < 0.001$; ns, non-significant. D and Dys, Dysbindin; T24, TRIM24; T32, TRIM32; miR, microRNA; neg, negative. (Modified from: Borlepawar et al., 2017, © the American Society for Biochemistry and Molecular Biology)

8.11 TRIM24 and TRIM32 affect cellular levels of Dysbindin via ubiquitination

E3 ubiquitin ligases degrade their substrate proteins via UPS. To find if TRIM24/32 exerted effects on Dysbindin via UPS, NRVCs were infected with several combinations of Ad-Dysbindin, Ad-TRIM24, Ad-TRIM32 viruses, and Ad-Ubiquitin (to accelerate ubiquitination) in the presence or absence of MG132 (a proteasomal inhibitor). Along these lines, primarily polyubiquitination of Dysbindin was confirmed in the presence of higher levels of ubiquitin (Figure 19A-B). We then analyzed the effect of proteasomal inhibitor MG132 on the E3 ubiquitin ligation and ubiquitination activity of TRIM24/32. The presence of TRIM24 significantly reduced

even the endogenous ubiquitin-mediated Dysbindin degradation, evident in Figure 19C-D, whereas, MG132 treatment completely abrogated the Dysbindin degradation by ubiquitin, indicating that the Dysbindin degradation is UPS-dependent. Similarly, MG132 treatment absolutely abrogated the Dysbindin degradation by TRIM32 irrespective of the ubiquitin presence (Figure 19F-G). Notably, overexpression of TRIM32 robustly increased ubiquitination of the proteins, whereas TRIM24 exhibited opposite effects (Figure 19E, 19H). Altogether, these data strongly show that TRIM32 acts as an UPS-dependent E3 ubiquitin ligase for Dysbindin, whereas TRIM24 exhibits a protective role.

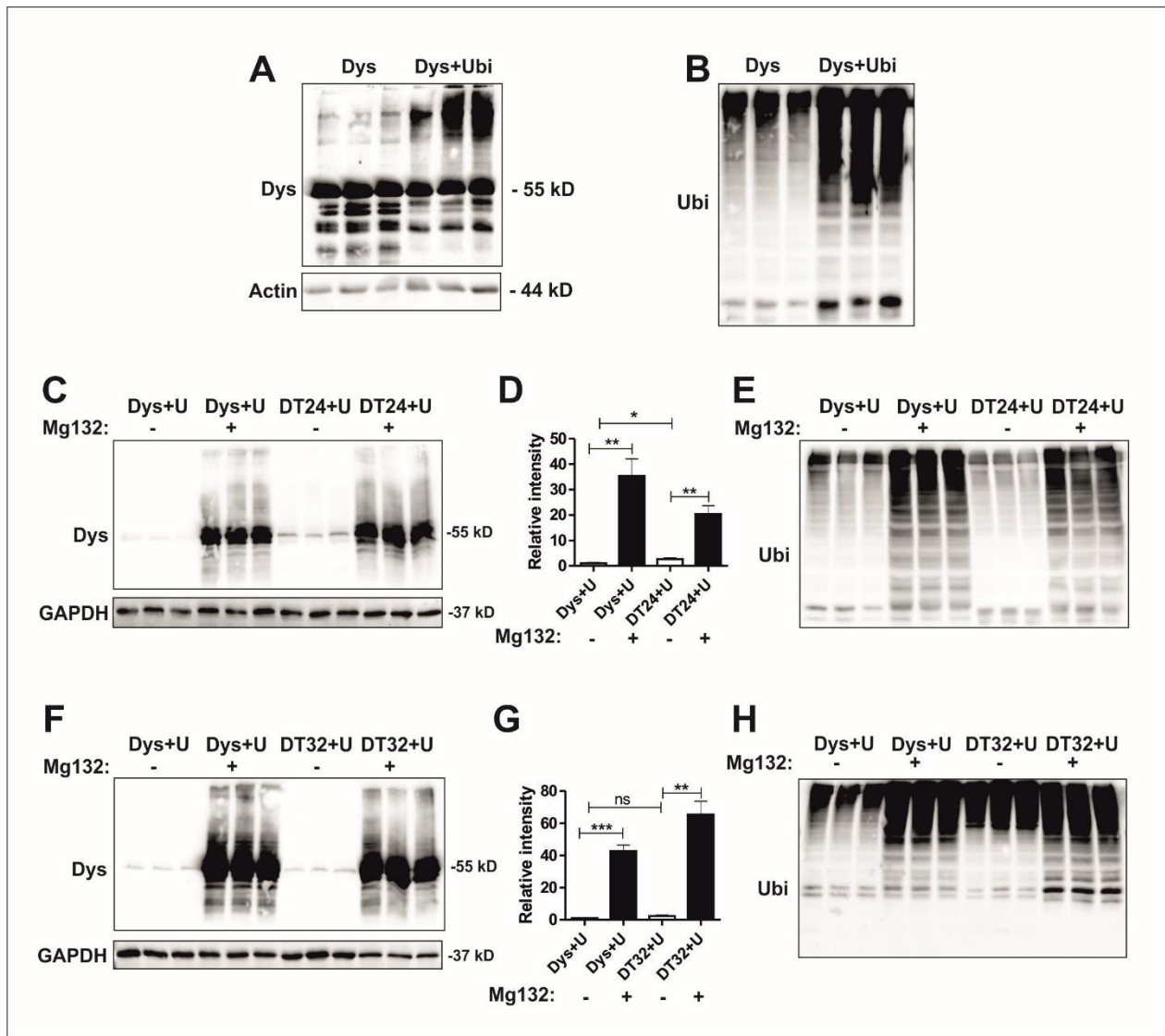


Figure 18: Dysbindin protein levels are regulated by TRIM24 and TRIM32 via ubiquitination. (A) Overexpression of ubiquitin in the presence of Dysbindin led to polyubiquitination of Dysbindin as confirmed by the appearance of high molecular weight bands in lanes 4–6 (ubiquitin overexpression is shown in **B**). **(C)** Effect of ubiquitin and UPS

inhibitor MG132 on Dysbindin protein levels when co-expressed with TRIM24; respective densitometry analysis presented in the graph **(D)** clearly shows that TRIM24 partially restricted Dysbindin degradation due to ubiquitin, whereas MG132 completely prevented Dysbindin degradation suggesting a direct involvement of the UPS system. **(E)** Ubiquitin immunoblot also indicates that the presence of TRIM24 reduces ubiquitin-driven polyubiquitination. Similarly, the presence of MG132 also attenuated the Dysbindin degradation due to TRIM32 **(F and G)**; nevertheless, in contrast to TRIM24, TRIM32 accelerated the polyubiquitination of cardiomyocyte proteins when co-expressed with ubiquitin (H). Statistical significance was determined using two-tailed Student's t-test. Error bars show mean \pm S.E. *, $p < 0.05$; **, $p < 0.01$; ***, $p < 0.001$; ns, non-significant. D and Dys, Dysbindin; T24, TRIM24; T32, TRIM32; U and Ubi, ubiquitin. (Modified from: Borlepawar et al., 2017, © the American Society for Biochemistry and Molecular Biology)

8.12 TRIM24 and TRIM32 have a differential effect on SRF signaling

Dysbindin has previously been identified as a robust inducer of hypertrophic Rho-dependent SRF signaling in NRVCs (Rangrez et al., 2013). To explore the potential effects of both TRIMs on Rho-dependent SRF signaling pathway, TRIM24/32 were overexpressed in the absence or presence of Dysbindin in NRVCs and activation of SRF signaling was assessed using the SRF response element (SRF-RE)-driven firefly luciferase activity with LacZ as a control. Interestingly, by virtue of Dysbindin protective role, TRIM24 exhibited activation of SRF signaling. Furthermore, TRIM24, when co-expressed with Dysbindin displayed an additive effect on the robust activation of SRF signaling by Dysbindin (Figure 20A). To the contrary, by virtue of its degrading role, overexpressed TRIM32 did not show a significant effect on SRF signaling compared with control; notwithstanding, it also strongly diminished the induction of SRF signaling by Dysbindin (Figure 20B). Correspondingly, knockdown of TRIM24 using a TRIM24-specific synthetic microRNA resulted in reduced SRF activation, but no significant difference was observed when this knockdown was followed by Dysbindin overexpression, compared with the overexpression of Dysbindin alone (Figure 20C). Although knockdown of endogenous TRIM32 resulted in a significant increase of SRF-luciferase activity in the presence of Dysbindin, no significant effect of TRIM32 knockdown was observed in the absence of Dysbindin (Figure 20D). Thus, opposite effects on Rho-dependent SRF signaling suggested differential effects of TRIM24/32 on also on functional aspects of cellular Dysbindin activity.

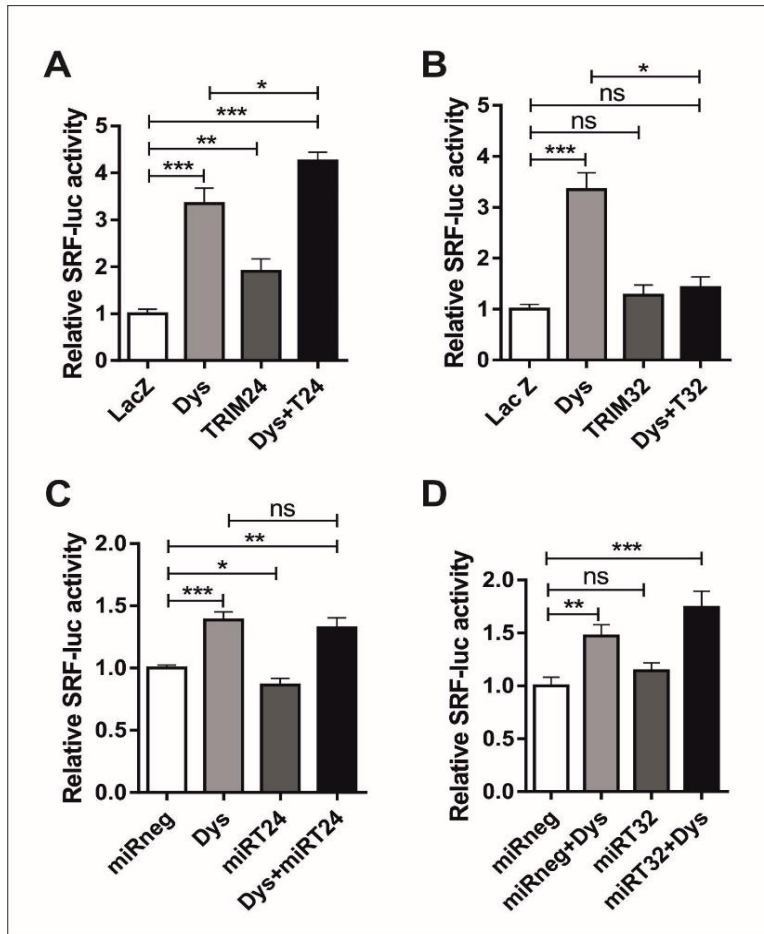


Figure 19: TRIM24 and TRIM32 antagonistically regulate SRF activity in NRVCs. Effect of TRIM24 (A) and TRIM32 (B) on Dysbindin-mediated luciferase activity determined by SRF-RE firefly luciferase reporter assay in NRVCs. Adenoviruses expressing Dysbindin (Ad-Dysbindin, 50 ifu), TRIM24 (Ad-TRIM24, 100 ifu), TRIM32 (Ad-TRIM32, 100 ifu), SRF-RE reporter-based firefly luciferase (Ad-SRF-luc, 20 ifu), and Renilla luciferase (Ad-Renilla-luc, 5 ifu, control) were used for infection in NRVCs. Adenovirus expressing -galactosidase (Ad-LacZ) was used as a control or to maintain the equal quantity of virus used for infection. Data shown are means of three independent experiments, n = 6. Synthetic microRNAs specific for TRIM24 (miRT24) (C) or TRIM32 (miRT32) (D) was used for knockdown of endogenous TRIMs in NRVCs to determine its effect on Dysbindin-mediated SRF signaling by luciferase assay. Synthetic microRNA not targeting any transcript (miRneg) was used as a negative control. Data shown are means of two independent experiments performed in sextuplicate. Statistical significance was determined using two-tailed Student's t-test. Error bars show mean \pm S.E. *, $p < 0.05$; **, $p < 0.01$; ***, $p < 0.001$; ns, non-significant. Dys, Dysbindin; T24, TRIM24; T32, TRIM32; miRT24, microRNA-TRIM24; miRT32, microRNA-TRIM32. (Modified from: Borlepawar et al., 2017, © the American Society for Biochemistry and Molecular Biology)

8.13 TRIM24 and TRIM32 inversely affect cell surface area in cardiomyocytes

To investigate the (patho-) physiological role of TRIM24/32 expression, we performed comparative analyses of the effects of Dysbindin, TRIM24, and TRIM32 on the growth and hypertrophy of NRVCs. The pro-hypertrophic effect of Dysbindin expression was evident as expected, where TRIM24 expression also exerted a similar effect resulting in increased cell

surface area (Figure 21A-B). In contrast, TRIM32 markedly reduced cell size when compared with cardiomyocytes expressing Dysbindin or TRIM24 by virtue of abrogation of Dysbindin levels and its pro-hypertrophic effects (Figure 21A-B).

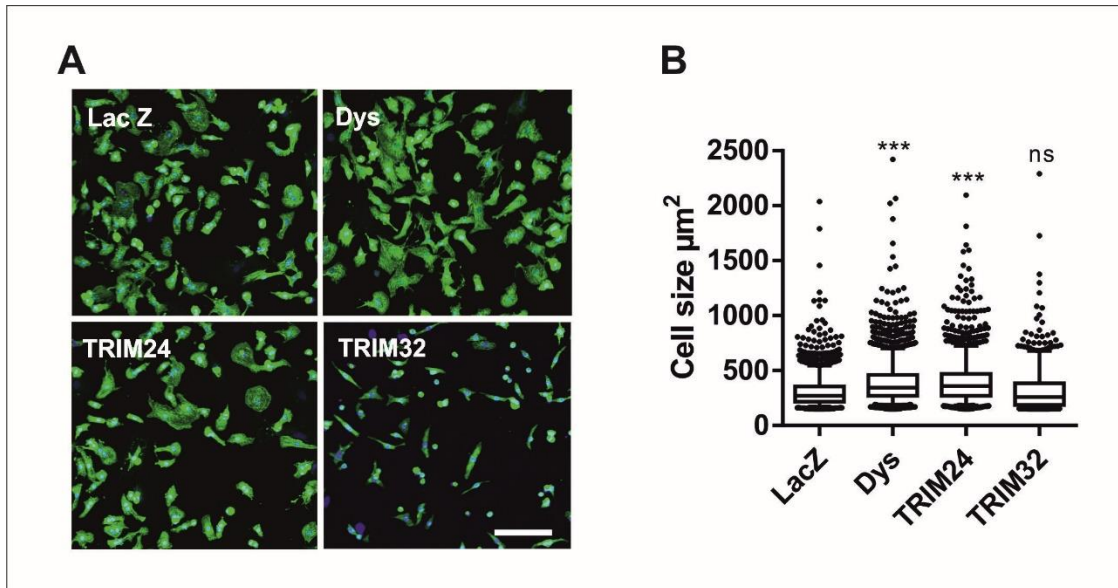


Figure 20: TRIM32 adversely affects cell surface area in cardiomyocytes. (A) Representative images for cell-size analysis after overexpression of particular proteins. NRVCMs were cultured on coverslips in triplicates, infected with adenovirus expressing LacZ (Ad-LacZ, control), Dysbindin (Ad-Dysbindin, 50 ifu), TRIM24 (Ad-TRIM24, 100 ifu), and TRIM32 (Ad-TRIM32, 100 ifu) for 72 h, and immunostained with α -actinin which is specific for sarcoplasmic z-disc. Nuclei were stained with DAPI. Cell size analysis was performed on images taken with a Keyence fluorescence microscope. (B) Cell surface area of the respective datasets was measured from randomly selected cells from three independent coverslips using ‘Macro Cell Count’ analyzer from BZ-II software. The experiment was repeated three times in triplicates. Data shown are means of two independent experiments performed in sextuplicates with ≥ 500 cells per condition. Scale bar (shown with a white line) represents 100 μm . Statistical significance was determined using two-tailed Student’s t-test. Error bars show mean \pm S.E. *, $p < 0.05$; **, $p < 0.01$; ***, $p < 0.001$; ns, non-significant. Dys, Dysbindin. (Modified from: Borlepawar et al., 2017, © the American Society for Biochemistry and Molecular Biology)

8.14 TRIM24 protects Dysbindin from TRIM32-mediated degradation and further promotes cardiomyocyte hypertrophy

Finally, we asked whether TRIM24 exhibits the potential to protect Dysbindin degradation and downstream signaling via inhibition of TRIM32-mediated Dysbindin degradation. Therefore, we repeated analysis of the pro-hypertrophic markers like cell surface area measurements, SRF signaling assays, and assessment of Dysbindin protein levels in a set of experimental conditions where Dysbindin was co-expressed with both TRIM24 and TRIM32 simultaneously in NRVCMs. Both TRIM24 and TRIM32 displayed consistency with their already seen effects in combination

with Dysbindin. Intriguingly, the anti-hypertrophic effects of TRIM32 were significantly blunted by the presence of TRIM24, resulting in larger cell size and increased SRF-signaling activity (Figure 22A-C). Moreover, in the presence of TRIM24, the potent effect of TRIM32 on Dysbindin degradation at the protein level is strongly abrogated (Figure 22D-E). Thus, possibly via competitive binding, TRIM24 effectively counteracted TRIM32-driven Dysbindin dysregulation with subsequent functional effects on cardiomyocyte growth and SRF signaling.

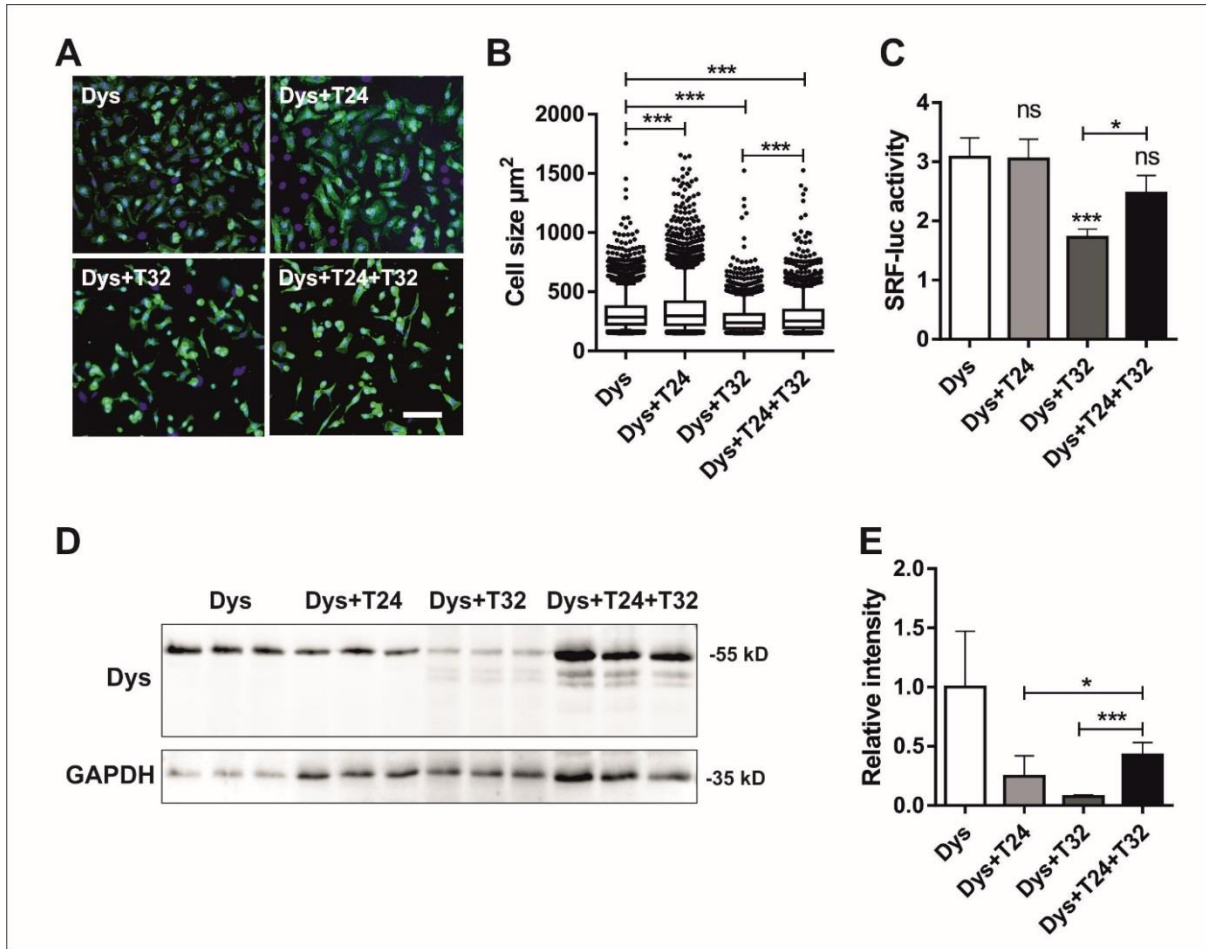


Figure 21: TRIM24 protects Dysbindin from TRIM32-mediated degradation. (A) Representative images for cell-size analysis. NRVCMs were cultured on coverslips in triplicate, infected with adenovirus expressing Dysbindin (Ad-Dysbindin, 50 ifu), TRIM24 (Ad-TRIM24, 100 ifu), TRIM32 (Ad-TRIM32, 100 ifu), and Ad-LacZ, as a filler adenovirus, for 72 h, and immunostained with α -actinin. Nuclei were stained with DAPI. Images were taken with a Keyence fluorescence microscope. (B) Cell surface area of the respective datasets was measured from randomly selected cells from three independent coverslips using 'Macro Cell Count' analyzer from BZ-II software. The experiment was repeated three times in triplicates. (C) Effect of TRIM24 and TRIM32 in different combinations with Dysbindin on SRF luciferase activity determined by SRF-RE firefly luciferase reporter assay in NRVCMs. Adenoviruses expressing Dysbindin (Ad-Dysbindin, 50 ifu), TRIM24 (Ad-TRIM24, 100 ifu), TRIM32 (Ad-TRIM32, 100 ifu), SRF-RE reporter-based firefly luciferase (Ad-SRF-luc, 20 ifu), and Renilla luciferase (Ad-Renilla, 5 ifu, control) were used for infection in NRVCMs. Data shown are means of three independent experiments performed in

s sextuplicate. **(D)** Immunoblot showing Dysbindin expression in protein isolated from NRVCs overexpressing Dysbindin in combination with TRIM24 and/or TRIM32; its densitometry analysis is depicted by a bar graph in **(E)**. Statistical significance was determined using two-tailed Student's t-test. Error bars show mean \pm S.E. *, $p < 0.05$; **, $p < 0.01$; ***, $p < 0.001$; ns, non-significant. Dys, Dysbindin; T24, TRIM24; T32, TRIM32. (Modified from: Borlepawar et al., 2017, © the American Society for Biochemistry and Molecular Biology)

8.15 TRIM32 expression adversely affects cell viability

Whenever an experiment with cell surface area was conducted in the current thesis, to our surprise, the total cell number of cultured NRVCs was remarkably reduced in the presence of overexpressed TRIM32 (Figure 23A-B). This prompted us to further investigate the potential causes of this reduced cell number effect by TRIM32. Of note, Dysbindin has previously been shown to play a supportive role in cell viability and proliferation in neurons (Nihonmatsu-Kikuchi et al., 2011); (Wang et al., 2014). Thus, we hypothesized that these growth supporting effects are suppressed by TRIM32 via Dysbindin degradation. To determine cellular viability, we performed MTT assays for cell viability in neonatal cardiomyocytes with an adenovirus-mediated expression of Dysbindin, TRIM24, and TRIM32. Cardiomyocyte survival indeed showed an inverse relation with the expression of TRIM32 but no effect was observed with Dysbindin or TRIM24 expression (Figure 23A), suggesting TRIM32 negatively affects cell viability independent of the anti-hypertrophic role. To confirm this negative effect of TRIM32 on cell viability and possibly induced cell death, we performed 'Terminal deoxynucleotidyl transferase dUTP nick end labeling' (TUNEL) assay which integrates labeled dNTPs along the fragmented DNA, one of the hallmarks of programmed cell death. The detrimental effect of TRIM32 on cell survival was consistent with TUNEL staining, with the percentage of apoptotic cells significantly surging up, when compared with the control cells expressing β -galactosidase. The number of TUNEL stained cells significantly went down with Dysbindin expression and remained unchanged with TRIM24 (Figure 23B-C). This data indicates that TRIM32 is a strong modulator of cell viability and apoptosis in NRVCs, independent of Dysbindin.

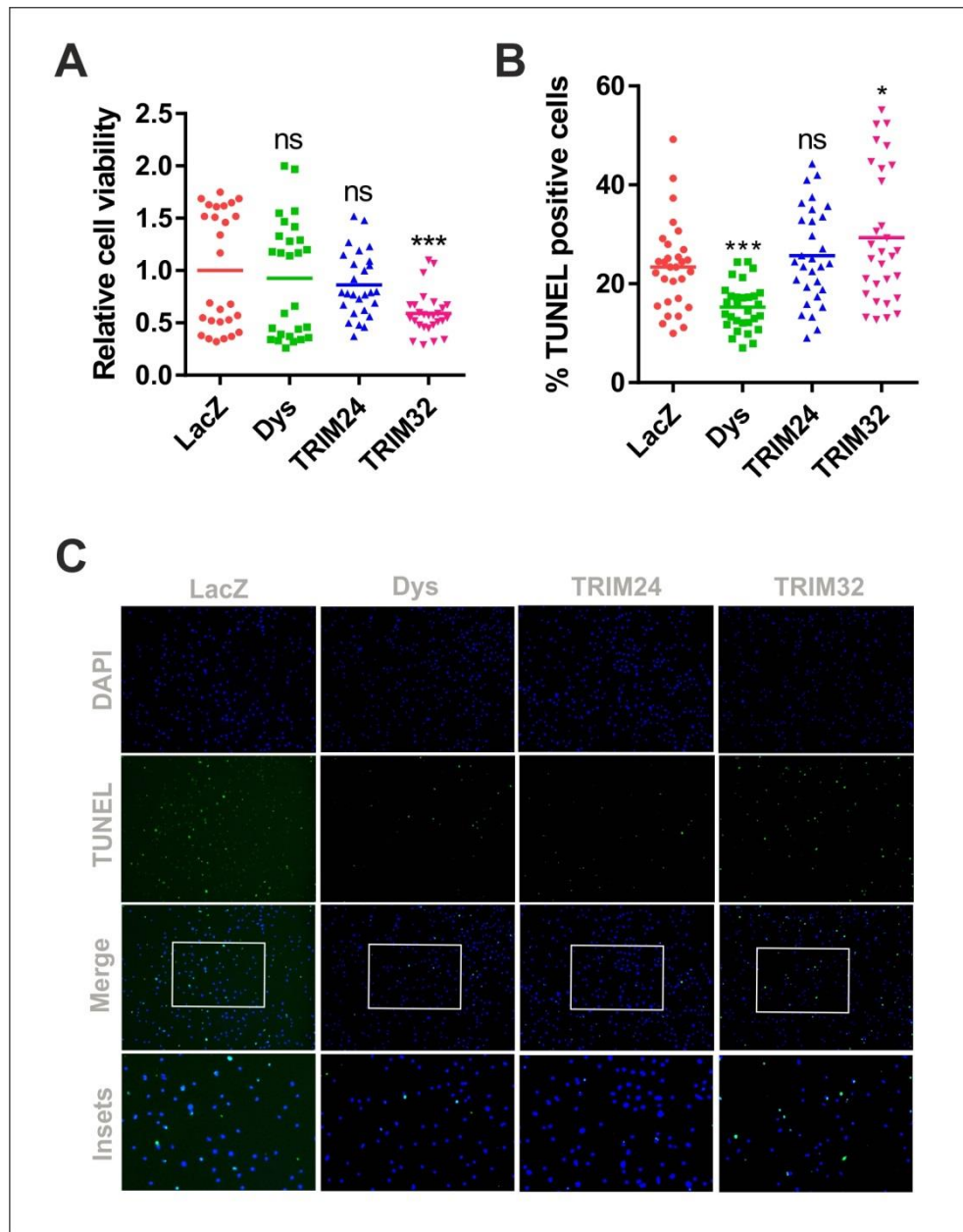


Figure 22: TRIM32 negatively affects cellular viability. (A) MTT assay for cell viability. Cultured NRVCMs were infected with adenovirus expressing Dysbindin (Ad-Dysbindin, 50 ifu), TRIM24 (Ad-TRIM24, 100 ifu), TRIM32 (Ad-TRIM32, 100 ifu) in serum-free media for 72 h. Adenovirus expressing-galactosidase (Ad-LacZ) was used as a control. After the incubation period, MTT-labeling reagent was added, and cells were incubated for 4 h in a humidified atmosphere. Subsequently, cells were subjected to overnight incubation with solubilization solution. Spectrophotometric absorbance was measured using a Tecan ELISA reader. Data shown are means of three independent experiments performed in sextuplicates. (C) Representative images for TUNEL and cleaved caspase-3 staining in NRVCMs. After adenovirus infection for 72 h, as mentioned above, NRVCMs underwent TUNEL staining. DAPI was used as a nuclear stain for total nuclei. Respective analysis for the percentage of TUNEL-positive (B) was performed with images taken from Keyence microscope. Nuclei count was performed with 'Macro Cell Count' analyzer. Data shown are means of two independent experiments performed in sextuplicates with >500 cells per condition. Scale bar (shown with a white line) represents 100 μ m. Statistical significance was determined using two-tailed Student's t-test. Error bars show mean \pm S.E. *, $p < 0.05$; **, $p < 0.01$; ***, $p < 0.001$; ns, non-significant.

Dys, Dysbindin. (Modified from: Borlepawar et al., 2017, © the American Society for Biochemistry and Molecular Biology)

8.16 TRIM32 expression induces apoptosis in NRVCMs

Apoptosis, the well-known controlled cell death process is a vital phenomenon in multicellular organisms. A tightly controlled apoptosis is the basic need of organisms where exaggerated growth can be terminated avoiding malignant growth resulting in cancers, while uncontrolled and exaggerated apoptosis can be pathological to the organism. A specific group of cysteine proteases named caspases is the main mediator of apoptosis. Caspases are activated after they undergo cleavage for initiation and execution of apoptosis in mammals. Caspase 2, 8, 9 and 10 are known to be initiators; whereas caspase 3, 6 and 7 are known as executioner caspases.

To further investigate the induction of apoptosis by TRIM32, NRVCMs were immunostained with the anti-cleaved-caspase 3 antibody. Caspase 3 being a nuclear protein, NRVCMs were stained along with other nuclei specific stain DAPI. The cleaved-caspase 3 vs. an overall number of nuclei allowed calculation of the percentage of apoptotic cells. TRIM32 showed a significant surge in supposedly caspase 3 mediated apoptosis after overexpression into cardiomyocytes, (Figure 24A-B). Magnified insets in the lower panel in Figure 24A display activation of caspase 3.

To further strengthen these results, NRVCMs were stained with Propidium iodide (PI), a DNA intercalating stain that is excluded from membrane permeability in viable cells, thus commonly used to identify dead cells in a population. Again, the detrimental effect of TRIM32 on cell survival was consistent with PI staining, with the percentage of dead cells surging up by 10% when compared with the control cells expressing -galactosidase (Figure 24C-D), implying induction of apoptosis and consequent cell death in NRVCMs. Unlike TUNEL-positive cells, which were reduced when Dysbindin was overexpressed compared with the LacZ (control) cell group (Figure 24B-C), cleaved caspase-3 or PI positive cells remained unchanged (Figure 24B, 24D). Notably, however, TRIM24 overexpression alone did not have any effect on apoptosis or cell death at all (Figure 24B, 24D). These data indicate that TRIM32 is a strong modulator of cell viability and apoptosis in NRVCMs.

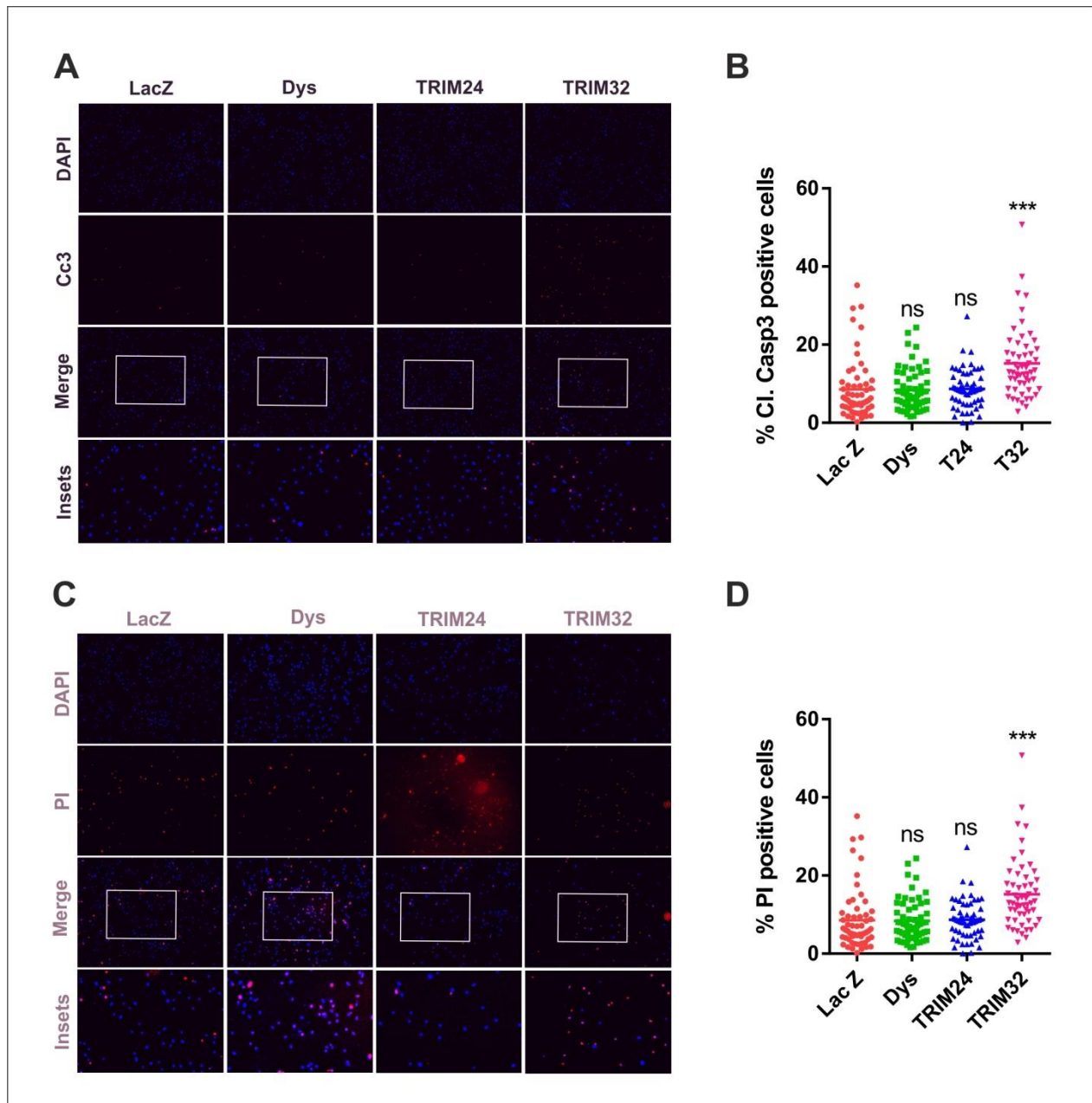


Figure 23: TRIM32 induces apoptosis and cell death in NRVCMs. (A) representative images and (B) analysis for cleaved caspase-3 staining in NRVCMs. (C) representative images and (D) analysis for PI staining in NRVCMs. After adenovirus infection for 72 h, as mentioned above, NRVCMs underwent immunostaining with cleaved caspase-3/PI. DAPI was used as a nuclear stain for total nuclei. Respective analysis for percentage of cleaved caspase-3-positive/PI was performed with images taken from Keyence fluorescence microscope. Nuclei count was performed with 'Macro Cell Count' analyzer for both DAPI and cleaved-caspase3/PI separately. Data shown are means of two independent experiments performed in sextuplicates with > 500 cells per condition. Statistical significance was determined using two-tailed Students *t*-test. Error bars show mean \pm SEM. *, $p < 0.05$; ***, $p < 0.001$; ns, non-significant. Scale bar (shown with a white line) represents 100 μ m. Dys, Dysbindin; Cc3, cleaved-caspase3; PI, propidium iodide. (Modified from: Borlepawar et al., 2017, © the American Society for Biochemistry and Molecular Biology)

8.17 TRIM32 induces apoptosis via regulation of Caspases

The next step was to ascertain the underlying mechanism of how exactly TRIM32 induces apoptosis in neonatal cardiomyocytes. To investigate whether TRIM32 induces apoptosis via mediators of apoptosis, caspases, we examined the effect of Dysbindin, TRIM24 and the TRIM32 expression on activation of specific executioner caspases by immunoblotting. As anticipated because of previously performed immunostaining, TRIM32 overexpression in NRVCs exhibited a compelling appearance of cleaved fragments around 18 kDa for caspase-3 (Figure 25A-B). A similar effect was observed with the activation of another important executioner caspase, caspase-7 (Figure 25C-D) compared with the respective control groups. In a bid to find more players in the activation of apoptosis by TRIM32, we looked out for interaction partners of caspase-3. In the literature, it was found that caspase3 is a known negative regulator of X-linked inhibitor of apoptosis (XIAP) (Hornle et al., 2011) and also exerts a positive influence on tumor protein53 (p53) expression (Hattangadi et al., 2004), a well-known carcinogenic marker that induces apoptosis in cancer cells. Moreover, XIAP is also suggested as a direct target of TRIM32, where TRIM32 ubiquitinated XIAP for degradation via UPS (Ryu et al., 2011). In line with these findings, TRIM32 expression was found to significantly downregulate XIAP protein levels (Figure 25E-F) in cardiomyocytes. Both TRIM24/32 have an established link with p53 in various other cell types in cancer-related studies (Allton et al., 2009); (Liu et al., 2014); (Jain et al., 2014). We found a significant reduction and a dramatic increase in p53 levels in the presence of Dysbindin and TRIM32, respectively (Figure 25G-H). Even though, TRIM24 is now an established interaction partner of p53 and studied as a clinical marker in various cancer-related studies, it had no effect on alteration of p53 in cardiomyocytes, suggesting only a tissue specific and not a general interaction between these two. Overall, these findings indicate that TRIM32 robustly activates apoptosis in NRVCs via activation of apoptosis modulators like caspases and p53, and inhibition of apoptosis inhibitor like XIAP.

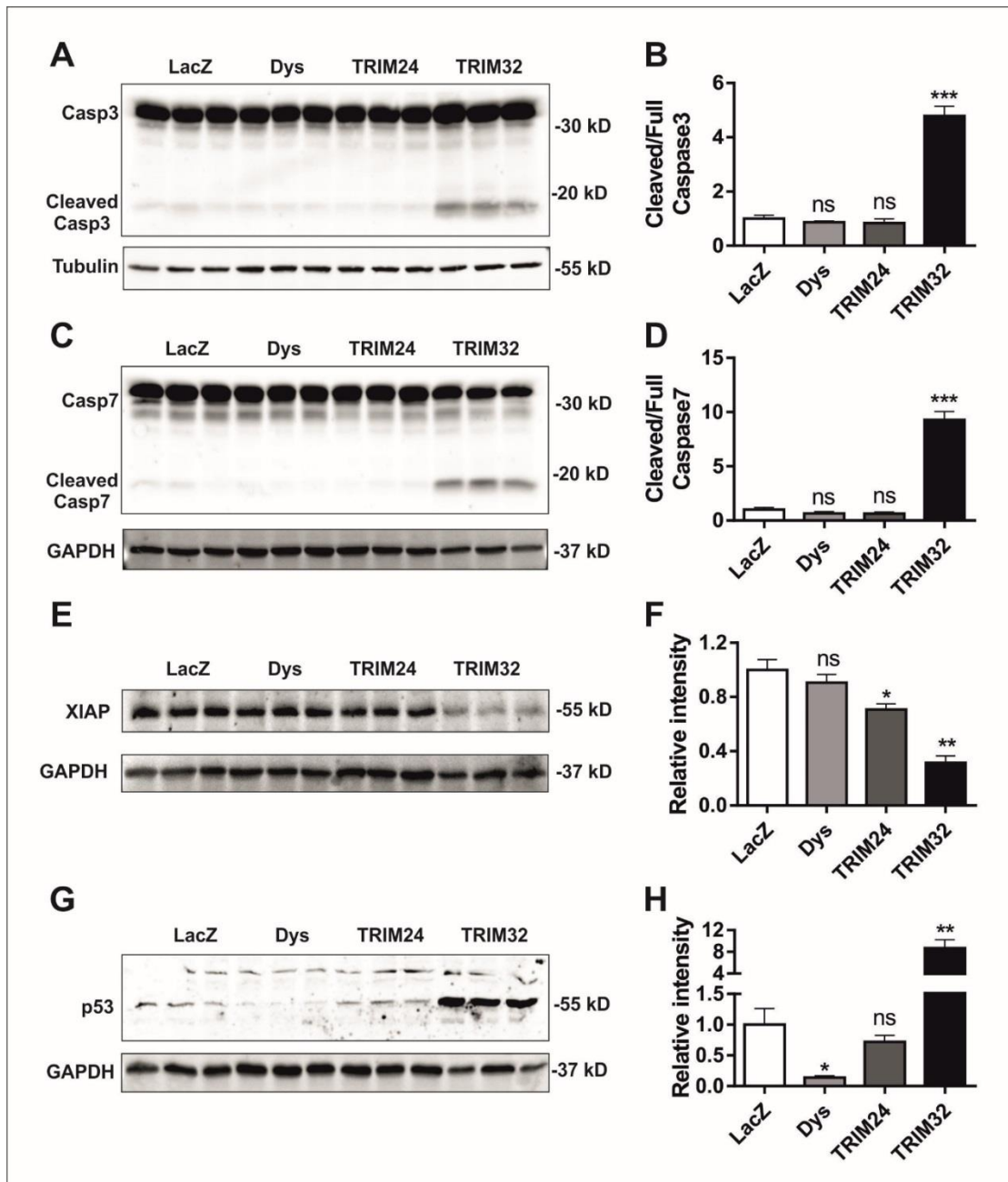


Figure 24: TRIM32 induces apoptosis in cardiomyocytes via cleavage and activation of caspases. (A) and (C) immunoblots showing expression of apoptosis execution markers, caspase-3, and caspase-7, with their cleaved fragments (~18 kDa), respectively, in NRVCs infected with adenovirus overexpressing Dysbindin (Ad-Dysbindin), TRIM24 (Ad-TRIM24), and TRIM32 (Ad-TRIM32). (B) and (D) densitometric analysis for caspase-3 and caspase-7 cleaved fragments performed against their respective un-cleaved fragments as a control. $n = 3$. (E) Immunoblot showing the expression of cellular apoptotic inhibitor protein XIAP and its densitometry analysis is presented in a bar graph (F) with GAPDH as a loading control. (G) Immunoblot showing the expression of cellular apoptotic inducer in cancerous cells, p53, and its densitometry analysis is presented in a bar graph (H) with GAPDH as a loading control. Statistical significance was determined using two-tailed Student's t-test. Error bars show mean \pm S.E. *, $p < 0.05$; **, $p < 0.01$; ***, $p < 0.001$; ns, non-significant. Cont, control; PE, phenylephrine; TAC, transverse aortic constriction. Casp3, caspase-3; Casp7, caspase-7; Dys, Dysbindin; p53, tumor protein 53; XIAP, an X-linked

inhibitor of apoptosis. (Modified from: Borlepawar et al., 2017, © the American Society for Biochemistry and Molecular Biology)

9 Discussion

The heart is a crucial organ pumping blood throughout the body of an organism by synchronous contraction and relaxation of the cardiac muscle. Homeostasis of the cardiac tissue and individual cells is necessary for normal heart function. Fine tuning of the cardiac muscle is maintained by numerous signal transduction pathways that mediate customary physiological functions and compensate for pathological injuries. The multifaceted process of cardiac pathophysiology constantly remains a top research field worldwide due to the high and steadily rising mortality associated with cardiovascular diseases according to WHO-CVDs data. Several intrinsic and extrinsic stimuli like physical stress, pressure overload, hypertension, *etc.* disturb cardiac homeostasis and affect signaling pathways causing disease phenotypes such as hypertrophy, cardiomyopathy, and subsequent heart failure. The unique characteristic of cardiomyocytes is that they are terminally differentiated in the embryo itself, and only grow in size by lateral hypertrophy postnatally. Hypertrophy is thus an inherent response to acute wall tension caused by various biochemical stresses in cardiomyocytes. At the molecular level, several signaling pathways and interacting networks have been implicated to the heart's molecular response to physiological and/or pathological biomechanical stressors (Frey and Olson, 2003); (Vega et al., 2003).

Various hypertrophic pathways mediated by Calcineurin (CnA-NFAT), glycogen synthase kinase (GSK)3 β , mitogen-activated protein (MAP) kinases, RhoA-SRF *etc.* have been well established through series of *in vitro* and *in vivo* studies and are highly correlated with human patients of cardiac hypertrophy and cardiomyopathy (Molkentin et al., 1998; Wilkins et al., 2004). CnA-NFAT signaling is found to be associated with other important hypertrophic pathways, such as signal transduction controlled by GSK3 β and MAPK (Vega et al., 2003). The RhoA-SRF mediated hypertrophic signaling pathway is crucial in this context. Rho family of small GTPase proteins, consisting of Rho, Rac, and Cdc42 subfamilies, regulates the sarcomere organization in cardiomyocytes, changes in which are hallmarks of hypertrophy (Hoshijima et al., 1998). These GTPase effectors are present upstream of a major cardiac signaling molecule, the serum

response factor (SRF) (Seeger et al., 2010). Through the activation of SRF, RhoA can induce the hypertrophic response in the heart. Recent discoveries related to RhoA-SRF axis have established Dysbindin, a schizophrenia core protein to be a strong inducer of cardiac hypertrophy *in vitro*, by virtue of direct interactions with hypertrophic proteins like RhoA and Myozap. In parallel, Dysbindin was also found to stimulate MEK1-ERK signaling independent of RhoA-SRF axis, activating hypertrophic and fetal gene programs that result in cardiac hypertrophy (Rangrez et al., 2013).

9.1 TRIM24 and TRIM32 are differentially regulated in cardiac hypertrophy and cardiomyopathy

TRIM24 was originally identified as transcriptional intermediary factor-1 α (TIF-1 α), a ligand-dependent co-repressor of retinoic acid receptor- α (Le Douarin et al., 1997), and has been reported to express aberrantly in human breast cancers correlating with poor patient survival (Thenot et al., 1997). TRIM32 is a ubiquitously expressed E3 ubiquitin ligase that is localized to the Z-line of skeletal muscle and has been shown to target desmin, actin, myosin, c-myc, NDRG2, etc. in addition to Dysbindin (Locke et al., 2009); (Kudryashova et al., 2005); (Cohen et al., 2012); (Mokhonova et al., 2015). TRIM32 is necessary for muscle regeneration by the process of myoblast proliferation and differentiation (Locke et al., 2009); (Kudryashova et al., 2005; Kudryashova et al., 2009); (Shieh et al., 2011); (Nicklas et al., 2012) and has also been associated with skeletal muscle atrophy (Cohen et al., 2012). Discovery of TRIM24 as one of the putative cardiac interaction partners of Dysbindin by Y2H assay (Table 13), and a potent endogenous presence in the heart (Figure 8B), prompted us for its cardiac-specific functional analysis. On the other hand, TRIM32 was incorporated in our experimental setup due to its established interaction with Dysbindin in the skeletal muscle (Locke et al., 2009).

To study the effects of TRIM24 and TRIM32 on cardiac functions of Dysbindin, first, we examined their expression levels in several models of cardiac hypertrophy. The differential upregulation of TRIM24 post PE infusion (Figure 9A-B), in cardiomyopathy patients of DCM (Figure 10A-B) and HCM (Figure 10D-E), suggested a hypertrophy-supporting role; whereas, unchanged levels after TAC prompted the role to be more specific towards certain types of cardiomyopathies. On the other hand, TRIM32 was significantly downregulated in all of the

mentioned hypertrophic conditions, suggesting a more general dysregulation of TRIM32 in pathological hypertrophy (Figure 9A, 9D, 10A, 10D). Interestingly, an inconsistent low molecular weight protein band was observed right below the expected TRIM32 band in the mouse hearts, which was highly up-regulated after TAC (Figure 9D). We hypothesize that this additional band represents a yet uncharacterized TRIM32 isoform that gets up-regulated in hypertrophic stress.

Collectively, the significant cardiac presence of TRIM24 and TRIM32 coupled with potent dysregulation in various cardiac disease conditions suggested the need for their functional characterization in the heart.

9.2 TRIM24 and TRIM32 interact with cardiac Dysbindin

To establish the possible Dysbindin-TRIM24/32 interaction, several co-IPs were performed in HEK293A cells using V5-Dysbindin, Flag-TRIM24, and Flag-TRIM32. In separate setups, TRIM24 and Dysbindin successfully pulled each other (Figure 11A-B), confirming an affinity towards each other. Expectedly, in line with skeletal muscle interaction, TRIM32 and Dysbindin were also confirmed to be interacting (Figure 11C-D). Dysbindin has been suggested to bind TRIM32 through its coiled-coil domain, as in the case of dystrobrevins interaction (Locke et al., 2009). To verify if the CC domain is a minimum necessary domain responsible for Dysbindin-TRIM24 interaction as well, Dysbindin expressing gene was segmented into four V5-fragments (Figure 12A). Various Co-IPs performed after co-expression of Dysbindin fragments with TRIM24 displayed that N-terminal+coiled-coil domain, coiled-coil domain, and full-length Dysbindin were able to pulldown TRIM24. Immunoprecipitation of TRIM24 in all three fragments containing the CC domain (Figure 12B) provides clear evidence that Dysbindin's CC domain is a minimal necessary domain responsible for Dysbindin-TRIM24 interaction.

After confirmation of Dysbindin interactions with TRIM24/32 into HEK293A cells, we reciprocated the interaction establishment in NRVCs, as these are primarily targeted cells in this thesis. For phenotypic characterization of suggested interactions in NRVCs, adenovirus-mediated overexpression (Figure 13A-F) and si/miRNA mediated knockdown (Figure 14A-F) of Dysbindin, TRIM24, and TRIM32 were verified. Localization of proteins in close vicinity of each other or in the same cellular compartment provides higher chances of interaction.

Antibodies specific for these proteins disclosed a high percentage of co-localization of Dysbindin with TRIM24 and TRIM32. TRIM24, a transcriptional intermediary factor, expectedly displayed a strong expression around the nucleus. By virtue of ubiquitous cellular presence, Dysbindin exhibited robust co-localization with perinuclear TRIM24 and cytoplasmic TRIM32 (Figure 16A). Justified by potent co-localization in cardiomyocytes and in the same lines of HEK Co-IPs, HA-Dysbindin successfully pulled TRIM24 and TRIM32 in NRVCs as well, confirming the interaction (Figure 15A-B).

Taken together, the data from various IPs and localization experiments confirmed the interaction of Dysbindin with TRIM24 and TRIM32 in the heart.

9.3 TRIM32 but not TRIM24 targets Dysbindin for UPS-mediated degradation

The characterization of Dysbindin in regard with a physiological role in the brain and its association with the psychiatric disorder schizophrenia is well proven by a series of research studies *in vitro*, in animal models, and in humans (Mullin et al., 2015); (Ghiani and Dell'Angelica, 2011). However, there was hardly an explanation about the putative role and regulation of this highly conserved and ubiquitously expressed protein in other cell types. Previously, our group has illustrated the cardiac role of Dysbindin as a pro-hypertrophic, SRF-signaling activator protein in NRVCs (Rangrez et al., 2013). To further disclose the molecular functions of Dysbindin in combination with its binding partners that potentially affect Dysbindin-associated hypertrophic pathways, a Y2H screen was performed, which presented TRIM24 as a potential binding partner, in addition to RhoA and others (Table 13). Another protein from the same family, TRIM32, had previously been reported as an E3 ubiquitin ligase of Dysbindin, targeting its UPS-mediated degradation in skeletal muscle cells.

On the basis of structural similarity between TRIM24 and TRIM32, with their famed roles in UPS targeted the degradation of various substrate proteins, we expected that both the proteins would display similar effects on Dysbindin levels, *i.e.* down regulating it. The overexpression of TRIM24 and TRIM32 in cardiomyocytes, however, displayed a completely different fate for endogenous Dysbindin. While TRIM32, targeted it for degradation, TRIM24 had no effect whatsoever on cellular Dysbindin levels (Figure 17A-D). On the contrary, microRNA-mediated

knockdown of TRIM24 and TRIM32 projected unaltered Dysbindin levels. It should also be noted that although TRIM24 and TRIM32 share similar N-terminal RBCC domains, they carry distinct C-terminal motifs and are categorized into different subgroups (in subgroup VI and VII, resp., Figure 7) (Ozato et al., 2008); (Borlepawar et al., 2018). It is therefore not surprising if two TRIMs exhibit contrasting effects in the same tissue for a given substrate, in this case, Dysbindin.

In the next steps to uncover the UPS dependency of TRIM24/32-mediated regulation, Dysbindin was overexpressed with various combinations of TRIM24/32, UPS-modulator ubiquitin and UPS-inhibitor drug MG132. Co-expression of Dysbindin with ubiquitin suggested overall higher ubiquitination of proteins in NRVCs, including Dysbindin (Figure 18A-B). The expression of TRIM24 along with ubiquitin increased cellular Dysbindin levels (Figure 18C-D), suggesting TRIM24 to be more protective of Dysbindin rather than degrading it. On the contrary, TRIM32 stimulated very low levels of Dysbindin, which were further diminished by the addition of ubiquitin (Figure 18F-G). The addition of MG132, the UPS-inhibitor drug, however, completely abrogated the degradation, where Dysbindin levels were noted to be ~60 times higher compared to TRIM32 affected levels (Figure 18C-D, 18F-G).

The above experiments collectively indicate that perinuclear TRIM24 does not, but cytoplasmic TRIM32 targets Dysbindin for UPS-mediated degradation in the heart.

9.4 TRIM24 is additive, whereas TRIM32 is inhibitory for SRF signaling

After examining the differential effects of TRIM24 and TRIM32 on Dysbindin levels in cardiomyocytes, the prime objective was to determine their role in SRF signaling, hypertrophic pathway induced by Dysbindin (Rangrez et al., 2013). TRIM24 activated SRF signaling, owing to its protective interaction with Dysbindin (Figure 19A); while its knockdown had no effect (Figure 19C), suggesting TRIM24 to be synergistic, but not necessary for SRF signaling. TRIM32 had no effect on basal SRF signaling, but strongly abrogated Dysbindin mediated activation (Figure 19B); whereas its knockdown did not inhibit Dysbindin mediated activation (Figure 19D), strongly indicating an inhibitory role through regulation of Dysbindin. The effects of TRIM24/32 on SRF signaling, as anticipated remained vastly dissimilar, suggesting a differential effect of TRIM24 and TRIM32 expression on Dysbindin-mediated SRF signaling.

The SRF signaling data, reported by dysregulation of SRF-reporter element further provides insight to the underlying molecular mechanism of hypertrophic SRF signaling, where TRIM24 promoted while TRIM32 restricted the pro-hypertrophic signaling via Dysbindin.

9.5 TRIM24 protects Dysbindin from TRIM32-mediated degradation

Through mapping and Co-IP experiments, the CC domain of Dysbindin was identified to be the minimal domain required for its interaction with TRIM24 (Figure 12A-B). Interestingly, the same CC domain is responsible for Dysbindin-TRIM32 interaction (Locke et al., 2009). Here, we expected TRIM24 to inhibit the degradative effects of TRIM32 at the protein level, possibly through competitive binding; after TRIM24 presence was found to have a protective effect on Dysbindin. The co-expression of both TRIM proteins with Dysbindin restored the cellular Dysbindin levels, i.e. even in the presence of TRIM32 (Figure 21D-E); suggesting that TRIM24 eventually protects Dysbindin from degradation via TRIM32. By virtue of either protection or degradation, the yin and yang function of TRIM24 and TRIM32 also regulates the pro-hypertrophic and SRF-activating effects of Dysbindin. TRIM24 not only protected Dysbindin levels but also its cardiac functions, which were observable after pro-hypertrophic analysis like higher cell surface area (Figure 21A-B) and elevated SRF signaling (Figure 21C).

The current study not only ascertains the interaction between Dysbindin-TRIM24/32, but it also provides mechanistic insight into the rare instances of proteins from the same family regulating a common substrate in a completely opposite manner, furthermore affecting downstream effects of the particular interaction.

9.6 TRIM32 affects cellular viability and induces apoptosis in cardiomyocytes

In this thesis, TRIM32 overexpression always resulted in distorted cellular architecture with an overall reduction in number of cells (Figure 20A, 21A). The reduction in total cell number was surprising, considering an equal cell seeding. TRIM family, known for selective proteolysis, has also been reported to play a role in the regulation of cell cycle and differentiation (Watanabe and Hatakemaya, 2017); directing a possibility of TRIM32 having an adverse effect on cell viability. On the other hand, Dysbindin had been proven to play a role in the proliferation of neurons (Nihonmatsu-Kikuchi et al., 2011) (Wang et al., 2014); providing a hypothesis that the

growth supplementary role of Dysbindin being affected by TRIM32. Analysis of cellular viability displayed a negative co-relation between TRIM32 and number of viable cells (Figure 22A). On the other hand, Dysbindin and TRIM24 had no effect whatsoever; suggesting detrimental effects of TRIM32 to be independent of reduction of cellular Dysbindin levels. The TUNEL assay for apoptosis consistently supported it, where the percentage of apoptotic cells increased with the introduction of TRIM32 (by ~ 10%, Figure 23B-C), suggesting it to be an apoptotic inducer. This induction was further confirmed when various immunostaining displayed an elevated percentage of cleaved-caspase3 (CC3) stained nuclei, a hallmark of apoptosis (Figure 23A-B); and Propidium iodide (PI) stained nuclei, a hallmark of cell death (Figure 23C-D) after TRIM32 overexpression, establishing it as an apoptotic inducer of cardiomyocytes.

Caspases are the initiators and executors of cellular apoptosis, who undergo cleavage after the induction of programmed cell death by stimuli like infections, nutrition depletion to carry out cellular apoptosis. Caspase-3, -7 and -9 are involved in the execution of the apoptosis. In various observations previously, TRIM32 has been found to play dual roles: its deficiency lead to increased proliferation and reduced apoptosis in neurons (Hillje et al., 2015); while, up-regulation promoted tumorigenesis in cancerous cells (Liu et al., 2014). In cardiomyocytes, however, TRIM32 induced cleavage of both Caspase-3 and -7, suggesting activation of the apoptosis (Figure 24A-D). Activation of caspase3 is well-known to lead inactivation of X-linked inhibitor of apoptosis (XIAP) and subsequent activation of p53 in order to perform programmed cell death (Hattangadi et al., 2004); (Hornle et al., 2011). Eponymously XIAP regulates apoptosis by inhibiting caspase-3 and -7 in healthy cells (Takahashi et al., 1998); (Scott et al., 2005). Notably, both XIAP and p53 are ubiquitination targets of TRIM32 (Ryu et al., 2011); (Liu et al., 2014). Through overexpression and knockdown experiments, Ryu et al. demonstrated TRIM32 to sensitize HEK293T cells to TNF α -induced apoptosis, where it co-localizes and interacts with XIAP after TNF α -induction, through CC and NHL domains, with RING domain carrying proteolysis in a tumor suppressive mechanism (Ryu et al., 2011). Similar proteolytic interaction was confirmed in NRVCs as well; where TRIM32 downregulated cellular XIAP levels, promoting apoptosis (Figure 24E-F). TRIM32 is known to be upregulated in tumorigenesis to negatively regulate tumor suppressor p53 (Liu et al., 2014); however, in this study, TRIM32 overexpression

rather resulted in strong upregulation of p53 (Figure 24G, 25H), suggesting a tissue-specific mechanism.

Recently, Chen et al. reported TRIM32 to inhibit cardiac hypertrophy by targeting hypertrophic AKT signaling, further implying it to be a possible therapeutic agent. After the current study, we speculate that the observed downregulation of TRIM32 in DCM/HCM is perhaps required for the development of pathological hypertrophy. It will thus be interesting to study this question *in vivo*, e.g. by restoring the downregulated TRIM32 levels after PE, TAC, DCM, and HCM; and subsequently assessing whether hypertrophy/heart failure still occurs. Nevertheless, the parallel effects of TRIM32 on cell survival can obscure the data, with the possibility of TRIM32 promoting heart failure due to increased cell death even if hypertrophy is inhibited. Answering this question is imperative before considering TRIM32 as a therapeutic agent in pathological cardiac hypertrophy (Chen et al., 2016).

Taken together, activation of p53, caspase-3/-7 and simultaneous inhibition of XIAP strongly contribute to the robust induction of apoptosis in NRVCs by TRIM32 overexpression.

9.7 Molecular mechanism of cardiac hypertrophy and apoptosis regulated by TRIM24/32

The post-translational regulation of Dysbindin in cardiomyocytes through its interaction partners TRIM24 and TRIM32 can be established as a novel mechanism of hypertrophic signaling after taking all results in the current thesis together. The study further implies TRIM32 to be a strong inducer of apoptosis in cardiomyocytes via concordant activation of apoptotic inducers like p53 and caspase-3/-7 and downregulation of inhibitor XIAP. Findings from this study and the known cardiac functions of Dysbindin from earlier work can be summarized in a model cartoon here (Figure 25).

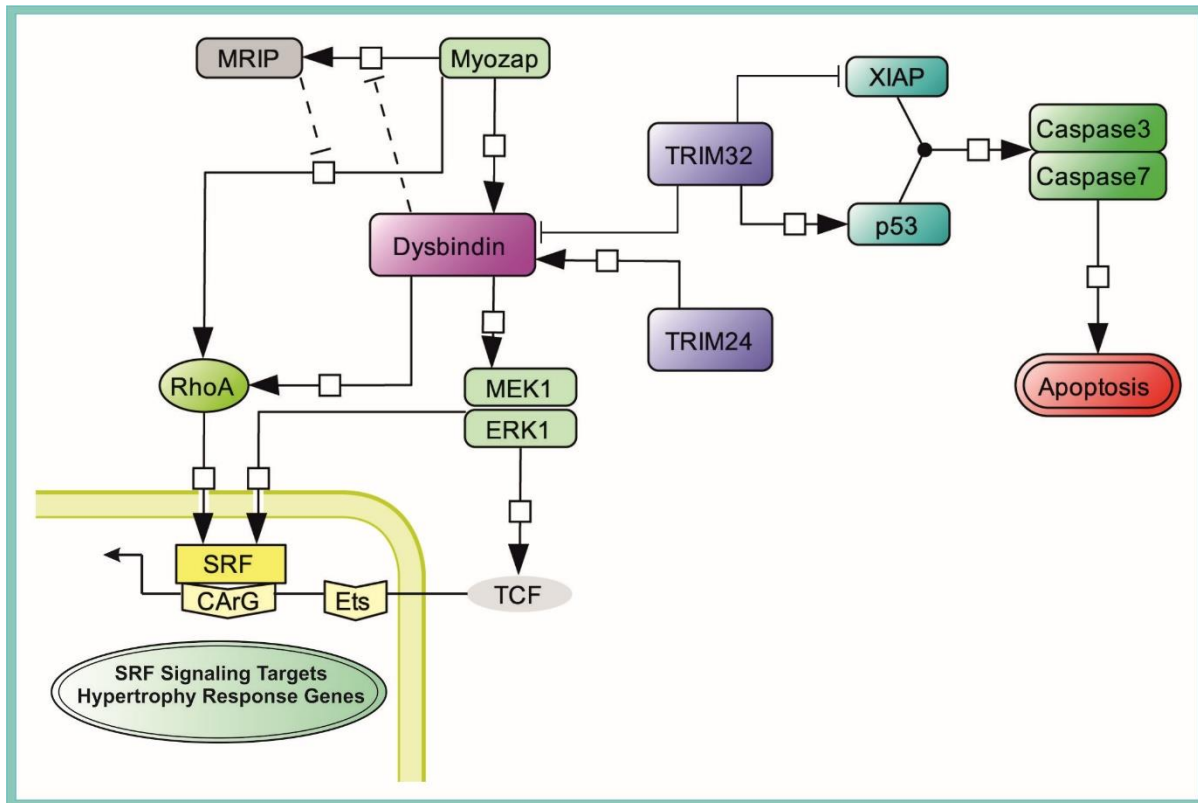


Figure 25: Pictorial representation of the effects of TRIM24/32 on Dysbindin levels and its downstream signaling in cardiomyocytes. Dysbindin activates SRF signaling through direct interaction with Myozap and RhoA, consequently leading to induction of SRF-responsive genes and hypertrophy. Based on the data from this study, we propose that TRIM24 protects Dysbindin and promotes Dysbindin-mediated hypertrophy and SRF signaling, whereas TRIM32 by virtue of Dysbindin degradation inhibits hypertrophy and SRF signaling. TRIM32 also induces apoptosis via activation of p53, caspase-3/-7, and inhibition of XIAP in Cardiomyocytes. (Borlepawar et al., 2017, © the American Society for Biochemistry and Molecular Biology)

In summary, this thesis is the first report to show a cardiac role for TRIM24 in general and a protective role in respect to Dysbindin degradation in particular. Moreover, the divergent effects of two TRIM proteins on a common substrate provide a novel pathway of post-translational regulation of Dysbindin. The association of Dysbindin/TRIM24/TRIM32 with SRF signaling makes this interaction interesting in the context of cardiac hypertrophy and cardiovascular diseases. The potent apoptotic effects of TRIM32 on NRVCMs are notable and might have wider implications in cardiac disease states that need to be thoroughly studied. Finally, the differential expressions of both TRIM24/32 in mouse models of biomechanical (PE) and biochemical (TAC) hypertrophy along with DCM and HCM suggest a direct involvement of these TRIMs in cardiac pathophysiology, which needs more attention to decipher the underlying maladaptive mechanisms. In broader terms, this study provides an initial characterization of two

members of the famed TRIM family of E3-ubiquitin ligases expressed in the heart that is useful for further *in vivo* and pathophysiological relevance.

9.8 Expression data suggest the involvement of additional TRIMs in heart function

Given the complexity of the cardiac function involving multiple molecular pathways and processes, only a few of the TRIMs have been shown to have a cardiac role before this thesis (three MuRFs, TRIM8, and TRIM72). In search of prospective studies, we hypothesized more TRIM family members to be mediating important cardiac functions. Using human Affymetrix data publicly available with Genevestigator (<https://genevestigator.com/gv/>), we traced down the expression of all TRIMs in various heart compartments. Several of the yet uncharacterized TRIMs were found to be significantly expressed in the heart, such as TRIM18, TRIM22, TRIM42, TRIM49, TRIM67, TRIM69, and TRIM73 (Figure 26), suggesting a wide possibility of cardio-specific studies regarding TRIM family of proteins. The expression of all TRIMs present in myocardium under cardiac disease settings like heart failure, cardiomyopathies, myocardial infarction, and atrial fibrillation was additionally determined to deduce the possible differential expression in the disease conditions. Interestingly, in addition to known cardiac TRIMs, several other TRIMs were found to be differentially regulated in these disease conditions, suggesting wider involvement of the tripartite protein family in cardiac pathogenesis (Figure 27).

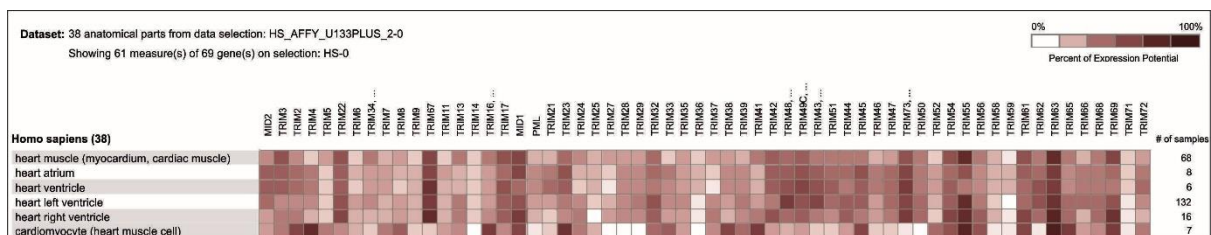


Figure 26: Expression of TRIM proteins in various heart compartments. Affymetrix data analysis indicates significant expression of various TRIMs in the heart and its sub-compartments (Borlepawar et al., 2018, Copyright © Elsevier).

The majority of the TRIMs which were found significantly expressed in the heart were also part of the specifically dysregulated TRIMs in cardiac disease conditions mentioned above. Although these bioinformatic findings need further *in vitro/in vivo* experimental validations; overall, these data highlight the potential of elaborated cardiac specific research for TRIMs in disease context (Figure 27).

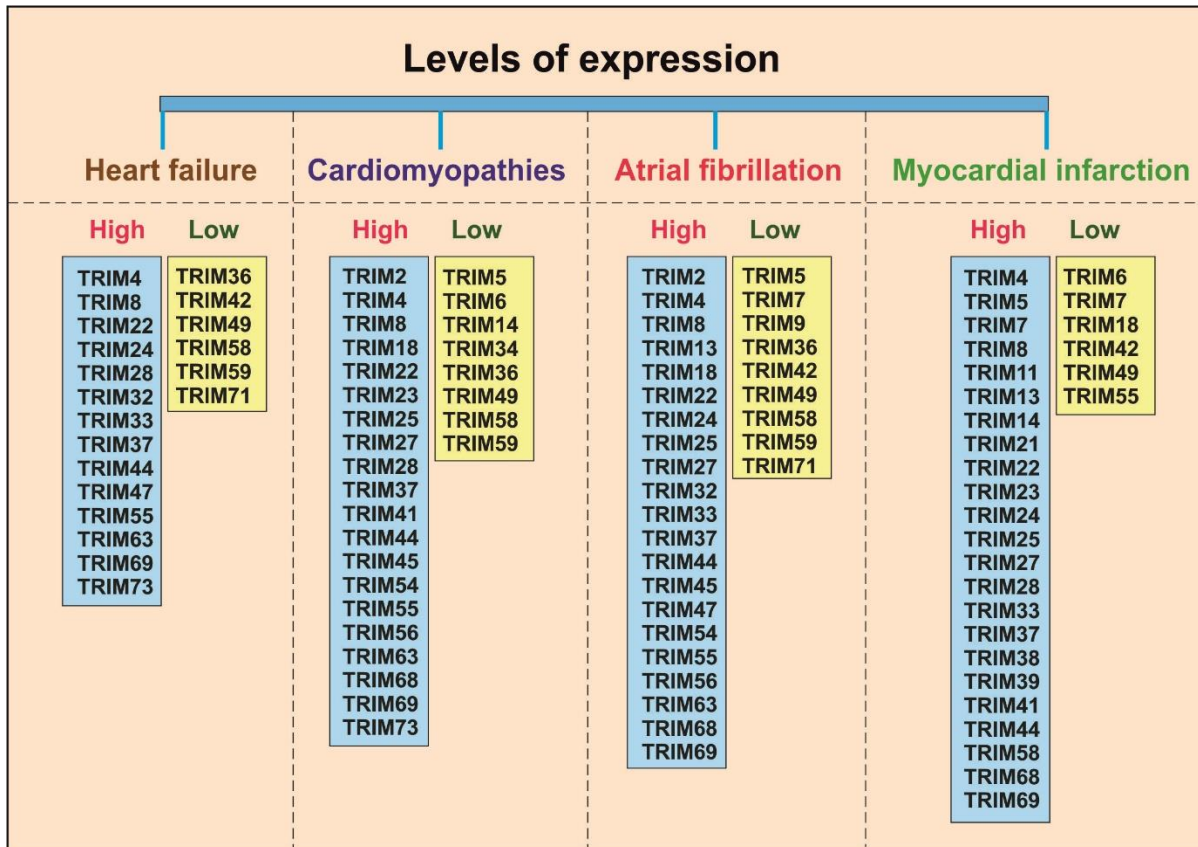


Figure 27: Expression of TRIM proteins in various cardiovascular diseases. Affymetrix data analysis indicates that several TRIM proteins are found to be differentially expressed in the heart under disease conditions like atrial fibrillation, cardiomyopathies, heart failure, and myocardial infarction (Borlepawar et al., 2018, Copyright © Elsevier).

9.9 Concluding remarks and wider prospectives

With ever-increasing studies targeting novel pathways and pathophysiology that harmfully affect cellular protein turnover, the toll of cardiovascular diseases remains high. PQC comprising protein degradation via autophagy and the UPS is essential in the cardiac context. Various perturbations in the tightly regulated PQC pathways give rise to several maladaptive diseases in humans like neurodegenerative Parkinson’s and Alzheimer’s, various cancerous growths, inflammatory Crohn’s disease, muscle related skeletal myopathies, and most important in the context of this thesis: various heart diseases including cardiac hypertrophy and heart failure. Several inherited cardiomyopathies are also associated with disruption of autophagy and/or increasing pathological protein aggregation, such as mutations in the sarcomeric Z-disc proteins BAG3 or desmin and its chaperone α B-crystallin, lead to proteotoxicity and dilated cardiomyopathy. Interestingly, several anti-cancer drugs such as tyrosine kinase inhibitors (e.g.

imatinib), anthracyclines (e.g. doxorubicin) or proteasome inhibitors (e.g. bortezomib) impair the UPS or autophagy, thereby indirectly causing artificial cardiomyopathy. Cardiac proteinopathy, a novel and more common disease condition found to cause cardiomyocyte decay, is largely neglected with the absence of effective therapies against it. Thus, there is an urgent need to develop innovative therapeutic approaches for curing cardiomyopathies and heart failure in the context of proteinopathies, where differentially regulated TRIMs can be employed as therapeutic agents. Thus, modulation of E3 ligases in the heart presents great potential as an alternative and target-directed therapeutic strategy. For example, an unbiased high-throughput screen by Jeff Robbin's lab has recently identified several potential E3 ligases like TRIM7, TRIM9, TRIM32, TRIM34a, and TRIM50 to accelerate or attenuate the formation of protein aggregates in cardiomyocytes (McLendon et al., 2017). Here TRIM32 specifically, can be expected to attenuate the aggregate formation via its capability of targeting aggregate-containing cardiac cells for an apoptosis- as studied in this thesis; or inhibiting hypertrophy- as suggested by (Chen et al., 2016) after examining the degree of apoptosis induction.

The downregulation of TRIM8 or TRIM21 has been proven to be beneficial for heart reconditioning after pressure overload and muscle deterioration and suggested as potential therapeutic approaches against pathological hypertrophy and heart failure. TRIM24, however, presents a different case, as it is additive to SRF-hypertrophy via its Dysbindin protection ability, but without having a robust hypertrophic effect itself. But, the transcriptional intermediary role of TRIM24, being capable of interactions with multiple transcription factors, suggests a need of its further characterization in the heart, and thus should be studied *in vivo* for any possible usage in clinical application. Moreover, it is also important to understand that E3 ligases selectively ubiquitinate distinct target proteins via numerous target binding domains. This very fact can be therapeutically exploited (i) to activate or supplement an E3- ligase that can selectively degrade a misfolded or unfolded protein of interest to reduce or dissolve protein aggregates formed, and (ii) to activate or inhibit downstream signaling pathways or cellular processes, in order to improve cardiac function in heart disease conditions.

10 Abbreviations

°C	Grad Celsius
λ	Lambda
Ad	Adenovirus
ADS	Digestive buffer with collagenase and pancreatin
AF	Alexa Fluor®- fluorescent dye
AHA	American Heart Association
AngII	Angiotensin II
APS	Ammonium persulfate
bp	Base pair
BSA	Bovine Serum Albumin
Ca ²⁺	Calcium
cDNA	Complementary DNA
CMV	Cytomegalovirus
Co-IP	Co-Immunoprecipitation
CVDs	Cardiovascular diseases
DAPI	4',6-Diamidin-2-phenylindol
DCM	Dilated Cardiomyopathy
ddH ₂ O	Double distilled water
DEPC	Diethyl pyrocarbonate
DMEM	Dulbecco's Modified Eagle Medium

DMSO	Dimethyl sulfoxide
DNA	Deoxyribonucleic acid
dNTP	Deoxyribonucleoside tri phosphate
DTT	Dithiothreitol
<i>E. coli</i>	<i>Escherichia coli</i>
ECL	Enhanced Chemiluminescence
EF	Ejections fraction
FCS	Fetal Calf Serum
Fig	Figure
FITC	Fluorescein Isothiocyanate
g	Gramm
GAPDH	Glyceraldehyde-3-phosphate-Dehydrogenase
h	Hour
HDAC	Histone-deacetylase
HCM	Hypertrophic cardiomyopathy
HW	Heart weight
HRP	Horseradish Peroxidase
hs	<i>homo sapiens</i>
HSF	Heat shock factors
HSPs	Heat shock proteins
IF	Immunofluorescence

ifu	Infectious units
IR	Ischemia-Reperfusion
kb	Kilo base pair
kDa	Kilo Dalton
KEGG	Kyoto Encyclopedia of Genes and Genomes
KO	Knockout
l	Liter
LacZ	Gene, coding for the enzyme β -Galactosidase
LB-Medium	Luria-Bertani Medium
LV	left ventricle
M	Molar
MAPK	Mitogen Activated Protein Kinase
MgCl ₂	Magnesium chloride
miRNeg	micro-RNA control
min	minute
miRNA	micro-RNA
mm	<i>mus musculus</i>
ml	Milliliter
mRNA	Messenger RNA
MuRFs	Muscle ring fingers
MW	Molecular weight

NaCl	Sodium chloride
NCS	Newborn Calf Serum
NFAT	Nuclear Factor of Activated T-cells
<i>nppa</i>	Natriuretic Peptide type A
<i>nppb</i>	Natriuretic Peptide type B
nm	Nanometer
NRVCMs	Neonatal Rat Ventricular cardiomyocytes
OD	Optical density
ORF	Open Reading Frame
PBS	Phosphate Buffered Saline
PCR	Polymerase Chain Reaction
PE	Phenylephrine
PFA	Paraformaldehyde
pH	Negative logarithm of the hydronium ion concentration
PQC	Protein quality control
PVDF	Polyvinyl difluoride
qPCR	Quantitative Real-Time PCR
Rcan1-4	Regulator of Calcineurin1-4
RCM	Restrictive cardiomyopathy
RNA	Ribonucleic acid
RNAi	RNA Interference

rn	<i>rattus norvegicus</i>
rpm	Revolutions per minute
RT	Room temperature
S	Seconds
SDS	Sodiumdodecylsulfate
SEM	Standard error of the mean
siRNA	small interfering RNA
SRF	Serum response factor
SRF-RE	Serum Response Factor Response Element
TAC	transverse aortic constriction
TAE	Tris-Acetate-EDTA Puffer
TBST	Tris-Buffered Saline Tween 20
TEMED	N,N,N',N'-Tetramethylethylenediamine
TF	Transcription factor
TG	Transgenic
TRIM	Tripartite motif containing
Tris	tris(hydroxymethyl)aminomethane
Triton X-100	Polyethylene glycol <i>p</i> -(1,1,3,3-tetramethylbutyl)-phenyl ether
U	Units
UPS	Ubiquitin Proteasome System
UV	Ultraviolet

v/v	Volume/Volume
w/v	Weight/Volume
WB	Western Blot
WHO	World Health Organization
WT	Wild type
X g	Centrifugal force

11 References

- Aasland, R., T.J. Gibson, and A.F. Stewart. 1995. The PHD finger: implications for chromatin-mediated transcriptional regulation. *Trends Biochem Sci.* 20:56-59.
- Albor, A., S. El-Hizawi, E.J. Horn, M. Laederich, P. Frosk, K. Wrogemann, and M. Kulesz-Martin. 2006. The interaction of Piasy with Trim32, an E3-ubiquitin ligase mutated in limb-girdle muscular dystrophy type 2H, promotes Piasy degradation and regulates UVB-induced keratinocyte apoptosis through NF kappa b. *J Biol Chem.* 281:25850-25866.
- Allton, K., A.K. Jain, H.M. Herz, W.W. Tsai, S.Y. Jung, J. Qin, A. Bergmann, R.L. Johnson, and M.C. Barton. 2009. Trim24 targets endogenous p53 for degradation. *P Natl Acad Sci USA.* 106:11612-11616.
- Arama, E., D. Dickman, Z. Kimchie, A. Shearn, and Z. Lev. 2000. Mutations in the beta-propeller domain of the Drosophila brain tumor (brat) protein induce neoplasm in the larval brain. *Oncogene.* 19:3706-3716.
- Arnold, S.E., K. Talbot, and C.G. Hahn. 2005. Neurodevelopment, neuroplasticity, and new genes for schizophrenia. *Prog Brain Res.* 147:319-345.
- Balch, W.E., R.I. Morimoto, A. Dillin, and J.W. Kelly. 2008. Adapting proteostasis for disease intervention. *Science.* 319:916-919.
- Banerjee, R., J. He, C. Spaniel, M.T. Quintana, Z. Wang, J. Bain, C.B. Newgard, M.J. Muehlbauer, and M.S. Willis. 2015. Non-targeted metabolomics analysis of cardiac Muscle Ring Finger-1 (MuRF1), MuRF2, and MuRF3 in vivo reveals novel and redundant metabolic changes. *Metabolomics.* 11:312-322.
- Bell, J.L., A. Malyukova, J.K. Holien, J. Koach, M.W. Parker, M. Kavallaris, G.M. Marshall, and B.B. Cheung. 2012. TRIM16 Acts as an E3 Ubiquitin Ligase and Can Heterodimerize with Other TRIM Family Members. *PLoS One.* 7.
- Bellini, M., J.C. Lacroix, and J.G. Gall. 1995. A Zinc-Binding Domain Is Required for Targeting the Maternal Nuclear-Protein Pwa33 to Lampbrush Chromosome Loops. *J Cell Biol.* 131:563-570.
- Benjamin, I.J., and D.R. McMillan. 1998. Stress (heat shock) proteins: molecular chaperones in cardiovascular biology and disease. *Circ Res.* 83:117-132.

- Bennardini, F., A. Wrzosek, and M. Chiesi. 1992. Alpha B-crystallin in cardiac tissue. Association with actin and desmin filaments. *Circ Res.* 71:288-294.
- Benson, M.A., S.E. Newey, E. Martin-Rendon, R. Hawkes, and D.J. Blake. 2001. Dysbindin, a novel coiled-coil-containing protein that interacts with the dystrobrevins in muscle and brain. *J Biol Chem.* 276:24232-24241.
- Bodine, S.C., E. Latres, S. Baumhueter, V.K. Lai, L. Nunez, B.A. Clarke, W.T. Poueymirou, F.J. Panaro, E. Na, K. Dharmarajan, Z.Q. Pan, D.M. Valenzuela, T.M. DeChiara, T.N. Stitt, G.D. Yancopoulos, and D.J. Glass. 2001. Identification of ubiquitin ligases required for skeletal muscle atrophy. *Science.* 294:1704-1708.
- Bogoyevitch, M.A., J. Gillespie-Brown, A.J. Ketterman, S.J. Fuller, R. Ben-Levy, A. Ashworth, C.J. Marshall, and P.H. Sugden. 1996. Stimulation of the stress-activated mitogen-activated protein kinase subfamilies in perfused heart. p38/RK mitogen-activated protein kinases and c-Jun N-terminal kinases are activated by ischemia/reperfusion. *Circ Res.* 79:162-173.
- Borden, K.L.B., and P.S. Freemont. 1996. The RING finger domain: A recent example of a sequence-structure family. *Curr Opin Struc Biol.* 6:395-401.
- Borlepawar, A., N. Frey, and A.Y. Rangrez. 2018. A systematic view on E3 ligase Ring TRIMmers with a focus on cardiac function and disease. *Trends Cardiovasc Med.* 29 (1), 1-8.
- Borlepawar, A., A.Y. Rangrez, A. Bernt, L. Christen, S. Sossalla, D. Frank, and N. Frey. 2017. TRIM24 protein promotes and TRIM32 protein inhibits cardiomyocyte hypertrophy via regulation of dysbindin protein levels. *J Biol Chem.* 292:10180-10196.
- Boudinot, P., L.M. van der Aa, L. Jouneau, L. Du Pasquier, P. Pontarotti, V. Briolat, A. Benmansour, and J.P. Levraud. 2011. Origin and evolution of TRIM proteins: new insights from the complete TRIM repertoire of zebrafish and pufferfish. *PLoS One.* 6:e22022.
- Brass, A.L., D.M. Dykxhoorn, Y. Benita, N. Yan, A. Engelman, R.J. Xavier, J. Lieberman, and S.J. Elledge. 2008. Identification of host proteins required for HIV infection through a functional genomic screen. *Science.* 319:921-926.
- Braunwald, E. 2017. Cardiomyopathies: An Overview. *Circ Res.* 121:711-721.
- Brokstad, K.A. 2016. The 2016 Nobel Prize in Physiology or Medicine. *Scand J Immunol.* 84:316.

- Buetow, L., and D.T. Huang. 2016. Structural insights into the catalysis and regulation of E3 ubiquitin ligases. *Nat Rev Mol Cell Biol.* 17:626.
- Cao, D.J., Z.V. Wang, P.K. Battiprolu, N. Jiang, C.R. Morales, Y. Kong, B.A. Rothermel, T.G. Gillette, and J.A. Hill. 2011. Histone deacetylase (HDAC) inhibitors attenuate cardiac hypertrophy by suppressing autophagy. *P Natl Acad Sci USA.* 108:4123-4128.
- Cao, T.Y., K.L.B. Borden, P.S. Freemont, and L.D. Etkin. 1997. Involvement of the rfp tripartite motif in protein-protein interactions and subcellular distribution. *J Cell Sci.* 110:1563-1571.
- Chasapis, C.T., and G.A. Spyroulias. 2009. RING finger E3 ubiquitin ligases: structure and drug discovery. *Curr Pharm Des.* 15:3716-3731.
- Chen, L., J. Huang, Y. Ji, X. Zhang, P. Wang, K. Deng, X. Jiang, G. Ma, and H. Li. 2016. Tripartite motif 32 prevents pathological cardiac hypertrophy. *Clin Sci (Lond).* 130:813-828.
- Chen, L.J., J. Huang, Y.X. Ji, F.H. Mei, P.X. Wang, K.Q. Deng, X. Jiang, G.S. Ma, and H.L. Li. 2017. Tripartite Motif 8 Contributes to Pathological Cardiac Hypertrophy Through Enhancing Transforming Growth Factor beta-Activated Kinase 1-Dependent Signaling Pathways. *Hypertension.* 69:249-+.
- Chen, Y., and D.J. Klionsky. 2011. The regulation of autophagy - unanswered questions. *J Cell Sci.* 124:161-170.
- Cohen, S., B. Zhai, S.P. Gygi, and A.L. Goldberg. 2012. Ubiquitylation by Trim32 causes coupled loss of desmin, Z-bands, and thin filaments in muscle atrophy. *J Cell Biol.* 198:575-589.
- Dai, D.F., E.J. Hsieh, Y. Liu, T. Chen, R.P. Beyer, M.T. Chin, M.J. MacCoss, and P.S. Rabinovitch. 2012. Mitochondrial proteome remodelling in pressure overload-induced heart failure: the role of mitochondrial oxidative stress. *Cardiovasc Res.* 93:79-88.
- Dorn, G.W., 2nd, J. Robbins, and P.H. Sugden. 2003. Phenotyping hypertrophy: eschew obfuscation. *Circ Res.* 92:1171-1175.
- Everett, R.D., and M.K. Chelbi-Alix. 2007. PML and PML nuclear bodies: implications in antiviral defence. *Biochimie.* 89:819-830.
- Fang, Z., L. Zhang, Q. Liao, Y. Wang, F. Yu, M. Feng, X. Xiang, and J. Xiong. 2017. Regulation of TRIM24 by miR-511 modulates cell proliferation in gastric cancer. *J Exp Clin Cancer Res.* 36:17.

- Fei, E.K., X.C. Ma, C.Q. Zhu, T. Xue, J. Yan, Y.X. Xu, J.N. Zhou, and G.H. Wang. 2010. Nucleocytoplasmic Shuttling of Dysbindin-1, a Schizophrenia-related Protein, Regulates Synapsin I Expression. *J Biol Chem.* 285:38630-38640.
- Ferrentino, R., M.T. Bassi, D. Chitayat, E. Tabolacci, and G. Meroni. 2007. MID1 Mutation Screening in a Large Cohort of Opitz G/BBB Syndrome Patients: Twenty-nine Novel Mutations Identified. *Hum Mutat.* 28.
- Fields, S., and O. Song. 1989. A novel genetic system to detect protein-protein interactions. *Nature.* 340:245-246.
- Fielitz, J., M.S. Kim, J.M. Shelton, S. Latif, J.A. Spencer, D.J. Glass, J.A. Richardson, R. Bassel-Duby, and E.N. Olson. 2007a. Myosin accumulation and striated muscle myopathy result from the loss of muscle RING finger 1 and 3. *J Clin Invest.* 117:2486-2495.
- Fielitz, J., E. van Rooij, J.A. Spencer, J.M. Shelton, S. Latif, R. van der Nagel, S. Bezprozvannaya, L. de Windt, J.A. Richardson, R. Bassel-Duby, and E.N. Olson. 2007b. Loss of muscle-specific RING-finger 3 predisposes the heart to cardiac rupture after myocardial infarction. *P Natl Acad Sci USA.* 104:4377-4382.
- Frank, D., R. Frauen, C. Hanselmann, C. Kuhn, R. Will, H.A. Katus, and N. Frey. 2008. Dyx1/Lmcd1 Mediates Cardiac Hypertrophy Both In Vitro And In Vivo. *Circulation.* 118:S393-S393.
- Franssen, C., J. Kole, R. Musters, N. Hamdani, and W.J. Paulus. 2017. alpha-B Crystallin Reverses High Diastolic Stiffness of Failing Human Cardiomyocytes. *Circ Heart Fail.* 10:e003626.
- Frantz, S., J. Bauersachs, and G. Ertl. 2009. Post-infarct remodelling: contribution of wound healing and inflammation. *Cardiovasc Res.* 81:474-481.
- Freemont, P.S. 2000. Ubiquitination: RING for destruction? *Curr Biol.* 10:R84-R87.
- Freemont, P.S., I.M. Hanson, and J. Trowsdale. 1991. A Novel Cysteine-Rich Sequence Motif. *Cell.* 64:483-484.
- Frey, N., and E.N. Olson. 2003. Cardiac hypertrophy: the good, the bad, and the ugly. *Ann Rev Physiol.* 65:45-79.
- Fu, C., D. Chen, R.J. Chen, Q.S. Hu, and G.H. Wang. 2015. The Schizophrenia-Related Protein Dysbindin-1A Is Degraded and Facilitates NF-Kappa B Activity in the Nucleus. *PLoS One.* 10.

- Fucini, P., C. Renner, C. Herberhold, A.A. Noegel, and T.A. Holak. 1997. The repeating segments of the F-actin cross-linking gelation factor (ABP-120) have an immunoglobulin-like fold. *Nat Struct Biol.* 4:223-230.
- Gavilan, M.P., C. Pintado, E. Gavilan, S. Jimenez, R.M. Rios, J. Vitorica, A. Castano, and D. Ruano. 2009. Dysfunction of the unfolded protein response increases neurodegeneration in aged rat hippocampus following proteasome inhibition. *Aging Cell.* 8:654-665.
- Ghiani, C.A., and E.C. Dell'Angelica. 2011. Dysbindin-containing complexes and their proposed functions in brain: from zero to (too) many in a decade. *ASN Neuro.* 3 (2).
- Golenhofen, N., M.D. Perng, R.A. Quinlan, and D. Drenckhahn. 2004. Comparison of the small heat shock proteins alphaB-crystallin, MKBP, HSP25, HSP20, and cvHSP in heart and skeletal muscle. *Histochem Cell Biol.* 122:415-425.
- Gomez-Pastor, R., E.T. Burchfiel, and D.J. Thiele. 2018. Regulation of heat shock transcription factors and their roles in physiology and disease. *Nat Rev Mol Cell Biol.* 19:4-19.
- Goodwin, J.F., H. Gordon, A. Hollman, and M.B. Bishop. 1961. Clinical aspects of cardiomyopathy. *Br Med J.* 1:69-79.
- Grigoryan, G., and A.E. Keating. 2008. Structural specificity in coiled-coil interactions. *Curr Opin Struct Biol.* 18:477-483.
- Groner, A.C., M. Brown, and J.P. Theurillat. 2016. Targeting transcriptional co-activators in advanced prostate cancer. *Cell Cycle.* 15:3333-3334.
- Han, D.S., H. Jang, C.S. Youn, and S.M. Yuk. 2015. A new surgical technique for concealed penis using an advanced musculocutaneous scrotal flap. *BMC Urol.* 15:54.
- Hattangadi, D.K., G.A. DeMasters, T.D. Walker, K.R. Jones, X. Di, I.F. Newsham, and D.A. Gewirtz. 2004. Influence of p53 and caspase 3 activity on cell death and senescence in response to methotrexate in the breast tumor cell. *Biochem Pharmacol.* 68:1699-1708.
- Haynes, S.R., C. Dollard, F. Winston, S. Beck, J. Trowsdale, and I.B. Dawid. 1992. The Bromodomain - a Conserved Sequence Found in Human, Drosophila and Yeast Proteins. *Nucleic Acids Res.* 20(10):2603.
- He, J., M.T. Quintana, J. Sullivan, L.P. T, J.G. T, J.C. Schisler, J.A. Hill, C.C. Yates, R.F. Mapanga, M.F. Essop, W.E. Stansfield, J.R. Bain, C.B. Newgard, M.J. Muehlbauer, Y. Han, B.A. Clarke, and M.S. Willis. 2015. MuRF2 regulates PPARgamma1 activity to protect against

- diabetic cardiomyopathy and enhance weight gain induced by a high fat diet. *Cardiovasc Diabetol.* 14:97.
- Henning, R.H., and B. Brundel. 2017. Proteostasis in cardiac health and disease. *Nat Rev Cardiol.*
- Hershko, A. 1996. Lessons from the discovery of the ubiquitin system. *Trends Biochem Sci.* 21:445-449.
- Hershko, A., and A. Ciechanover. 1982. Mechanisms of intracellular protein breakdown. *Annu Rev Biochem.* 51:335-364.
- Higgs, R., J. Ni Gabhann, N. Ben Larbi, E.P. Breen, K.A. Fitzgerald, and C.A. Jefferies. 2008. The E3 ubiquitin ligase Ro52 negatively regulates IFN-beta production post-pathogen recognition by polyubiquitin-mediated degradation of IRF3. *J Immunol.* 181:1780-1786.
- Hillje, A.L., E. Beckmann, M.A. Pavlou, C. Jaeger, M.P. Pacheco, T. Sauter, J.C. Schwamborn, and L. Lewejohann. 2015. The neural stem cell fate determinant TRIM32 regulates complex behavioral traits. *Front cell Neurosci.* 9:75.
- Hornle, M., N. Peters, B. Thayaparasingham, H. Vorsmann, H. Kashkar, and D. Kulms. 2011. Caspase-3 cleaves XIAP in a positive feedback loop to sensitize melanoma cells to TRAIL-induced apoptosis. *Oncogene.* 30:575-587.
- Hoshijima, M., V.P. Sah, Y. Wang, K.R. Chien, and J.H. Brown. 1998. The low molecular weight GTPase Rho regulates myofibril formation and organization in neonatal rat ventricular myocytes. Involvement of Rho kinase. *J Biol Chem.* 273:7725-7730.
- Hutter, M.M., R.E. Sievers, V. Barbosa, and C.L. Wolfe. 1994. Heat-Shock Protein Induction in Rat Hearts - a Direct Correlation between the Amount of Heat-Shock Protein-Induced and the Degree of Myocardial Protection. *Circulation.* 89:355-360.
- Ishizaka, N., H. de Leon, J.B. Laursen, T. Fukui, J.N. Wilcox, G. De Keulenaer, K.K. Griendling, and R.W. Alexander. 1997. Angiotensin II-induced hypertension increases heme oxygenase-1 expression in rat aorta. *Circulation.* 96:1923-1929.
- Jain, A.K., K. Allton, A.D. Duncan, and M.C. Barton. 2014. TRIM24 is a p53-induced E3-ubiquitin ligase that undergoes ATM-mediated phosphorylation and autodegradation during DNA damage. *Mol Cell Biol.* 34:2695-2709.

- Javanbakht, H., F. Diaz-Griffero, M. Stremlau, Z. Si, and J. Sodroski. 2005. The contribution of RING and B-box 2 domains to retroviral restriction mediated by monkey TRIM5alpha. *J Biol Chem.* 280:26933-26940.
- Kaizuka, T., and N. Mizushima. 2016. Atg13 Is Essential for Autophagy and Cardiac Development in Mice. *Mol Cell Biol.* 36:585-595.
- Kampinga, H.H., J. Hageman, M.J. Vos, H. Kubota, R.M. Tanguay, E.A. Bruford, M.E. Cheetham, B. Chen, and L.E. Hightower. 2009. Guidelines for the nomenclature of the human heat shock proteins. *Cell Stress Chaperones.* 14:105-111.
- Khan, M.M., S. Strack, F. Wild, A. Hanashima, A. Gasch, K. Brohm, M. Reischl, S. Carnio, D. Labeit, M. Sandri, S. Labeit, and R. Rudolf. 2014. Role of autophagy, SQSTM1, SH3GLB1, and TRIM63 in the turnover of nicotinic acetylcholine receptors. *Autophagy.* 10:123-136.
- Klionsky, D.J. 2008. Autophagy revisited: a conversation with Christian de Duve. *Autophagy.* 4:740-743.
- Kopitz, J., G.O. Kisen, P.B. Gordon, P. Bohley, and P.O. Seglen. 1990. Nonselective autophagy of cytosolic enzymes by isolated rat hepatocytes. *J Cell Biol.* 111:941-953.
- Korovila, I., M. Hugo, J.P. Castro, D. Weber, A. Hohn, T. Grune, and T. Jung. 2017. Proteostasis, oxidative stress and aging. *Redox Biol.* 13:550-567.
- Kudryashova, E., D. Kudryashov, I. Kramerova, and M.J. Spencer. 2005. Trim32 is a ubiquitin ligase mutated in limb girdle muscular dystrophy type 2H that binds to skeletal muscle myosin and ubiquitinates actin. *J Mol Biol.* 354:413-424.
- Kudryashova, E., J. Wu, L.A. Havton, and M.J. Spencer. 2009. Deficiency of the E3 ubiquitin ligase TRIM32 in mice leads to a myopathy with a neurogenic component. *Hum Mol Genet.* 18:1353-1367.
- Kuwahara, K., and K. Nakao. 2011. New molecular mechanisms for cardiovascular disease:transcriptional pathways and novel therapeutic targets in heart failure. *J Pharmacol Sci.* 116:337-342.
- Larimore, J., S.A. Zlatic, A. Gokhale, K. Tornieri, K.S. Singleton, A.P. Mullin, J. Tang, K. Talbot, and V. Faundez. 2014. Mutations in the BLOC-1 subunits dysbindin and muted generate divergent and dosage-dependent phenotypes. *J Biol Chem.* 289:14291-14300.

- Le Douarin, B., A.L. Nielsen, J. You, P. Chambon, and R. Losson. 1997. TIF1 alpha: a chromatin-specific mediator for the ligand-dependent activation function AF-2 of nuclear receptors? *Biochem Soc Trans.* 25:605-612.
- Lemckert, F.A., A. Bournazos, D.M. Eckert, M. Kenzler, J.M. Hawkes, T.L. Butler, B. Ceely, K.N. North, D.S. Winlaw, J.R. Egan, and S.T. Cooper. 2016. Lack of MG53 in human heart precludes utility as a biomarker of myocardial injury or endogenous cardioprotective factor. *Cardiovasc Res.* 110:178-187.
- Li, H.H., M.S. Willis, P. Lockyer, N. Miller, H. McDonough, D.J. Glass, and C. Patterson. 2007. Atrogin-1 inhibits Akt-dependent cardiac hypertrophy in mice via ubiquitin-dependent coactivation of Forkhead proteins. *J Clin Invest.* 117:3211-3223.
- Li, W., Q. Zhang, N. Oiso, E.K. Novak, R. Gautam, E.P. O'Brien, C.L. Tinsley, D.J. Blake, R.A. Spritz, N.G. Copeland, N.A. Jenkins, D. Amato, B.A. Roe, M. Starcevic, E.C. Dell'Angelica, R.W. Elliott, V. Mishra, S.F. Kingsmore, R.E. Paylor, and R.T. Swank. 2003. Hermansky-Pudlak syndrome type 7 (HPS-7) results from mutant dysbindin, a member of the biogenesis of lysosome-related organelles complex 1 (BLOC-1). *Nat Genet.* 35:84-89.
- Li, Z., and P. Srivastava. 2004. Heat-shock proteins. *Curr Protoc Immunol.* Appendix 1:Appendix 1T.
- Lin, L., W.H. Zhao, B. Sun, X.Y. Wang, and Q. Liu. 2017. Overexpression of TRIM24 is correlated with the progression of human cervical cancer. *Am J Transl Res.* 9:620-628.
- Liu, J., C. Zhang, X.L. Wang, P. Ly, V. Belyi, Z.Y. Xu-Monette, K.H. Young, W. Hu, and Z. Feng. 2014. E3 ubiquitin ligase TRIM32 negatively regulates tumor suppressor p53 to promote tumorigenesis. *Cell Death Differ.* 21:1792-1804.
- Locke, M., C.L. Tinsley, M.A. Benson, and D.J. Blake. 2009. TRIM32 is an E3 ubiquitin ligase for dysbindin. *Hum Mol Genet.* 18:2344-2358.
- Lodka, D., A. Pahuja, C. Geers-Knorr, R.J. Scheibe, M. Nowak, J. Hamati, C. Kohncke, B. Purfurst, T. Kanashova, S. Schmidt, D.J. Glass, I. Morano, A. Heuser, T. Kraft, R. Bassel-Duby, E.N. Olson, G. Dittmar, T. Sommer, and J. Fielitz. 2016. Muscle RING-finger 2 and 3 maintain striated-muscle structure and function. *J Cachexia Sarcopenia Muscle.* 7:165-180.

- Lovering, R., I.M. Hanson, K.L. Borden, S. Martin, N.J. O'Reilly, G.I. Evan, D. Rahman, D.J. Pappin, J. Trowsdale, and P.S. Freemont. 1993. Identification and preliminary characterization of a protein motif related to the zinc finger. *P Natl Acad Sci USA*. 90:2112-2116.
- Lupas, A. 1996. Coiled coils: new structures and new functions. *Trends Biochem Sci*. 21:375-382.
- Ma, L., L.L. Yuan, J. An, M.C. Barton, Q.Y. Zhang, and Z.L. Liu. 2016. Histone H3 lysine 23 acetylation is associated with oncogene TRIM24 expression and a poor prognosis in breast cancer. *Tumor Biol*. 37:14803-14812.
- Ma, X., E. Fei, C. Fu, H. Ren, and G. Wang. 2011. Dysbindin-1, a schizophrenia-related protein, facilitates neurite outgrowth by promoting the transcriptional activity of p53. *Mol Psychiatr*. 16:1105-1116.
- Maron, B.J., J.A. Towbin, G. Thiene, C. Antzelevitch, D. Corrado, D. Arnett, A.J. Moss, C.E. Seidman, J.B. Young, A. American Heart, H.F. Council on Clinical Cardiology, C. Transplantation, C. Quality of, R. Outcomes, G. Functional, G. Translational Biology Interdisciplinary Working, E. Council on, and Prevention. 2006. Contemporary definitions and classification of the cardiomyopathies: an American Heart Association Scientific Statement from the Council on Clinical Cardiology, Heart Failure and Transplantation Committee; Quality of Care and Outcomes Research and Functional Genomics and Translational Biology Interdisciplinary Working Groups; and Council on Epidemiology and Prevention. *Circulation*. 113:1807-1816.
- Mattox, T.A., M.E. Young, C.E. Rubel, C. Spaniel, J.E. Rodriguez, T.J. Grevengoed, M. Gautel, Z.L. Xu, E.J. Anderson, and M.S. Willis. 2014. MuRF1 activity is present in cardiac mitochondria and regulates reactive oxygen species production in vivo. *J Bioenerg Biomembr*. 46:173-187.
- McLendon, P.M., G. Davis, J. Gulick, S.R. Singh, N. Xu, N. Salomonis, J.D. Molkentin, and J. Robbins. 2017. An Unbiased High-Throughput Screen to Identify Novel Effectors That Impact on Cardiomyocyte Aggregate Levels. *Circ Res*. 121:604-616.
- Mearini, G., S. Schlossarek, M.S. Willis, and L. Carrier. 2008. The ubiquitin-proteasome system in cardiac dysfunction. *Biochim Biophys Acta*. 1782:749-763.
- Meroni, G., and G. Diez-Roux. 2005. TRIM/RBCC, a novel class of 'single protein RING finger' E3 ubiquitin ligases. *Bioessays*. 27:1147-1157.

- Mestril, R., S.H. Chi, M.R. Sayen, K. O'Reilly, and W.H. Dillmann. 1994. Expression of inducible stress protein 70 in rat heart myogenic cells confers protection against simulated ischemia-induced injury. *J Clin Invest.* 93:759-767.
- Meyer, H.J., and M. Rape. 2014. Enhanced Protein Degradation by Branched Ubiquitin Chains. *Cell.* 157:910-921.
- Meyer, M., S. Gaudieri, D.A. Rhodes, and J. Trowsdale. 2003. Cluster of TRIM genes in the human MHC class I region sharing the B30.2 domain. *Tissue Antigens.* 61:63-71.
- Miano, J.M. 2010. Role of serum response factor in the pathogenesis of disease. *Lab Invest.* 90:1274-1284.
- Miano, J.M., N. Ramanan, M.A. Georger, K.L. de Mesy Bentley, R.L. Emerson, R.O. Balza, Jr., Q. Xiao, H. Weiler, D.D. Ginty, and R.P. Misra. 2004. Restricted inactivation of serum response factor to the cardiovascular system. *P Natl Acad Sci USA.* 101:17132-17137.
- Mizushima, N., and M. Komatsu. 2011. Autophagy: renovation of cells and tissues. *Cell.* 147:728-741.
- Mocanu, M.M., S.E. Steare, M.C. Evans, J.H. Nugent, and D.M. Yellon. 1993. Heat stress attenuates free radical release in the isolated perfused rat heart. *Free Radic Biol Med.* 15:459-463.
- Mokhonova, E.I., N.K. Avliyakov, I. Kramerova, E. Kudryashova, M.J. Haykinson, and M.J. Spencer. 2015. The E3 ubiquitin ligase TRIM32 regulates myoblast proliferation by controlling turnover of NDRG2. *Hum Mol Genet.* 24:2873-2883.
- Molkentin, J.D., J.R. Lu, C.L. Antos, B. Markham, J. Richardson, J. Robbins, S.R. Grant, and E.N. Olson. 1998. A calcineurin-dependent transcriptional pathway for cardiac hypertrophy. *Cell.* 93:215-228.
- Moosmann, P., O. Georgiev, B. Le Douarin, J.P. Bourquin, and W. Schaffner. 1996. Transcriptional repression by RING finger protein TIF1 beta that interacts with the KRAB repressor domain of KOX1. *Nucleic Acids Res.* 24:4859-4867.
- Morimoto, R.I. 1993. Cells in stress: transcriptional activation of heat shock genes. *Science.* 259:1409-1410.
- Morreale, F.E., and H. Walden. 2016. Types of Ubiquitin Ligases. *Cell.* 165:248-248 e241.

- Mullin, A.P., M.K. Sadanandappa, W. Ma, D.K. Dickman, K. VijayRaghavan, M. Ramaswami, S. Sanyal, and V. Faundez. 2015. Gene dosage in the dysbindin schizophrenia susceptibility network differentially affect synaptic function and plasticity. *Neurosci.* 35:325-338.
- Naga Prasad, S.V., G. Esposito, L. Mao, W.J. Koch, and H.A. Rockman. 2000. Gbetagamma-dependent phosphoinositide 3-kinase activation in hearts with in vivo pressure overload hypertrophy. *J Biol Chem.* 275:4693-4698.
- Nakai, A., O. Yamaguchi, T. Takeda, Y. Higuchi, S. Hikoso, M. Taniike, S. Omiya, I. Mizote, Y. Matsumura, M. Asahi, K. Nishida, M. Hori, N. Mizushima, and K. Otsu. 2007. The role of autophagy in cardiomyocytes in the basal state and in response to hemodynamic stress. *Nat Med.* 13:619-624.
- Nakatogawa, H., K. Suzuki, Y. Kamada, and Y. Ohsumi. 2009. Dynamics and diversity in autophagy mechanisms: lessons from yeast. *Nat Rev Mol Cell Biol.* 10:458-467.
- Nicklas, S., A. Otto, X. Wu, P. Miller, S. Stelzer, Y. Wen, S. Kuang, K. Wrogemann, K. Patel, H. Ding, and J.C. Schwamborn. 2012. TRIM32 regulates skeletal muscle stem cell differentiation and is necessary for normal adult muscle regeneration. *PloS One.* 7:e30445.
- Nihonmatsu-Kikuchi, N., R. Hashimoto, S. Hattori, S. Matsuzaki, T. Shinozaki, H. Miura, S. Ohota, M. Tohyama, M. Takeda, and Y. Tatebayashi. 2011. Reduced rate of neural differentiation in the dentate gyrus of adult dysbindin null (sandy) mouse. *PloS One.* 6:e15886.
- Niida, M., M. Tanaka, and T. Kamitani. 2010. Downregulation of active IKK beta by Ro52-mediated autophagy. *Mol Immunol.* 47:2378-2387.
- Ortega, A., E. Rosello-Lleti, E. Tarazon, M.M. Molina-Navarro, L. Martinez-Dolz, J.R. Gonzalez-Juanatey, F. Lago, J.D. Montoro-Mateos, A. Salvador, M. Rivera, and M. Portoles. 2014. Endoplasmic reticulum stress induces different molecular structural alterations in human dilated and ischemic cardiomyopathy. *PloS One.* 9:e107635.
- Owen, M.J., N.M. Williams, and M.C. O'Donovan. 2004. Dysbindin-1 and schizophrenia: from genetics to neuropathology. *J Clin Invest.* 113:1255-1257.
- Ozato, K., D.M. Shin, T.H. Chang, and H.C. Morse, 3rd. 2008. TRIM family proteins and their emerging roles in innate immunity. *Nat Rev Immunol.* 8:849-860.

- Parlakian, A., D. Tuil, G. Hamard, G. Tavernier, D. Hentzen, J.P. Concordet, D. Paulin, Z. Li, and D. Daegelen. 2004. Targeted inactivation of serum response factor in the developing heart results in myocardial defects and embryonic lethality. *Mol Cell Biol.* 24:5281-5289.
- Perera, S., M.R. Holt, B.S. Mankoo, and M. Gautel. 2011. Developmental regulation of MURF ubiquitin ligases and autophagy proteins nbr1, p62/SQSTM1 and LC3 during cardiac myofibril assembly and turnover. *Dev Biol.* 351:46-61.
- Pfeffer, M.A., and E. Braunwald. 1990. Ventricular remodeling after myocardial infarction. Experimental observations and clinical implications. *Circulation.* 81:1161-1172.
- Phizicky, E.M., and S. Fields. 1995. Protein-protein interactions: methods for detection and analysis. *Microbiol Rev.* 59:94-123.
- Pizon, V., A. Iakovenko, P.F. Van Der Ven, R. Kelly, C. Fatu, D.O. Furst, E. Karsenti, and M. Gautel. 2002. Transient association of titin and myosin with microtubules in nascent myofibrils directed by the MURF2 RING-finger protein. *J Cell Sci.* 115:4469-4482.
- Powell, S.R., J. Herrmann, A. Lerman, C. Patterson, and X. Wang. 2012. The ubiquitin-proteasome system and cardiovascular disease. *Prog Mol Biol Transl Sci.* 109:295-346.
- Quintana, M.T., J. He, J. Sullivan, T. Grevengoed, J. Schisler, Y. Han, J.A. Hill, C.C. Yates, W.E. Stansfield, R.F. Mapanga, M.F. Essop, M.J. Muehlbauer, C.B. Newgard, J.R. Bain, and M.S. Willis. 2015. Muscle ring finger-3 protects against diabetic cardiomyopathy induced by a high fat diet. *BMC Endocr Disord.* 15:36.
- Rangrez, A.Y., A. Bernt, R. Poyanmehr, V. Harazin, I. Boomgaarden, C. Kuhn, A. Rohrbeck, D. Frank, and N. Frey. 2013. Dysbindin is a potent inducer of RhoA-SRF-mediated cardiomyocyte hypertrophy. *J Cell Biol.* 203:643-656.
- Reymond, A., and R. Brent. 1995. p16 proteins from melanoma-prone families are deficient in binding to Cdk4. *Oncogene.* 11:1173-1178.
- Reymond, A., G. Meroni, A. Fantozzi, G. Merla, S. Cairo, L. Luzi, D. Riganelli, E. Zanaria, S. Messali, S. Cainarca, A. Guffanti, S. Minucci, P.G. Pelicci, and A. Ballabio. 2001. The tripartite motif family identifies cell compartments. *EMBO J.* 20:2140-2151.
- Ritossa, F. 1962. New Puffing Pattern Induced by Temperature Shock and Dnp in *Drosophila*. *Experientia.* 18:571-&.

- Rodrigo-Brenni, M.C., and R.S. Hegde. 2012. Design principles of protein biosynthesis-coupled quality control. *Dev Cell*. 23:896-907.
- Rosciglione, S., C. Theriault, M.O. Boily, M. Paquette, and C. Lavoie. 2014. Galphas regulates the post-endocytic sorting of G protein-coupled receptors. *Nat Commun*. 5:4556.
- Ryu, Y.S., Y. Lee, K.W. Lee, C.Y. Hwang, J.S. Maeng, J.H. Kim, Y.S. Seo, K.H. You, B. Song, and K.S. Kwon. 2011. TRIM32 protein sensitizes cells to tumor necrosis factor (TNF α)-induced apoptosis via its RING domain-dependent E3 ligase activity against X-linked inhibitor of apoptosis (XIAP). *J Biol Chem*. 286:25729-25738.
- Sadowski, M., and B. Sarcevic. 2010. Mechanisms of mono- and poly-ubiquitination: Ubiquitination specificity depends on compatibility between the E2 catalytic core and amino acid residues proximal to the lysine. *Cell Div*. 5.
- Sanbe, A., H. Osinska, J.E. Saffitz, C.G. Glabe, R. Kaye, A. Maloyan, and J. Robbins. 2004. Desmin-related cardiomyopathy in transgenic mice: a cardiac amyloidosis. *P Natl Acad Sci USA*. 101:10132-10136.
- Santoro, M.G. 2000. Heat shock factors and the control of the stress response. *Biochem Pharmacol*. 59:55-63.
- Schindler, U., H. Beckmann, and A.R. Cashmore. 1993. HAT3.1, a novel Arabidopsis homeodomain protein containing a conserved cysteine-rich region. *Plant J*. 4:137-150.
- Sciarretta, S., V.S. Boppana, M. Umapathi, G. Frati, and J. Sadoshima. 2015. Boosting autophagy in the diabetic heart: a translational perspective. *Cardiovasc Diagn Ther*. 5:394-402.
- Scott, F.L., J.B. Denault, S.J. Riedl, H. Shin, M. Renatus, and G.S. Salvesen. 2005. XIAP inhibits caspase-3 and -7 using two binding sites: evolutionarily conserved mechanism of IAPs. *EMBO J*. 24:645-655.
- Seeger, T.S., D. Frank, C. Rohr, R. Will, S. Just, C. Grund, R. Lyon, M. Luedde, M. Koegl, F. Sheikh, W. Rottbauer, W.W. Franke, H.A. Katus, E.N. Olson, and N. Frey. 2010. Myozap, a Novel Intercalated Disc Protein, Activates Serum Response Factor-Dependent Signaling and Is Required to Maintain Cardiac Function In Vivo. *Circ Res*. 106:880-U120.
- Sergeeva, I.A., I.B. Hooijkaas, J.M. Ruijter, I. van der Made, N.E. de Groot, H.J. van de Werken, E.E. Creemers, and V.M. Christoffels. 2016. Identification of a regulatory domain

- controlling the Nppa-Nppb gene cluster during heart development and stress. *Development*. 143:2135-2146.
- Shieh, P.B., E. Kudryashova, and M.J. Spencer. 2011. Limb-girdle muscular dystrophy 2H and the role of TRIM32. *Handb Clin Neurol*. 101:125-133.
- Shore, P., and A.D. Sharrocks. 1995. The MADS-box family of transcription factors. *Eur J Biochem*. 229:1-13.
- Short, K.M., and T.C. Cox. 2006. Subclassification of the RBCC/TRIM superfamily reveals a novel motif necessary for microtubule binding. *J Biol Chem*. 281:8970-8980.
- Slack, F.J., and G. Ruvkun. 1998. A novel repeat domain that is often associated with RING finger and B-box motifs. *Trends Biochem Sci*. 23:474-475.
- Song, R., W. Peng, Y. Zhang, F. Lv, H.K. Wu, J. Guo, Y. Cao, Y. Pi, X. Zhang, L. Jin, M. Zhang, P. Jiang, F. Liu, S. Meng, C.M. Cao, and R.P. Xiao. 2013. Central role of E3 ubiquitin ligase MG53 in insulin resistance and metabolic disorders. *Nature*. 494:375-379.
- Sotiropoulos, A., D. Gineitis, J. Copeland, and R. Treisman. 1999. Signal-regulated activation of serum response factor is mediated by changes in actin dynamics. *Cell*. 98:159-169.
- Starcevic, M., and E.C. Dell'Angelica. 2004. Identification of snapin and three novel proteins (BLOS1, BLOS2, and BLOS3/reduced pigmentation) as subunits of biogenesis of lysosome-related organelles complex-1 (BLOC-1). *J Biol Chem*. 279:28393-28401.
- Su, H., and X. Wang. 2010. The ubiquitin-proteasome system in cardiac proteinopathy: a quality control perspective. *Cardiovasc Res*. 85:253-262.
- Su, M., J. Wang, L. Kang, Y. Wang, Y. Zou, X. Feng, D. Wang, F. Ahmad, X. Zhou, R. Hui, and L. Song. 2014. Rare variants in genes encoding MuRF1 and MuRF2 are modifiers of hypertrophic cardiomyopathy. *Int J Mol Sci*. 15:9302-9313.
- Sun, Y., B. Ji, Y. Feng, Y. Zhang, D. Ji, C. Zhu, S. Wang, C. Zhang, D. Zhang, and Y. Sun. 2017. TRIM59 facilitates the proliferation of colorectal cancer and promotes metastasis via the PI3K/AKT pathway. *Oncol Rep*. 38:43-52.
- Suzuki, H., T. Kaizuka, N. Mizushima, and N.N. Noda. 2015. Structure of the Atg101-Atg13 complex reveals essential roles of Atg101 in autophagy initiation. *Nat Struct Mol Biol*. 22:572-580.

- Tai, E., and S. Benchimol. 2009. TRIMming p53 for ubiquitination. *P Natl Acad Sci USA*. 106:11431-11432.
- Takahashi, R., Q. Deveraux, I. Tamm, K. Welsh, N. Assa-Munt, G.S. Salvesen, and J.C. Reed. 1998. A single BIR domain of XIAP sufficient for inhibiting caspases. *J Biol Chem*. 273:7787-7790.
- Takeshige, K., M. Baba, S. Tsuboi, T. Noda, and Y. Ohsumi. 1992. Autophagy in yeast demonstrated with proteinase-deficient mutants and conditions for its induction. *J Cell Biol*. 119:301-311.
- Tamkun, J.W. 1995. The Role of Brahma and Related Proteins in Transcription and Development. *Curr Opin Genet Dev*. 5:473-477.
- Taneike, M., O. Yamaguchi, A. Nakai, S. Hikoso, T. Takeda, I. Mizote, T. Oka, T. Tamai, J. Oyabu, T. Murakawa, K. Nishida, T. Shimizu, M. Hori, I. Komuro, T.S. Takuji Shirasawa, N. Mizushima, and K. Otsu. 2010. Inhibition of autophagy in the heart induces age-related cardiomyopathy. *Autophagy*. 6:600-606.
- Teyssier, C., C.Y. Ou, K. Khetchoumian, R. Losson, and M.R. Stallcup. 2006. Transcriptional intermediary factor 1alpha mediates physical interaction and functional synergy between the coactivator-associated arginine methyltransferase 1 and glucocorticoid receptor-interacting protein 1 nuclear receptor coactivators. *Mol Endocrinol*. 20:1276-1286.
- Thenot, S., C. Henriquet, H. Rochefort, and V. Cavailles. 1997. Differential interaction of nuclear receptors with the putative human transcriptional coactivator hTIF1. *J Biol Chem*. 272:12062-12068.
- Tomar, D., R. Singh, A.K. Singh, and C.D. Pandya. 2012. TRIM13 regulates ER stress induced autophagy and clonogenic ability of the cells. *Biochim Biophys Acta*. 1823:316-326.
- Torok, M., and L.D. Etkin. 2001. Two B or not two B? Overview of the rapidly expanding B-box family of proteins. *Differentiation*. 67:63-71.
- Vega, R.B., R. Bassel-Duby, and E.N. Olson. 2003. Control of cardiac growth and function by calcineurin signaling. *J Biol Chem*. 278:36981-36984.

- Venturini, L., J. You, M. Stadler, R. Galien, V. Lallemand, M.H. Koken, M.G. Mattei, A. Ganser, P. Chambon, R. Losson, and H. de The. 1999. TIF1gamma, a novel member of the transcriptional intermediary factor 1 family. *Oncogene*. 18:1209-1217.
- Vincent, S.R., D.A. Kwasnicka, and P. Fretier. 2000. A novel RING finger-B box-coiled-coil protein, GERP. *Biochem Biophys Res Commun*. 279:482-486.
- Wakayama, Y., Y. Matsuzaki, S. Yamashita, M. Inoue, T. Jimi, H. Hara, A. Unaki, S. Iijima, and H. Masaki. 2010. Dysbindin, syncoilin, and beta-synemin mRNA levels in dystrophic muscles. *Int J Neurosci*. 120:144-149.
- Wallace, D.C. 2005. A mitochondrial paradigm of metabolic and degenerative diseases, aging, and cancer: a dawn for evolutionary medicine. *Annual review of genetics*. 39:359-407.
- Walther, D.M., P. Kasturi, M. Zheng, S. Pinkert, G. Vecchi, P. Ciryam, R.I. Morimoto, C.M. Dobson, M. Vendruscolo, M. Mann, and F.U. Hartl. 2015. Widespread Proteome Remodeling and Aggregation in Aging *C. elegans*. *Cell*. 161:919-932.
- Wang, H., Y.F. Yuan, Z. Zhang, H. Yan, Y.Q. Feng, and W. Li. 2014. Dysbindin-1C Is Required for the Survival of Hilar Mossy Cells and the Maturation of Adult Newborn Neurons in Dentate Gyrus. *J Biol Chem*. 289:29060-29072.
- Wang, X., H. Osinska, R. Klevitsky, A.M. Gerdes, M. Nieman, J. Lorenz, T. Hewett, and J. Robbins. 2001. Expression of R120G-alphaB-crystallin causes aberrant desmin and alphaB-crystallin aggregation and cardiomyopathy in mice. *Circ Res*. 89:84-91.
- Wilkins, B.J., Y.S. Dai, O.F. Bueno, S.A. Parsons, J. Xu, D.M. Plank, F. Jones, T.R. Kimball, and J.D. Molkentin. 2004. Calcineurin/NFAT coupling participates in pathological, but not physiological, cardiac hypertrophy. *Circ Res*. 94:110-118.
- Willis, M.S., A. Bevilacqua, T. Pulinilkunnil, P. Kienesberger, M. Tannu, and C. Patterson. 2014a. The role of ubiquitin ligases in cardiac disease. *J Mol Cell Cardiol*. 71:43-53.
- Willis, M.S., M. Rojas, L. Li, C.H. Selzman, R.H. Tang, W.E. Stansfield, J.E. Rodriguez, D.J. Glass, and C. Patterson. 2009a. Muscle ring finger 1 mediates cardiac atrophy in vivo. *Am J Physiol Heart Circ Physiol*. 296:H997-H1006.
- Willis, M.S., J.C. Schisler, L. Li, J.E. Rodriguez, E.G. Hilliard, P.C. Charles, and C. Patterson. 2009b. Cardiac muscle ring finger-1 increases susceptibility to heart failure in vivo. *Circ Res*. 105:80-88.

- Willis, M.S., K.M. Wadosky, J.E. Rodriguez, J.C. Schisler, P. Lockyer, E.G. Hilliard, D.J. Glass, and C. Patterson. 2014b. Muscle ring finger 1 and muscle ring finger 2 are necessary but functionally redundant during developmental cardiac growth and regulate E2F1-mediated gene expression in vivo. *Cell Biochem Funct.* 32:39-50.
- Yahara, I. 1996. Stress-inducible cellular responses. Introduction. *Exs.* 77:XI-XII.
- Yamada, Y., K.I. Takayama, T. Fujimura, D. Ashikari, D. Obinata, S. Takahashi, K. Ikeda, S. Kakutani, T. Urano, H. Fukuhara, Y. Homma, and S. Inoue. 2017. A novel prognostic factor TRIM44 promotes cell proliferation and migration, and inhibits apoptosis in testicular germ cell tumor. *Cancer Sci.* 108:32-41.
- Yoshigai, E., S. Kawamura, S. Kuhara, and K. Tashiro. 2009. Trim36/Haprin plays a critical role in the arrangement of somites during *Xenopus* embryogenesis. *Biochem Biophys Res Commun.* 378:428-432.
- Yu, W., B. Gao, N. Li, J. Wang, C. Qiu, G. Zhang, M. Liu, R. Zhang, C. Li, G. Ji, and Y. Zhang. 2017. Sirt3 deficiency exacerbates diabetic cardiac dysfunction: Role of Foxo3A-Parkin-mediated mitophagy. *Biochim Biophys Acta.* 1863:1973-1983.
- Zhang, X., G. Azhar, J. Chai, P. Sheridan, K. Nagano, T. Brown, J. Yang, K. Khrapko, A.M. Borrás, J. Lawitts, R.P. Misra, and J.Y. Wei. 2001a. Cardiomyopathy in transgenic mice with cardiac-specific overexpression of serum response factor. *Am J Physiol Heart Circ Physiol.* 280:H1782-1792.
- Zhang, X., J. Chai, G. Azhar, P. Sheridan, A.M. Borrás, M.C. Furr, K. Khrapko, J. Lawitts, R.P. Misra, and J.Y. Wei. 2001b. Early postnatal cardiac changes and premature death in transgenic mice overexpressing a mutant form of serum response factor. *J Biol Chem.* 276:40033-40040.
- Zhang, Y., H.K. Wu, F.X. Lv, and R.P. Xiao. 2016. MG53 is a double-edged sword for human diseases. *Sheng li xue bao.* 68:505-516.
- Zheng, N., P. Wang, P.D. Jeffrey, and N.P. Pavletich. 2000. Structure of a c-Cbl-UbcH7 complex: RING domain function in ubiquitin-protein ligases. *Cell.* 102:533-539.
- Zhu, H.X., P. Tannous, J.L. Johnstone, Y.L. Kong, J.M. Shelton, J.A. Richardson, V. Lei, B. Levine, B.A. Rothermel, and J.A. Hill. 2007. Cardiac autophagy is a maladaptive response to hemodynamic stress. *J Clin Invest.* 117:1782-1793.

Zolk, O., C. Schenke, and A. Sarikas. 2006. The ubiquitin-proteasome system: focus on the heart. *Cardiovasc Res.* 70:410-421.

Zwadlo, C., and J. Borlak. 2005. Disease-associated changes in the expression of ion channels, ion receptors, ion exchangers and Ca(2+)-handling proteins in heart hypertrophy. *Toxicol Appl Pharmacol.* 207:244-256.

12 Curriculum vitae

Personal information

Ankush Borlepawar, MSc

Born on 24th February 1990 in Nanded, India

Education

- 1. Master of Science:** AgriGenomics (Final grade: 1.7) February, 2015
Christian-Albrechts-Universität zu Kiel - Kiel, Germany
 - 2. Bachelor of Science:** Biotechnology (Percentage: 76.46 %) March, 2011
MGM's College of CS & IT (SRTM University) - Nanded, India
-

Research Experience

- 1. PhD student** August, 2015 to July, 2019
Clinic for Internal Medicine III – Cardiology and Angiology, UK-SH, Campus Kiel
- 2. Master's thesis** May to November, 2014
Department of Plant Nutrition and Soil Sciences, University of Kiel, Germany

List of publications

Borlepawar, A., A.Y. Rangrez. 2016. Multi- facets of Serum Response Factor in the Cardiac Pathophysiology. *Biochem Mol Biol J.* 2:2.

Borlepawar, A.*, A.Y. Rangrez*, A. Bernt, L. Christen, S. Sossalla, D. Frank, and N. Frey. 2017. TRIM24 protein promotes and TRIM32 protein inhibits cardiomyocyte hypertrophy via regulation of dysbindin protein levels. *The Journal of biological chemistry.* 292:10180-10196. PMID: 28465353

Borlepawar, A., N. Frey, and A.Y. Rangrez. 2018. A systematic view on E3 ligase Ring TRIMmers with a focus on cardiac function and disease. *Trends Cardiovasc Med.* 29(1):1-8. PMID: 29880235

Borlepawar, A., N. Frey, and D. Frank. 2019. Editorial commentary: Epithelial-to-Mesenchymal transition and G protein-coupled receptors: A novel possibility for cardiac regeneration? *Trends Cardiovasc Med.* 29(4):205-206. PMID: 30268649

Frank, D., A. Y. Rangrez, C. Friedrich, S. Dittmann, B. Stallmeyer, P. Yadav, A. Bernt, E. Schulze-Bahr, **A. Borlepawar**, W.H. Zimmermann, S. Peischard, G. Seebohm, W. Linke, H. Baba, M. Krüger, A. Unger, P. Usinger, N. Frey, and E. Schulze-Bahr. A cardiac α -actin (*ACTC1*) gene mutation causes atrial-septal defects associated with late-onset dilated cardiomyopathy. *Under review.*

13 Acknowledgment

At the dawn of the most vital step in my academic career, the Ph.D. thesis, it is imperative for me to be grateful to the countless hands that helped me to succeed in this long and monumental effort.

First of all, I would like to thank Prof. Dr. Norbert Frey for providing me the opportunity in his cutting edge lab consisting of advanced tools for molecular cardiology research without any funding or academic restrictions. Your continued support, suggestions, and guidance, sometimes even from behind the curtains have provided me ample freedom for the completion of the current thesis. I'm also thankful to Prof. Dr. Derk Frank for the constant encouragement and provision of opportunities that have boosted my academic profile.

One of the highlights of my stay in the lab was the formation of personal bonds with the wonderful colleagues. My most humble gratitude is towards immediate colleagues Lynn, Nessrin, Kathi, Anca, Franzi, Suzi, Anushka and Alexandra for constant support and uplifting during my thesis. Many thanks to Lucia, for being very patient while proofreading the entire thesis. From my early times Vio, Linda, Greta, Christin, Vanessa, and Alexander never made me feel like an outsider and that helped a lot to be a member of the group in no time. Gabi always helped with countless official documentation and never-ending support for the lab material and no amount of thanks are enough for her help. The scientific and other discussions with people like Simone, Frauke and Christopher were helpful in the journey. Various lab mates Inga, Wiona, and Angela were immensely helpful for the constant help and ease of the experimental work. The discussions with uncountable medical students were extremely cheerful and always helped to bring out the fun part of the scientific work.

Family is something that trusts and encourages one to be the best in whatever one does in their life. I'm extremely lucky to have you in my life Anna-Aai, Tai-Bhauji, Bhau-Vahini, May-Tata, Gauravi, Gautami, Granth, Sarvesha, Anvik my in-laws and my fiancée Shravanti. You always think of me as the most ideal person and that boosts my spirit with unfathomable confidence.

Other than innumerable reasons, I'm really thankful for your constant support from allowing me to study out of India to smooth completion of my Ph.D. thesis.

Another important aspect of my gratitude goes to my teachers in bachelor's studies specifically Dr. Mangesh Kothari, Smt. Yogini Joshi, Dr. S. Shah Quadri and several others, who always supported my idea of studying in Germany and encouraged me for same. My friends from Nanded, especially Shivshankar Kumdale and Sunij Paldewar also are worth mention as you are my go to people and support system back in India, you are special buddies.

The vital backbone of my stay away from home was my second family of friends. Gaurav, Kiran, Smit, Amit, Abhijeet, and Jaydeep, you are like brothers and you know how much you mean to me. Exceptionally close friends like Jay-Riddhi, Kanishk, Niharika, Sandeep, Prashant-Maneet, Jay B., Ruchit, Dinesh and Linda made my stay from masters to Ph.D. very eventful and joyous. Innumerable other Indian and non-Indian friends were always supportive and respectful, that made my journey easier one.

Lastly, my most distinct gratitude goes towards my supervisor PD Dr. Ashraf Yusuf Rangrez. Not many PhDs are lucky enough to have a friend, who is constantly available to every stupid question and is a no-matter-what supportive supervisor. Ashraf da, your unprecedented help from the very beginning of my work has no match. Every smallest suggestion and directions in microbiology, biochemistry, molecular biology, and cardiac physiology has helped me to understand the basic nuances of scientific work. Your guidance regarding basic lab protocols, presentation of work in lab-meetings and conferences, understanding the need of experiments and further planning them, manuscript writing for scientific journals have converted me from the mud to a tough vessel in the research field. The constant non-scientific and family-related discussions with you have made me a better person who is loved and respected by family, friends, and colleagues. Ashraf da, for all the direct and indirect guidance and support, I'm forever indebted to you and cannot imagine a better supervisor than you. Thank you.